Geosphere, published online on 21 February 2014 as doi:10.1130/GES00952.1

Geosphere

Field and microanalytical isotopic investigation of ultradepleted in ^{18}O Paleoproterozoic "Slushball Earth" rocks from Karelia, Russia

I.N. Bindeman, N.S. Serebryakov, A.K. Schmitt, J.A. Vazquez, Y. Guan, P. Ya. Azimov, B. Yu. Astafiev, J. Palandri and L. Dobrzhinetskaya

Geosphere published online 21 February 2014;
doi: 10.1130/GES00952.1

Notes

Geosphere, published online on 21 February 2014 as doi:10.1130/GES00952.1

Field and microanalytical isotopic investigation of ultradepleted in ^{18}O Paleoproterozoic "Slushball Earth" rocks from Karelia, Russia

I.N. Bindeman[1], N.S. Serebryakov[2], A.K. Schmitt[3], J.A. Vazquez[4], Y. Guan[5], P. Ya. Azimov[6], B. Yu. Astafiev[6], J. Palandri[1], and L. Dobrzhinetskaya[7]

[1]*Department of Geological Sciences, 1272 University of Oregon, Eugene, Oregon 97403, USA*
[2]*Institute of Petrography, Mineralogy and Geology of Ore Deposits (IGEM), Russian Academy of Sciences, Staromonetny per, 35, Moscow, Russia*
[3]*Department of Earth and Space Sciences, University of California, Los Angeles, Los Angeles, California 90095, USA*
[4]*U.S. Geological Survey, Menlo Park, California 94025, USA*
[5]*Geological and Planetary Sciences Division, California Institute of Technology, Pasadena, California 91125, USA*
[6]*Institute of Precambrian Geology and Geochronology, Russian Academy of Sciences, St. Petersburg 199034, Russia*
[7]*Department of Earth Sciences, University of California, Riverside, California 92521, USA*

ABSTRACT

The 1.85 Ga Belomorian Belt, Karelia, Russia, hosts ultralow $\delta^{18}O$ and δD (as low as –27.3‰ and –235‰ standard mean ocean water [SMOW], respectively), high-Al gneisses and amphibolites that we attribute to the Paleoproterozoic "Slushball Earth" glaciation. They now occur in at least 11 localities spanning 450 km. To constrain distribution of ^{18}O-depleted rocks, we performed detailed field mapping in Khitostrov, where $\delta^{18}O$ values are the lowest. Using 430 new and previously published laser fluorination isotope analyses, we show that the elongated, concentrically zoned area of $\delta^{18}O$ depletion is greater than 6 × 2 km in areal extent, ~10 times larger than previously thought. Relationships between $\delta^{17}O$ versus $\delta^{18}O$ strictly adhere to the equilibrium terrestrial mass-dependent fractionation with a slope of 0.527. We also report the results of ion microprobe U-Pb geochronology of zircons coupled with co-registered oxygen isotope spot analyses for mafic intrusions and host gneisses in six localities. The 2.9–2.7 Ga gneiss zircon cores are normal in $\delta^{18}O$ (5‰–7‰). They show truncated oscillatory cathodoluminescence (CL) patterns and rounded shape indicative of original igneous crystallization with subsequent detrital overprinting. A younger 2.6–2.55 Ga metamorphic zircon domain with normal $\delta^{18}O$, low Th/U, dark cathodoluminescence, and also with rounded crystal morphology is commonly preserved. Cores are surrounded by ubiquitous rims highly depleted in $\delta^{18}O$ (re-)crystallized with Svecofennian (1.85–1.89 Ga) ages. Rims are interpreted as metamorphic due to bright and uniform CL and Th/U <0.05. Mafic intrusions preserve few igneous zircon crystals between ca. 2.23 and 2.4 Ga in age, but neoblastic zircon in these intrusions originated mostly during 1.85 Ga Svecofennian metamorphism. The $\delta^{18}O$-age relationship for metamorphic rims in zircon and corundum grains suggests that $\delta^{18}O$ values of fluids were subtly increasing with time during metamorphism. Large metamorphic corundum grains have ~3‰ intracrystalline $\delta^{18}O$ isotope zonation from –24 to –21‰, which likely developed during interaction with metamorphic fluids. The Zr-in-rutile geothermometer temperatures are in the range of 760 to 720 °C, in accordance with mineral assemblages and amphibolite metamorphic grade. High and irregular rare-earth element (REE) abundance in cores and rims of many zircons correlates with high phosphorus content and is explained by nanometer-scale xenotime and monazite inclusions, likely in metamict zones during 1.85 Ga Svecofennian metamorphism. A survey of oxygen isotopes in ultrahigh-pressure diamond and coesite-bearing metamorphic terrains around the world reveals normal to high-$\delta^{18}O$ values, suggesting that the low $\delta^{18}O$ in metamorphic rocks of Dabie Shan, Kokchetav, and in Karelia, are genetically unrelated to metamorphism. We discuss alternative ways to achieve extreme $\delta^{18}O$ depletion by kinetic, Rayleigh, and thermal diffusion processes, and by metamorphism. We prefer an interpretation where the low-$\delta^{18}O$ and high-Al signature of the rocks predates metamorphism, and is caused by shallow hydrothermal alteration and partial dissolution of the protolith surrounding shallow mafic intrusions by glacial meltwaters during pan-global Paleoproterozoic "Slushball Earth" glaciations between ca. 2.4 and ca. 2.23 Ga.

INTRODUCTION

There are now 11 known localities spanning over 450 km across the Belomorian Belt, which formed in the Late Archean–Early Proterozoic, where we have observed remarkably ^{18}O depleted rocks (as low as –27.3‰ standard mean ocean water [SMOW], Fig. 1)[1]. Ultralow-$\delta^{18}O$ rocks crop out over many tens to hundreds of meters, and comprise chiefly four lithologies: Al-rich paragneisses, 2.4 Ga high-Mg gabbronoritic intrusions, amphibolites at the contact between the two, and high-Fe intrusions with a tentative age of 2.3–2.1 Ga. The $\delta^{18}O$ depletions often display a "bulls-eye" concentric pattern with progressively greater ^{18}O depletion in the proximity of the intrusions (Fig. 2), which are

Geosphere; April 2014; v. 10; no. 2; ; doi:10.1130/GES00952.1; 16 figures; 3 tables; 1 supplemental file.
Received 28 May 2013 ♦ Revision received 4 January 2014 ♦ Accepted 29 January 2014 ♦ Published online 21 February 2014

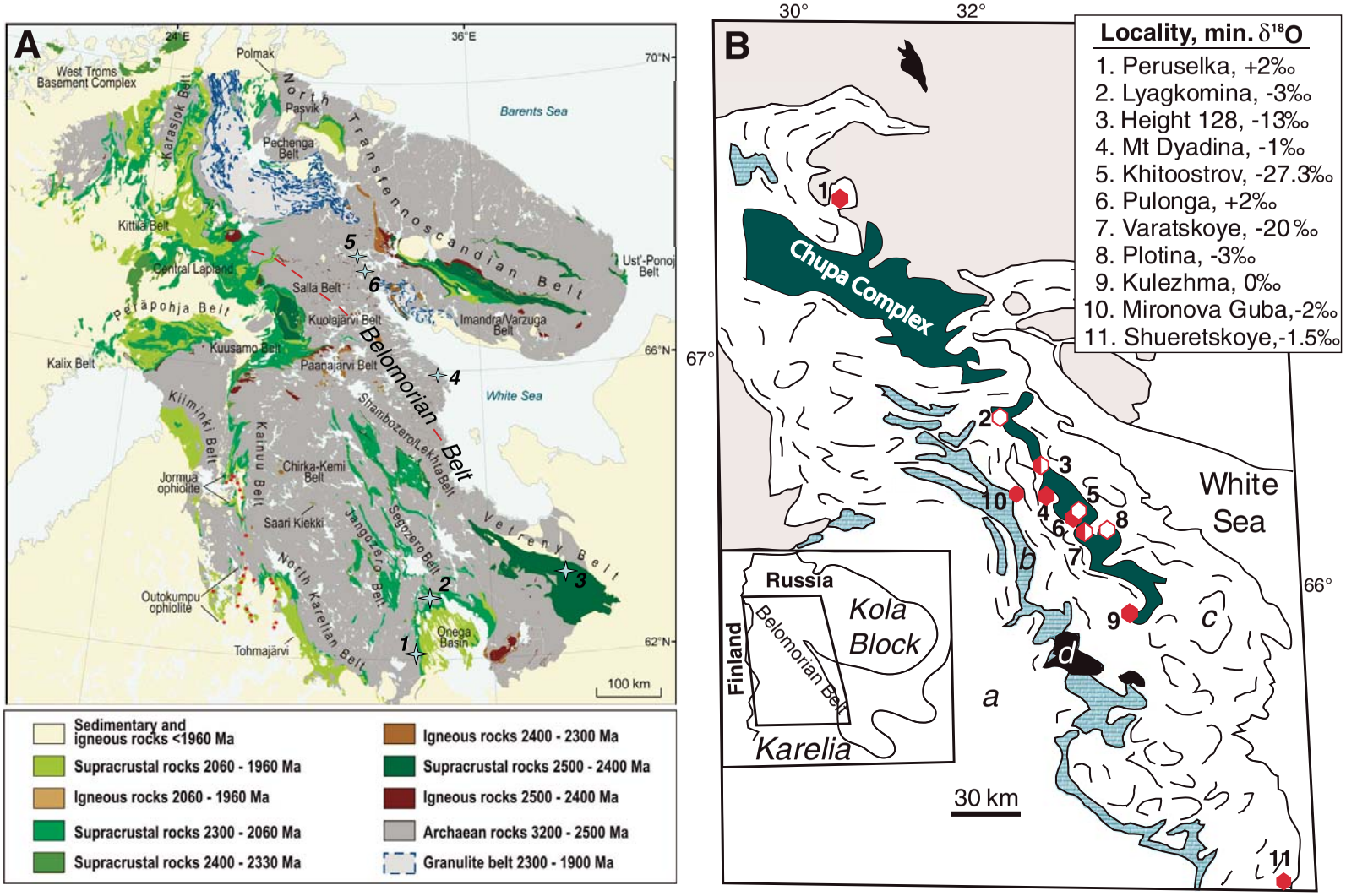

Figure 1 (*Continued on following page*). Geology of Karelia and the Belomorian Belt with study locations. (A) Tectonic and igneous architecture of Kola and Karelia separated by the Belomorian Belt; note the NW-SE–trending rifts of 2.4–2.5 Ga. The degree of metamorphism increases from the Vetreny-Shambozero-Kuolasjarvi Belts (weakly metamorphosed, greenschist), the Belomorian Belt (amphibolitic grade), to eclogite-granultites along the shore of the White Sea (e.g., Miller and Milkevich, 1995; Slabunov et al., 2006). Location of studied ca. 2.5–2.4 Ga supracrustal and volcanic samples of Sumian and Sariolian age, which are described in the text, Table 3, and Table A1 in the Supplemental File (see footnote 2), are shown by stars: supracrustal rocks: 1—Onega Basin, 2—Segozero, 3—Vetreny Belt; eclogites: 4—Gridino, 5—Kuruvara, 6—Salma. The map is adopted and modified after Hanski and Melezhik (2013). (B) Simplified geologic map of the Belomorian Belt with structural elements showing the location of the Paleoproterozoic–Neoarchean Chupa allochthonous nappe and studied localities with ultralow-$\delta^{18}O$ values, spanning 450 km (source map is after Balagansky et al., 1986; Bibikova et al., 2004). Legend: (a) Karelian and Kola Archean blocks; (b) Archean metavolcanic and metasedimentary units; (c) other nappes of the Belomorian Belt; (d) gabbronorite and layered intrusions (2.45–2.4 Ga). Lowest $\delta^{18}O$ values are shown for each locality. Filled symbols indicate $\delta^{18}O$-depleted rocks hosted by 2.4 Ga high-Mg druzitic gabbronorites; open symbols are isotope depletions inside of Chupa gneiss; and half-filled symbols indicate a depletion occurring in both 2.4 Ga metagabbronorites and Chupa gneiss.

Geosphere, published online on 21 February 2014 as doi:10.1130/GES00952.1

Geosphere, published online on 21 February 2014 as doi:10.1130/GES00952.1

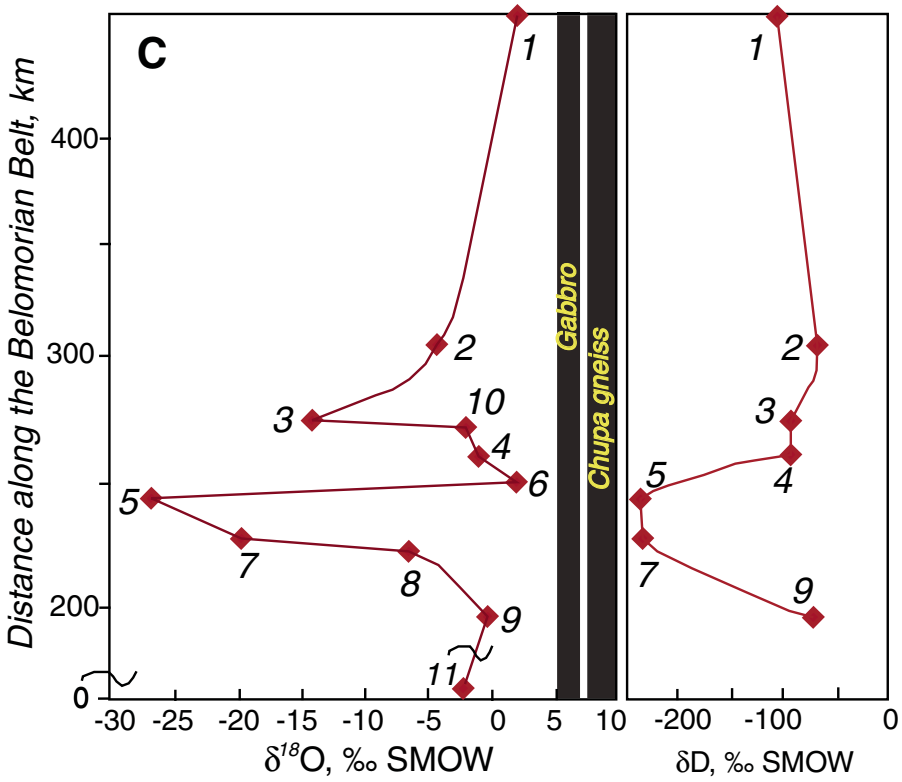

Figure 1 (*Continued*). (C) Distribution of lowest δ^{18}O and δD values along the Belomorian Belt (numbers correspond to localities in Fig. 1B); values are updated after Bindeman and Serebryakov (2011), see Table A1 in the Supplemental File (see footnote 2) for new data.

similar to trends observed around shallow intrusions in modern meteoric-hydrothermal systems (Taylor, 1974). A feature of aluminoferrous Karelian rocks (Fig. 3) is that the maximum level of ^{18}O depletion is also characterized by the highest concentration of Al, insoluble major and trace elements in the paragneisses, most notably in their high-Al/Si, Ti, and Zr concentrations. These features can be explained by residuum enrichment during partial dissolution of silicate minerals in hydrothermal process at large water/rock ratios (Bindeman and Serebryakov, 2011). It is also undoubtedly important to resolve the influence of ca. 1.85–1.89 Ga metamorphic processes, and in particular the effects of synmetamorphic fluid flow, on the protolith of these rocks. Preservation of diverse δ^{18}O protolithic values during and after high-grade metamorphism has been described in other terranes (e.g., Valley and O'Neil, 1984; Fu et al., 2012), but synmetamorphic origin of ultralow δ^{18}O Karelia rocks is advocated by some researchers (e.g., Ustinov et al., 2008). Karelian rocks represent the current world record in the level of ^{18}O depletion. The only known terrestrial oxygen reservoir that could conceivably cause rocks and minerals to attain such low δ^{18}O values is glacial meteoric water (e.g., Bindeman, 2011). We thus envision high-temperature water-rock interaction in a subglacial rift zone where ca. 2.4 Ga and perhaps younger Paleoproterozoic mafic intrusions have caused the depletion in the pre–1.85 Ga metamorphic protoliths. Because Karelia was located at near equatorial latitudes during most of the Paleoproterozoic (Evans and Pisarevsky, 2008), these ultralow-δ^{18}O, high-Al paragneisses were interpreted to represent the first direct evidence for pan-global "Slushball Earth" glaciation (Bindeman et al., 2010). Dating of the intrusions can also serve as a novel method to constrain the individual glaciations, or the total duration of a pan-global freeze. The current geologic and geochronologic data suggest three to four individual glaciations between 2.5 and 2.26 Ga (Young, 2004; Hoffman, 2009; Bekker, 2011; Hoffman, 2013; Rasmussen et al., 2013). Which of the three events caused the appearance of atmospheric oxygen and disappearance of mass independent sulfur-isotope fractionation is a matter of current debate.

Here, we expand our previous isotopic mapping of the Belomorian Belt and present 430 new analyses of individual minerals, mostly garnet, by laser fluorination (Fig. 2; see Table A1 in the Supplemental File[2]). We also report new analyses for the southernmost low-δ^{18}O locality, Shueretskoye (Fig. 1B), which expands the zone of known low-δ^{18}O localities to 450 km across the Belomorian Belt. We also present 216 high-spatial resolution geochronologic and oxygen isotope spot analyses from 11 rock units at six localities, with auxiliary trace-element analyses of zircon. Zircon is unique for these mineral assemblages in that it retains normal-δ^{18}O cores, which survived hydrothermal alteration and subsequent metamorphism. Metamorphic recrystallization during ca. 1.85 Ga Svecofennian metamorphism formed some neoblastic low-δ^{18}O zircons in equilibrium with other metamorphic minerals but mostly triggered the epitaxial crystallization of low-δ^{18}O rims onto normal-δ^{18}O cores. In order to determine the age of depletion, we use the age of the youngest detrital zircon core in the paragneisses to constrain the age of last deposition prior to hydrothermal alteration and metamorphism. We further have determined the ages and δ^{18}O values of zircons in mafic intrusions that are present in the vicinity of the ultralow-δ^{18}O rock halo. In an attempt to constrain hydrothermal alteration in nonmetamorphic equivalents of the gabbronorite

[1]Here and below, "normal-δ^{18}O" rocks are defined as being in the +5.5 to 6.5‰ range characteristic of δ^{18}O values for mantle-derived basic rocks and silicic products of their differentiation; differentiation causes subtle increase of δ^{18}O with increasing SiO_2 ("mantle array" of Bindeman, 2008). Normal-δ^{18}O minerals and fluids are in high-temperature (T) isotopic equilibrium with (and within) these rocks; their δ^{18}O values are different from the bulk rock by small (typically less than 1–2‰ at high T) mineral-specific, temperature-dependent fractionation factors (e.g., Taylor, 1974). Physical weathering and isochemical metamorphism do not change bulk δ^{18}O value of rocks despite changes in modal mineral identity. This paper also refers to high-δ^{18}O gneisses, with values >7.5‰, formed by metamorphism of high-δ^{18}O supracrustal sedimentary protoliths. Low-δ^{18}O rocks (0 to 5.5‰) represent the result of hydrothermal interaction of low-δ^{18}O meteoric water with normal- and high-δ^{18}O rocks and minerals, leading to heterogeneous lowering of δ^{18}O values in rocks. The "ultralow"-δ^{18}O rocks featured in this paper (δ^{18}O <<0‰ standard mean ocean water [SMOW]) are formed by high-T interaction of "ultralow"-δ^{18}O glacial meltwater with rocks.

[2]Supplemental File. Laser fluorination analyses and supplementary tables and figures. If you are viewing the PDF of this paper or reading it offline, please visit http://dx.doi.org/10.1130/GES00952.S1 or the full-text article on www.gsapubs.org to view the supplemental file.

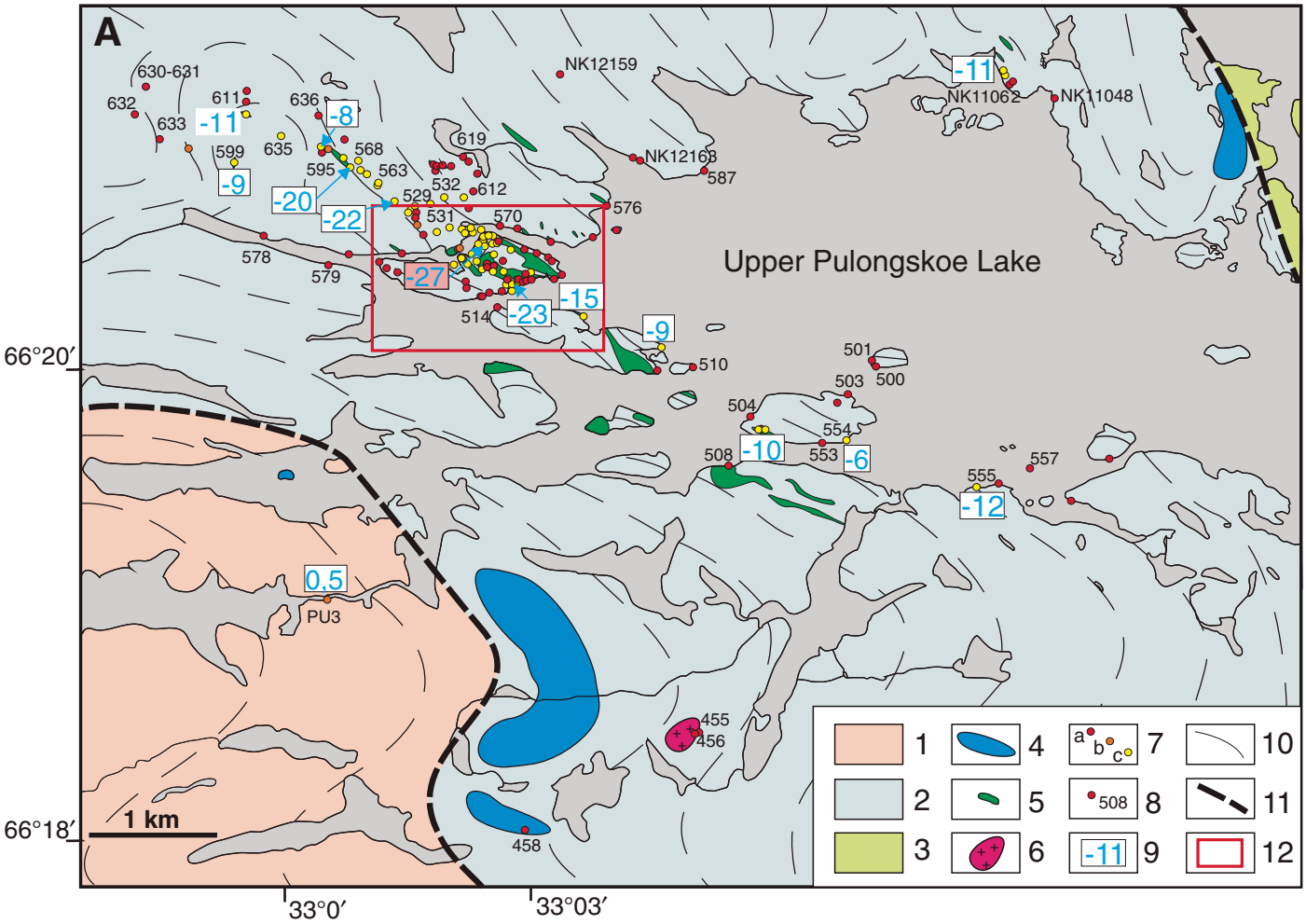

Figure 2 (*Continued on following page*). **Geologic maps with isotopic sampling locations. (A) Geologic map of Upper Pulongskoye Lake area (modified after Bibikova et al., 1994; Myskova et al., 2000, 2003; Serebryakov, 2004, and based on our field mapping). Legend: 1—Kotozero gneiss nappe; 2—Chupa gneiss nappe; 3—Khetolambino gneiss nappe; 4—High-Mg gabbronorites of ca. 2.45 Ga age (druzites); 5—High-Fe gabbro of 2.3 to 2.1 Ga age range; 6—Archean (2.8 Ga) granites; 7—Sampling localities and sample numbers with: (a) normal-$\delta^{18}O$ ($\delta^{18}O$ of garnet >5‰), (b) low $\delta^{18}O$ (0–5‰), (c) ultralow $\delta^{18}O$ (0 to –27‰); 8—sample numbers; 9—minimal values shown at each location; 10—measured metamorphic strikes and orientations; 11—major faults; 12—detailed study area shown on panel (B). (B) Geologic map of Khitostrov locality (source map after Serebryakov, 2004, modified by current fieldwork). Legend: 1—Bi-Gt Chupa gneiss; 2—Ky-Bi-Gt Chupa gneiss (near the contact with Crn rocks; it lacks Qz and has large Ky); 3—Fe-gabbro and gabbro-amphibolite; 4—migmatized Gt-amphibolites; 5—St-Gt-Bi-Ts-Pl-rock with St-Pl pseudomorphs over Ky; 6—Crn-St-Grt-Ged-Prg-Pl-rock with Crn-St-Pl pseudomorphs over Ky (near contacts with 5) and with large idiomorphic crystals of Crn (in central part, with maximum $\delta^{18}O$ depletion); 7—plagioclasites; 8—late pegmatites; 9—faults; 10—strike and dip. Mineral abbreviations used on this figure and throughout the paper, given alphabetically: Amph—amphibole, Ant—antophillite, Bi—biotite, Cam—Ca-amphibole, Chl—chlorite, Crn—corundum, Ged—gedrite amphibole, Gt—garnet, Ky—kyanite, Opx—orthopyroxene, Pl—plagioclase, Prg—pargasitic amphibole, Px—pyroxene, Ru—rutile, Qz—quartz, Ts—Tschermakitic Amphibole, St—staurolite, Zrc—zircon. (C) Isotope contour map of the area around Khitostrov, drawn as a result of isotope mapping and based on earlier data published in Bindeman and Serebryakov (2011); see Table A1 in the Supplemental File (see footnote 2) for newly determined $\delta^{18}O$ values of minerals, rock types, and exact sampling localities. Notice that isotope contour lines show association with a gabbroic intrusion, forming a concentric bulls-eye pattern, which is elongated along the regional fault.**

Geosphere, published online on 21 February 2014 as doi:10.1130/GES00952.1

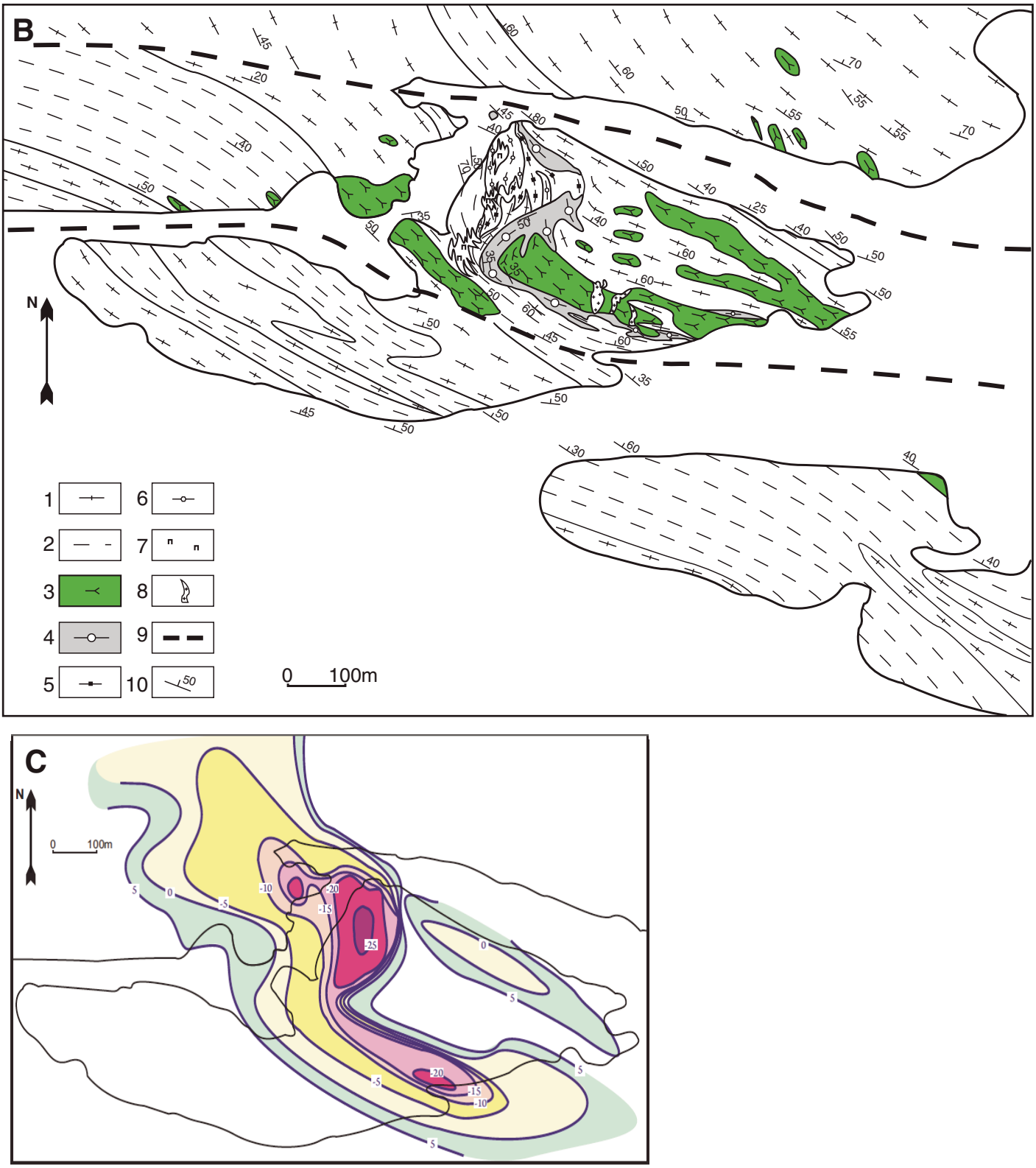

Figure 2 (*Continued*).

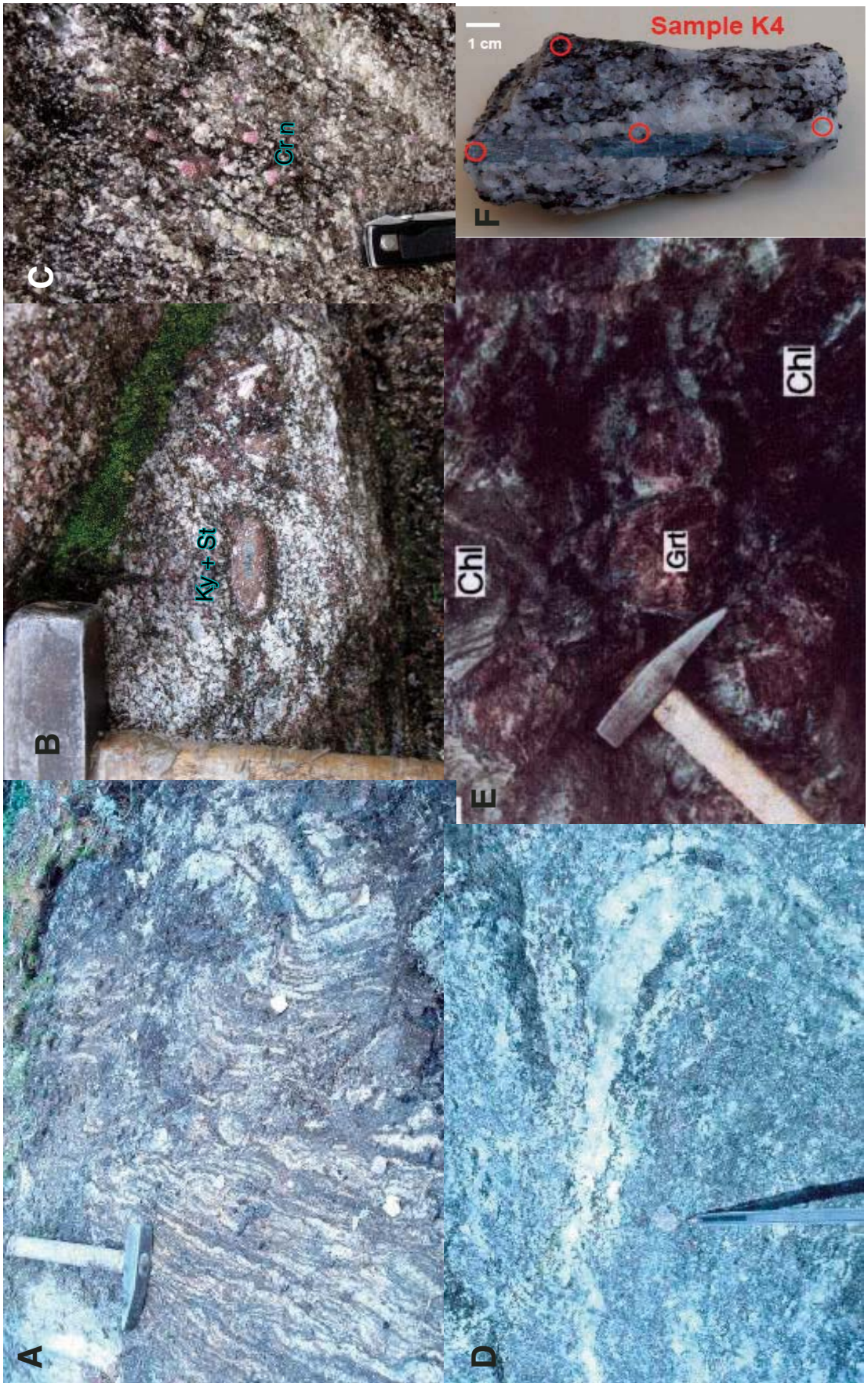

Figure 3. Field relations among different rock types. (A) Chupa gneiss with large garnets. (B) Staurolite-plagioclase pseudomorphs coating large kyanite crystal at Khitostrov. (C) Rock with large corundum crystals. (D) Most $\delta^{18}O$-depleted rock with plagioclasite leucosome and large crystal of corundum; pen is pointing to corundum, Khitostrov locality. (E) Large crystal of almandinic garnet inside of chloritic rock at Mount Dyadina locality. (F) Large crystal of kyanite in desilicified Chupa gneiss, Khitostrov.

and gneiss complex, we investigated Sumian and Sariolian ca. 2.4–2.2 Ga Karelian supracrustal rocks for their $\delta^{18}O$ composition: basaltic pillow rims, amygdaloidal vugs, varves from lacustrine periglacial lakes, as well as Tertiary basalts and their alteration products (vugs) from Antarctica for comparison purposes.

METHODS

Sampling and Laser Fluorination Analyses

For isotopic mapping of the Belomorian Belt, hand specimens were processed in the field to extract 1–2 mg of garnet and other major phases. The separates were then transferred to the University of Oregon Stable Isotope Laboratory. For the majority of mapping samples, a single crystal of garnet was analyzed (Table A1 in the Supplemental File [see footnote 2]). Bulk oxygen isotope analyses of 0.5–2 mg aliquots of garnet and/or mineral separates of plagioclase, ruby corundum, kyanite, biotite, amphibole, zircon, monazite, and rutile were conducted using laser fluorination (e.g., Bindeman, 2008). Samples were heated with a 35W NewWave Research infrared laser in the presence of purified BrF_5 reagent to liberate oxygen. The O_2 gas generated in the laser chamber was purified through a series of cryogenic traps held at liquid nitrogen temperature and a mercury diffusion pump to remove traces of fluorine-bearing waste gases. The oxygen was converted to CO_2 gas in a small, heated platinum-graphite converter, the yields were measured, and then the CO_2 gas was analyzed using a Thermo Scientific MAT 253 mass spectrometer in a dual inlet mode. Four to seven garnet standard aliquots (UOG, $\delta^{18}O$ = 6.52‰ and GMG, $\delta^{18}O$ = 5.75‰) were analyzed together with the unknowns during each of seven analytical sessions. Measurements of unknowns were adjusted to correct for day-to-day variability, and precision of the standards was typically <0.1‰ (1 standard deviation).

Because Karelian samples span the largest yet measured terrestrial range in $\delta^{18}O$, we additionally performed three isotope (16, 17, 18) oxygen isotope measurements including ^{17}O of several Khitostrov samples spanning a 37‰ range in $\delta^{18}O$, by measuring the isotopes in O_2 gas directly without conversion to CO_2, to check for mass independent isotope fractionation. The procedure includes twice collecting the gas on chilled 13 Å molecular sieve to prevent $^{14}NF^+$ (mass/charge = 33) contamination. This interference was monitored by scanning for $^{14}NF_2^+$ (mass/charge = 52), which was below detection, suggesting the absence of contaminants in the O_2 gas.

Ion Microprobe U-Pb Dating, Oxygen Isotope, and Trace-Element Analysis

Zircons were extracted from crushed samples using standard density separation procedures involving heavy liquids and magnetic separation. Extracted zircons were mounted in the center of a round (2.54 cm in diameter) epoxy mount along with standards and polished to expose crystal interiors. The crystals were imaged by backscatter electron (BSE) and cathodoluminescence (CL) methods prior to analysis. Ion microprobe U-Pb dating of zircons (Table 1) was performed at University of California, Los Angeles (UCLA) using the CAMECA IMS 1270 large magnet-radius ion microprobe, applying routine instrumental and calibration procedures based on zircon standard AS3 (Schmitt et al., 2003; Bindeman et al., 2010). A subset of zircons was dated using the Stanford–U.S. Geological Survey (USGS) sensitive high-resolution ion microprobe reverse-geometry (SHRIMP-RG) ion microprobe at Stanford University using a U-Pb dating protocol that is calibrated to zircon standard R33 (419 Ma, Black et al., 2004) and includes trace-element analysis. Sample AB3513 was dated by SHRIMPII in VSEGEI, St. Petersburg, Russia, and used TEMORA (Black et al., 2004) zircon as age standard.

Oxygen isotope analyses of zircons were performed at UCLA using methods described in Trail et al. (2007). After repolishing the mount to level the crystal topography and remove all traces of oxygen implanted during the U-Pb dating analysis, a ~3 nA Cs^+ primary beam at 25 µm spot diameter was targeted directly onto the same crystal domains used for dating. Beam size and repolishing likely resulted in core/rim overlap in some analyses, especially for small zircons such as in sample K5 (Bindeman et al., 2010). Instrumental fractionation was calibrated using bracketing and interspersed analyses of zircon standards mounted together with the unknowns. Standard values were as follows: AS3, $\delta^{18}O$ = 5.31‰ (Trail et al., 2007), KIM5, $\delta^{18}O$ = 5.09‰ (Valley, 2003), and TEMORA, $\delta^{18}O$ = 8.20‰ (Valley, 2003). Instrumental mass fractionation factors (IMFs) varied between ~1 and 3‰, with shifts occurring after exchanging sample mounts, but $\delta^{18}O$ drift was absent for runs of individual mounts. Uncertainties for individual spot analyses (Table 1) are based on the external reproducibility of the standards in each analytical session, and average ~0.2‰. In addition, we analyzed zircon rims by pressing euhedral grains into indium metal along with standards. Because zircon prismatic growth domains are thus laterally extensive perpendicular to the direction of ion beam penetration, the composition of the outermost rims of zircon can thus be analyzed to a depth of ~1 µm. In another experiment, we applied a ~0.5 µm Ga^+ beam to detect oxygen isotope variations in an ~25 µm lateral profile. This technique (a novel method, developed for this work by AKS using the UCLA CAMECA 1270 ion microprobe) used pre-implantation of the analysis area with Cs^+ to enhance secondary ion yields, and simultaneous Faraday cup measurements of $^{16}O^-$ with ion counting of $^{18}O^-$ using a Hamamatsu Mark III electron multiplier. The instrumental fractionation value determined on 91500 zircon was ~–40‰, with a spot-to-spot reproducibility of ~1‰ (1 standard deviation [s.d.]). Analyses of zircons are presented in Table 1.

Analysis of oxygen isotopes within a large corundum crystal from sample K1 (Fig. 4) was conducted with a CAMECA 7fGEO ion microprobe at California Institute of Technology (Caltech). Given the large crystal size (~1–2 cm), synthetic corundum (–6.37‰ SMOW, determined by laser fluorination at the University of Oregon) was mounted around the margins and Instrumental Mass Fractionation (IMF) corrections were applied using standards in close proximity to the unknown. We estimate the overall error associated with these corrections to be ~0.5–1‰ (1 s.d.). The range of observed core-to-rim variability was independently confirmed by laser fluorination analysis (Fig. 4).

Analyses of trace-element concentrations in zircons (Table A4 in the Supplemental File [see footnote 2]) were performed with the Stanford-USGS SHRIMP-RG using a negative O_2 primary beam and a mass resolution of 8000–8500 in order to resolve potential interferences for rare-earth elements. Concentrations were calculated from Zr_2O^+-normalized secondary ion yields relative to those from an in-house concentration standard (MAD, Barth and Wooden, 2010), which was calibrated to zircon standard SL13 (Mattinson et al., 2006) as well as synthetic zircon measured by electron microprobe (Claiborne et al., 2006). Zirconium concentrations in rutiles were measured by laser ablation–inductively coupled plasma mass spectrometry (LA-ICP MS) at ETH-Zurich (Marcus Walle, analyst) and are presented in Figure 5.

RESULTS

Mapping of Isotopic Anomalies

The spatial distribution of the most ^{18}O-depleted rocks at the Khitostrov locality was mapped over four field seasons between 2009 and 2013 and is based on 639 mineral $\delta^{18}O$ analyses (430 new in Table A1 in the Supplemental

TABLE 1. SUMMARY OF U-Pb ($^{207}Pb/^{206}Pb$) ZIRCON AGES AND IN SITU ZIRCON OXYGEN ISOTOPES IN KARELIA SAMPLES

Locality, sample Spot identification	Core and/ or rim	$\delta^{18}O$ (‰)	1 s.d. (‰) external	$^{207}Pb/^{206}Pb$ age (Ma)	± age (Ma)	Radiogenic (%)	Th/U	U (ppm)
Varatskoye								
Sample AB_3513, corundum-bearing rock over gneiss for V41: Cam: –19.08‰; Grt: –18.76‰; D/H Amph = –233‰								
Mount M833, dated in St. Petersburg in 2009, O isotopes at UCLA April 2011								
AB3513_3.1	C	6.7	0.15	2562	9.4	100.0	0.14	593
AB3513_3.1.2	R	–18.4	0.15	1867	110	100.3	6.42	13
AB3513_3.2.1	C	6.2	0.15	2558	7.1	99.5	0.10	846
AB_3513_3.2.2	R	–19.5	0.15					
AB_3513_3.3.1	C	7.9	0.15	2537	10	99.6	0.22	385
AB_3513_3.3.2	R	–17.8	0.15	1897	72	99.8	4.32	20
AB_3513_3.4.1	C	4.0	0.15	2807	6.2	99.8	0.09	921
AB_3513_3.4.2	R	–18.7	0.15	1888	44	100.0	2.85	27
AB_3513_3.5.1	R	–19.3	0.15	1810	110	100.1	4.16	20
AB_3513_3.6.1	R	–19.5	0.15	1921	86	99.9	6.20	13
AB_3513_1.1.1	C	4.8	0.15	2835	36	100.0	0.30	273
AB_3513_1.1.2	R	–18.7	0.15					
AB_3513_1.3.1	C	5.8	0.15	2613	69	99.9	1.42	55
AB_3513_1.2.2	C	6.5	0.15	2831	34	100.0	0.39	199
AB_3513_1.2.1	C	6.4	0.15	2745	37	99.7	0.20	356
AB_3513_1.4.1	R	–19.0	0.15		47			
AB_3513_1.5.1	R	–18.6	0.15	1912	61	99.8	3.62	16
AB_3513_1.6.1	C	4.8	0.15					
AB_3513_1.6.2	R	–19.5	0.15	1996	100	99.9	0.20	401
AB_3513_1.3.3	R	–18.7	0.15					
Sample B51, metamorphosed ca. 2.45 Ga mafic intrusion: Plag: –14.07‰, Cam: –15.92‰; D/H Amph = –227‰								
Mount KAR-1, U-Pb in Stanford, 03 March 2011, repolishing, and O isotopes in April 2011 at UCLA								
B51-1.1	R	–17.38	0.35	1851	17	100.1	0.09	89
B51-1.2	C	–17.98	0.35	1873	14	100.0	0.18	117
B51-2.1	R	–17.66	0.35	1843	12	100.4	0.16	153
B51-2.2	C	–18.49	0.35	1885	13	99.9	0.15	122
B51-3.1	R	–18.05	0.35	1877	12	99.7	0.20	169
B51-3.2	R	–18.00	0.35	1837	11	100.0	0.16	226
B51-4.1	R	–18.42	0.35	1874	13	100.0	0.10	159
B51-4.2	C	–18.29	0.35	1886	13	99.8	0.09	136
B51-5.1	C			1889	15	99.9	0.22	177
B51-6.1	C	–18.39	0.35	1901	12	99.9	0.19	154
B51-7.1	R	–17.24	0.35	1851	13	100.1	0.15	127
B51-7.2	C	–17.94	0.35	1893	15	100.3	0.20	140
B51-8.1	R			1845	14	100.4	0.12	129
B51-8.2	R	–17.94	0.35	1875	19	99.7	0.16	143
B51-9.1	R	–17.26	0.35	1885	14	99.9	0.17	125
B51-10.1	C	–17.90	0.35	1879	17	99.7	0.14	95
B51-10.2	R	–17.53	0.35	1850	15	100.5	0.16	141
B51-11.1	R	–17.66	0.35	1855	14	100.0	0.15	142
B51-12.1	R	–17.94	0.35	1877	13	99.6	0.13	157
B51-13.1	R	–18.22	0.35	1906	14	99.4	0.19	138
B51-14.1	R	–17.67	0.35	1878	12	99.9	0.16	158
B51-15.1	C	–18.51	0.35	1868	11	100.0	0.19	187
Kulezhma								
Sample KY21, metamorphosed ca. 2.1 Ga mafic intrusion: Grt: 3.06‰								
Mount Picabo, U-Pb dating in UCLA, 19 Jan 2012								
KY21_@13	R			1842	49	99.3	0.14	17
KY21_@9	R			1868	5	99.9	0.08	400
KY21_@10	C			2025	4	99.7	0.23	2234
KY21_@15	C			2029	11	98.2	0.50	1917
KY21_@6	C			2051	6	99.8	0.23	997
KY21_@5	C			2057	3	100.0	0.19	1273
KY21_@12r	R			2058	9	99.6	0.65	1628
KY21_@2	C			2059	5	99.9	0.91	2422
KY21_@11	C			2065	4	100.0	0.49	861
KY21_@14	C			2066	5	100.0	1.01	1498
KY21_@8c	C			2068	3	100.0	0.84	949
KY21_@8r	R			2068	6	100.0	0.83	1076
KY21_@7	C			2076	10	99.8	0.27	864
KY21_@1	C			2089	7	99.8	0.25	557
KY21_@4	C			2101	7	99.9	0.54	2365
KY21_@3	C			2117	3	100.0	0.69	2957
KY21_@12c	C			2122	7	100.0	1.86	425
Height 128 m								
Sample KV10, metamorphosed kyanite-bearing gneiss: Plag: –4.3‰; Cam: –7.73‰; Grt: –9.05‰								
Mount L1, O isotopes in UCLA 24 August 2010, dating at UCLA, January 2012								
KV10_kw1_c	C	8.6	0.09	2588	11	99.9	0.05	217
KV10_1_2	C	4.0	0.09	2771	6	99.8	0.81	239
KV10_kw2_c	C	4.5	0.12	2660	3	100.0	0.05	381
KV10_kw3_c	C	8.6	0.14					
KV10_kw3_r	C	6.5	0.12					
KV10_2_1	R	–8.2	0.07	1848	100	99.9	0.00	5.94
KV10_2_2	C/R	1.0	0.11	2681	14	99.5	0.38	128

(*Continued*)

Geosphere, published online on 21 February 2014 as doi:10.1130/GES00952.1

TABLE 1. SUMMARY OF U-Pb ($^{207}Pb/^{206}Pb$) ZIRCON AGES AND IN SITU ZIRCON OXYGEN ISOTOPES IN KARELIA SAMPLES (*Continued*)

Locality, sample Spot identification	Core and/ or rim	$\delta^{18}O$ (‰)	1 s.d. (‰) external	$^{207}Pb/^{206}Pb$ age (Ma)	± age (Ma)	Radiogenic (%)	Th/U	U (ppm)
KV10_kw4_c	C	8.6	0.09	2615	10	99.9	0.10	351
KV10_3_21	C	7.8	0.09	2602	7	100.0	0.07	414
KV10_kw5_c	C	8.0	0.08					
KV10_4_2	C	8.0	0.11	2570	3	100.0	0.19	685
KV10_5_2	C	4.5	0.06	2673	14	99.7	0.80	46
KV10_5_3	C/R	3.8	0.08					
KV10_kw6_c	C	7.9	0.08					
KV10_kw6_r	R	–6.2	0.11					
KV10_kw7_c	C	6.1	0.08					
KV10_kw7_r	R	–9.1	0.11					
KV10_kw8_c	C	8.0	0.11					
KV10_kw8_r	R	–4.4	0.07					
KV10_kw9_c	C	5.4	0.08					
KV10_kw9_r	R	0.8	0.07					
KV10_kw10_c	C	5.3	0.09					
Lyagkomina								
Sample L1, metamorphosed corundum-bearing gneiss: Cam: –3.05‰; Grt: –4.8‰								
Mount L1, O isotopes in UCLA 24 August 2010, dating at Stanford, then at UCLA, January 2012								
L1_15_1	C	4.0	0.08	2640	17	99.8	0.01	34
L1_15_2	C	7.1	0.10	2736	4	99.8	0.44	392
L1_14_1	C	2.1	0.11	2654	14	99.8	0.02	52
L1_13_1	R	–4.2	0.09					
L1_13_2	C	7.1	0.11	2742	5	99.6	0.53	1065
L1_12_1	C/R	2.4	0.09	2465	77	99.6	0.21	9.4
L1_12_2	C	5.0	0.10	2602	5	99.9	0.38	532
L1_10_1	C	6.5	0.07	2715	3	99.3	0.24	890
L1_9_1	C	7.0	0.11	2707	6	99.6	0.39	230
L1_7_1	C	7.8	0.06	2715	5	99.4	0.50	288
L1_11_1	R	–3.1	0.10			124.0	0.02	3.3
L1_11_2	C	7.2	0.12	2695	6	99.2	0.37	330
L1_6_1	C	6.9	0.09	2707	13	99.3	0.27	127
L1_8_1	C/R	4.0	0.09	2503	49	99.8	0.11	11
L1_8_2	C/R	3.2	0.10	2499	9	99.9	0.24	179
L1_5_1	C	7.2	0.11	2743	9	100.1	0.39	215
L1_4_1	C	6.7	0.09	2747	2	99.9	0.22	648
L1_4_1c	C			2707	3	99.7	0.36	983
L1_3_1	C	7.7	0.10	2754	7	99.9	0.66	217
L1_2_1	R	6.2	0.14	2606	7	99.4	0.17	769
L1_1_1	R	7.2	0.09	2646	5	100.0	0.19	423
L1_1_1c	C			2761	8	99.8	0.45	140
Dyadina Gora								
Sample DG150, metamorphosed ca. 2.45 Ga mafic intrusion: Plag: 7.30‰, Cpx: 4.98‰								
Mount KAR-2, dating in UCLA, 21 May 2011								
DG150@11	C			2393	11	99.8	0.72	319
DG150@4	C			2057	17	99.8	0.18	725
DG150@1	C			1815	16	99.6	0.16	462
DG150@10	C			1878	13	99.9	0.12	616
DG150@12	C			1859	10	99.8	0.14	532
DG150@13	C			1870	10	99.6	0.18	519
DG150@15	C			1810	12	99.6	0.12	923
DG150@21	C			1851	13	99.8	0.06	903
DG150@3	C			1863	11	99.9	0.06	889
DG150@5	C			1867	20	99.8	0.09	263
DG150@6	C			1810	29	99.7	0.12	369
DG150@7	C			1861	10	99.8	0.02	415
DG150@8	C			1822	10	99.7	0.11	368
DG150@9	C			1835	19	99.8	0.08	419
Mount KAR-1, U-Pb in Stanford, March 2011								
DG150-1.1	C			1856	10	99.4	0.18	211
DG150-2.1	C			1852	8	99.8	0.06	303
DG150-3.1	C			1885	13		0.36	148
DG150-4.1	C			1893	11	99.2	0.21	191
DG150-5.1	C			1864	21	99.7	0.12	185
DG150-6.1	C			1867	10	99.9	0.09	243
DG150-7.1	C			1876	10	99.5	0.09	345
DG150-8.1	C			1882	8	99.5	0.11	318
Khitostrov								
Sample X245, metamorphosed high-Fe (ca. 2.1–2.3 Ga) mafic intrusion: Plag: 6.48‰, Cam: 4.96‰								
Mount KAR-1, U-Pb in Stanford, March 2011								
X245-2.1	C			2228	7	99.6	2.41	276
X245-1.1	C			1864	16	99.9	0.86	1384
X245-3.1	C			1873	5	100.4	1.93	1262
X245-4.1	C			1878	6	99.9	1.07	1196
X245-5.1	C					100.8	11.72	1141
X245-6.1	C			1952	7	99.9	2.80	1104
X245-7.1	C			1885	5	99.9	1.61	776
X245-8.1	C			1884	6	100.1	1.18	1252

(*Continued*)

TABLE 1. SUMMARY OF U-Pb ($^{207}Pb/^{206}Pb$) ZIRCON AGES AND IN SITU ZIRCON OXYGEN ISOTOPES IN KARELIA SAMPLES (*Continued*)

Locality, sample Spot identification	Core and/ or rim	$\delta^{18}O$ (‰)	1 s.d. (‰) external	$^{207}Pb/^{206}Pb$ age (Ma)	± age (Ma)	Radiogenic (%)	Th/U	U (ppm)
Mount KAR-2, dating in UCLA, 21 May 2011								
X245@1	C			1813	9	99.2	0.42	1036
X245@10	C			1821	21	99.0	0.33	391
X245@11	C			1837	17	99.6	2.25	648
X245@12	C			1804	7	99.4	0.48	1826
X245@14	C			1853	6	99.7	3.31	2333
X245@16	C			1843	12	99.5	0.44	532
X245@18	C			1854	8	99.6	0.45	670
X245@2	C			1812	11	99.3	0.58	1197
X245@4	C			1827	31	99.4	0.41	500
X245@5	C			1892	24	99.4	0.26	122
X245@6	C			1835	13	99.1	0.45	463
X245@8	C			1816	11	99.2	0.68	797
X245@9	C			1836	20	99.2	0.30	231
Sample X451, metamorphosed ca. 2.1–2.3 Ga mafic intrusion Qz: –3.46‰; Cam: –7.32‰								
Mount KAR-2, dating in UCLA, 21 May 2011								
X451@2	C			1988	73	99.2	0.34	21
X451@6	C			1854	45	99.6	0.24	47
Sample X588, metamorphosed high-Fe (ca. 2.1–2.3Ga) mafic intrusion Plag: 5.74‰								
Mount X588, dating in UCLA, 25 October 2013								
X588_z@7	C			1883	14	99.5	0.49	373
X588_z@8	C			1872	27	99.8	0.14	61
X588_z@20	C			1913	18	100.0	0.03	73
X588_z@9	C			1866	34	99.3	0.45	59
X588_z@1	C			1879	6	99.9	1.04	1416
X588_z@2	C			2096	20	99.3	13.20	346
X588_z@4	C			1859	10	99.6	0.37	832
X588_z@3	C			1852	5	99.9	0.40	1769
X588_z@6	C			1836	20	99.7	0.50	123
X588_z@12	C			1818	8	99.5	0.44	948
Sample X424, corundum-bearing rock, the lowest in $\delta^{18}O$: Plag: –23.49‰; Cam: –25.48‰; Grt: –26.54‰								
UCLA, April 2011, indium mount, lightly polished zircon rims in an attempt to find lowest $\delta^{18}O$ zircons								
X424@1	R	1.04	0.26					
X424@2	R	–15.46	0.26					
X424@3	R	–27.17	0.26					
X424@4	R	4.61	0.26					
X424@5	R	–6.57	0.26					
X424@6	R	–3.79	0.26					
X424@7	R	–26.83	0.26					
X424@8	R	–25.69	0.26					
X424@9	R	–19.64	0.26					
X424@10	R	7.19	0.26					
X424@11	R	3.98	0.26					
X424@12	R	1.89	0.26					
X424@13	R	5.16	0.26					
X424@14	R	7.08	0.26					
X424@15	R	2.96	0.26					
X424@16	R	0.28	0.26					
X424@17	R	2.45	0.26					
Hole5@1	R	–26.21	0.26					
Hole5@2	R	–5.83	0.26					
Hole5@3	R	–12.50	0.26					
Hole5@4	R	–27.30	0.26					
Hole5@5	R	–8.95	0.26					
Hole5@6	R	–25.45	0.26					
Hole5@7	R	–24.66	0.26					
Hole5@8	R	–26.83	0.26					
Hole5@9	R	–20.30	0.26					
Hole5@10	R	–25.75	0.26					
K5@1	R	5.52	0.26					
K5@2	R	1.75	0.26					
K5@3	R	6.94	0.26					
Sample K5, corundum-bearing rock: Plag: –20.05‰; Grt: –23.23‰; Cam: –22.88‰; rutile: –27.9‰; bulk Zrc: –15‰, –17.97‰, –19.85‰								
Mount KAR-1, U-Pb in Stanford, 03 March 2011, dating, repolishing, and O isotopes in April 2011 at UCLA								
K5-3.1	C			2880	14	99.6	0.18	231
K5-2.1a	C			2764	10	99.7	0.35	145
K5-5.1	C			2950	4	100.2	0.50	546
K5-5.2	R	–25.50	0.35	1886	7	100.2	0.03	368
K5-6.1	C			2846	20	100.2	0.27	366
K5-6.2	R			2576	10	99.9	0.02	543
K5-7.1	C	6.18	0.35	2802	3	100.3	0.31	1196
K5-8.1	C			2646	10	100.7	0.04	772
K5-9.1	C	2.72	0.35	2543	48	99.8	0.01	1399
K5-10.1	R	6.35	0.35	2590	15	99.8	0.04	241
K5-10.2	C	6.75	0.35	2783	4	99.5	0.90	536
K5-11.1	C			2975	34	100.1	0.42	64
K5-4.1	R			2124	12	99.8	0.02	174
K5-4.2	C			2619	3	100.3	0.01	1469

(*Continued*)

Geosphere, published online on 21 February 2014 as doi:10.1130/GES00952.1

TABLE 1. SUMMARY OF U-Pb ($^{207}Pb/^{206}Pb$) ZIRCON AGES AND IN SITU ZIRCON OXYGEN ISOTOPES IN KARELIA SAMPLES (*Continued*)

Locality, sample Spot identification	Core and/ or rim	$\delta^{18}O$ (‰)	1 s.d. (‰) external	$^{207}Pb/^{206}Pb$ age (Ma)	± age (Ma)	Radiogenic (%)	Th/U	U (ppm)
Mount Karelia-1, dating and O isotopes in UCLA, 27 July 2009, published in Bindeman et al. (2010)								
K5_z1@1	R	–24.8	0.37	1824	16	99.6	0.027	470
K5_z1@2	C	–25.1	0.37	1846	16	99.7	0.013	380
K5_z1@3	C	–26.2	0.37	1836	16	99.4	0.026	390
K5_z10@1	R	3.0	0.37	2461	10	99.6	0.034	920
K5_z10@2	C	7.3	0.37	2648	5	99.9	0.0055	1350
K5_z11@1	C	6.4	0.37	2621	6	99.7	0.006	940
K5_z11@2	C	7.8	0.37	2637	7	99.7	0.005	1050
K5_z12@1	C	–26.1	0.37	2065	18	99.4	0.019	460
K5_z12@2	R	–16.9	0.37	1870	27	98.6	0.047	410
K5_z13@1	C	4.9	0.37	2556	8	99.7	0.0056	900
K5_z14@1	R	3.3	0.37	1827	18	99.4	0.142	530
K5_z15@1	C	5.2	0.37	2355	12	99.6	0.039	550
K5_z2@1	C	7.1	0.37	2705	12	99.8	0.016	660
K5_z2@2	R	5.4	0.37	2554	6	99.8	0.015	670
K5_z3@1	R	7.1	0.37	2592	7	99.8	0.0053	850
K5_z3@2	C	5.8	0.37	2583	8	99.8	0.017	480
K5_z3@3	R	5.8	0.37	2676	4	99.9	0.052	1580
K5_z4@1	R	1.7	0.37	1843	23	99.0	0.017	340
K5_z4@2	R	–2.9	0.37	2695	6	99.9	0.155	1100
K5_z4@3	C	4.9	0.37	2556	6	99.6	0.019	1040
K5_z5@1	C	5.1	0.37	2556	9	99.7	0.057	780
K5_z5@2	R	7.0	0.37	2506	30	99.0	0.088	630
K5_z6@1	R	6.6	0.37	2641	4	99.6	0.024	1060
K5_z6@2	C	4.6	0.37	2641	6	99.6	0.019	900
K5_z6@3	R	3.7	0.37	2636	9	99.8	0.0094	1110
K5_z7@1	R	–24.1	0.37	1831	15	99.6	0.011	450
K5_z7@2	C	–23.9	0.37	1813	12	99.5	0.008	460
K5_z7@3	R	–24.4	0.37	1843	19	99.5	0.017	460
K5_z8@1	C	6.1	0.37	2557	11	99.8	0.0057	630
K5_z8@2	R	6.5	0.37	2507	14	99.7	0.007	510
K5_z9@1	R	4.7	0.37	2613	6	99.7	0.088	730
K5_z9@2	R	5.7	0.37	2645	14	99.8	0.077	1010
K5_z9@3	C	6.3	0.37	2648	6	99.8	0.071	970

Note: $\delta^{18}O$ and δD values shown to the right of sample description are for major minerals analyzed by laser fluorination and thermal conversion elemental analysis. Where both ages and oxygen-isotope values are listed, they were performed in overlapping spot after repolishing. See Figure 6 for cathodoluminescence images of selected zircon crystals. Abbreviations: C—core; Cam—Ca-Amphibole; Cpx—clinopyroxene; D/H Amph—amphibole; Grt—garnet; O—oxygen; Plag—plagioclase; Qz—quartz; R—rim; UCLA—University of California, Los Angeles; Zrc—zircon.

File [see footnote 2] and 209 analyses published in Bindeman and Serebryakov, 2011) that form the basis for an isotope contour map (Fig. 2C). In order to determine rock $\delta^{18}O$ values, we relied on garnet because it (1) is present in nearly all of these rocks and is an alteration-resistant mineral with a high closure temperature; (2) is chemically and isotopically inert under retrograde metamorphism, and thus best suited to record peak-metamorphic and protolithic compositions; (3) has a comparatively simple stoichiometry with little (~0.2‰) variation in the oxygen isotope fractionation factor α among common types of garnet (Kohn and Valley, 1998); and (4) serves as a good proxy for the whole-rock oxygen isotope composition (with calculated $1000\ln\alpha_{WR\text{-}Grt}$ = 0‰ and +0.5‰ for mafic and silicic Karelian lithologies, respectively; Bindeman and Serebryakov, 2011).

The new data suggest that the extent of the Khitostrov isotope anomaly is much larger than first described (Fig. 2A). Our current estimates indicate that the isotopic depletion zone now covers a >6 × 2 km area. Most ^{18}O depletions of Khitostrov and the area inside and beyond Upper Pulongskoye Lake trace the elongated high-Fe mafic body but also extend to a wider area around it. Significant (–7 to –10‰) ^{18}O depletion also characterizes rather ordinary looking gneiss and amphibolite without or with very limited desilication (Table A1 in the Supplemental File [see footnote 2]). Zones of maximal ^{18}O depletion are correlated in the field with desilication trends leading to disappearance of quartz and enrichment in kyanite and corundum (e.g., Figs. 3 and 4), and these trends are used to identify and target low-$\delta^{18}O$ areas in the field. Based on our present investigations, we suspect that expanding isotope mapping may require random sampling of ordinary looking gneisses and amphibolites, which lack visible evidence of desilication.

The second-lowest values of $\delta^{18}O$ and δD ever documented (–20‰ and –232‰, respectively) were identified at Varatskoye, ~20 km south of Khitostrov (Fig. 1). There as well, the isotopically anomalous rocks are associated with high-Mg amphibolites, gneisses, and a contact between gneiss and amphibolite contacts, and are accompanied by desilication leading to the enrichment in Al, Ti, and other aqueous-fluid insoluble trace elements. For Varatskoye and other localities, we previously presented isotope profiles (Bindeman and Serebryakov, 2011).

Here we also report low-$\delta^{18}O$ values for Shueretskoye locality (Table A1 in the Supplemental File [see footnote 2], samples SH-) measured in four samples with garnets (up to 10 cm) inside of amphibolites of the southernmost Belomorian Belt, earlier described by Glebovitsky and Bushmin (1983). The Shueretskoye garnet deposit is located 150 km to the southeast along the Belomorian Belt (Fig. 1B). The discovery of low-$\delta^{18}O$ values there expands the zone of known $\delta^{18}O$ depletion of Karelia to 450 km. We also report $\delta^{18}O$ analyses of eclogites of the Belomorian Belt (e.g., Shipansky et al., 2012), which represent higher-metamorphic grade, devolatilized equivalents of gneisses and gabbros of the Belomorian Belt (Table A1 in the Supplemental File [see footnote 2]).

Isotope Diversity and Zoning of Minerals

Individual minerals from single hand specimens from the Khitostrov locality are heterogeneous and zoned in $\delta^{18}O$ by 1–2.5‰, and were interpreted to be caused by cm-scale oxygen

Geosphere, published online on 21 February 2014 as doi:10.1130/GES00952.1

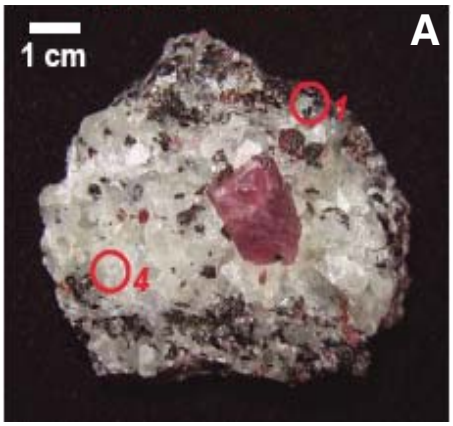

isotope heterogeneity in the protolith, which is typical for modern hydrothermal systems (Bindeman et al., 2010). However, isotope mapping at the outcrop scale also revealed that some isotope diversity is synmetamorphic, related to fluid activity of variable $\delta^{18}O$ (but generally ultralow $\delta^{18}O$ with values of ~–27 to –10‰) isotopic composition (Bindeman and Serebryakov, 2011). In particular, this diversity is observed on the contact of plagioclase-rich leucosomes (called plagioclasites) containing large corundum crystals (e.g., Figs. 3D and 4 and Table A2 in the Supplemental File [see footnote 2]). These plagioclasites are thought to have formed under the presence of synmetamorphic fluids and be metasomatic in origin (e.g., Serebryakov and Aristov, 2004; Serebryakov and Rusinov, 2004). We analyzed an individual large crystal of corundum extracted from the contact zone between melanosome and leucosome in the paragneiss using an ion microprobe, and it shows isotopic zonation with a low-$\delta^{18}O$ core (–24‰), and heavier $\delta^{18}O$ values closer to the rim (–21 to –22‰), next to the plagioclase leucosome (Fig. 4). Serebryakov (2004) and several other researchers consider leucosome to be metasomatic in origin rather than the result of a true partial melting. We performed Zr-in-rutile thermometry on rocks in the corundum-bearing assemblages (Fig. 5), and the temperatures range from ~765 °C for rutiles enclosed in corundum to 720 °C for rutiles in the matrix, in agreement with upper to mid-amphibolite–facies metamorphism in these samples, and above wet solidus temperature for these rocks.

We performed melting-crystallization simulations with the MELTS (Ghiorso and Sack, 1995) program using high-Al lithologies as the protolith and 6 kbar pressure and 3–6 wt% water (Table A3 in the Supplemental File [see footnote 2]). Low degree, 15%–25%, partial melts have 12–20 wt% water and a general composition of plagioclasite, suggesting that hydrous partial melting of high-Al lithologies can generate a plagioclase-rich (up to 90%) "metasomatic" leucosome with corundum (Fig. 3D and Table A2 in the Supplemental File [see footnote 2]). Moreover, water and temperature variations in the

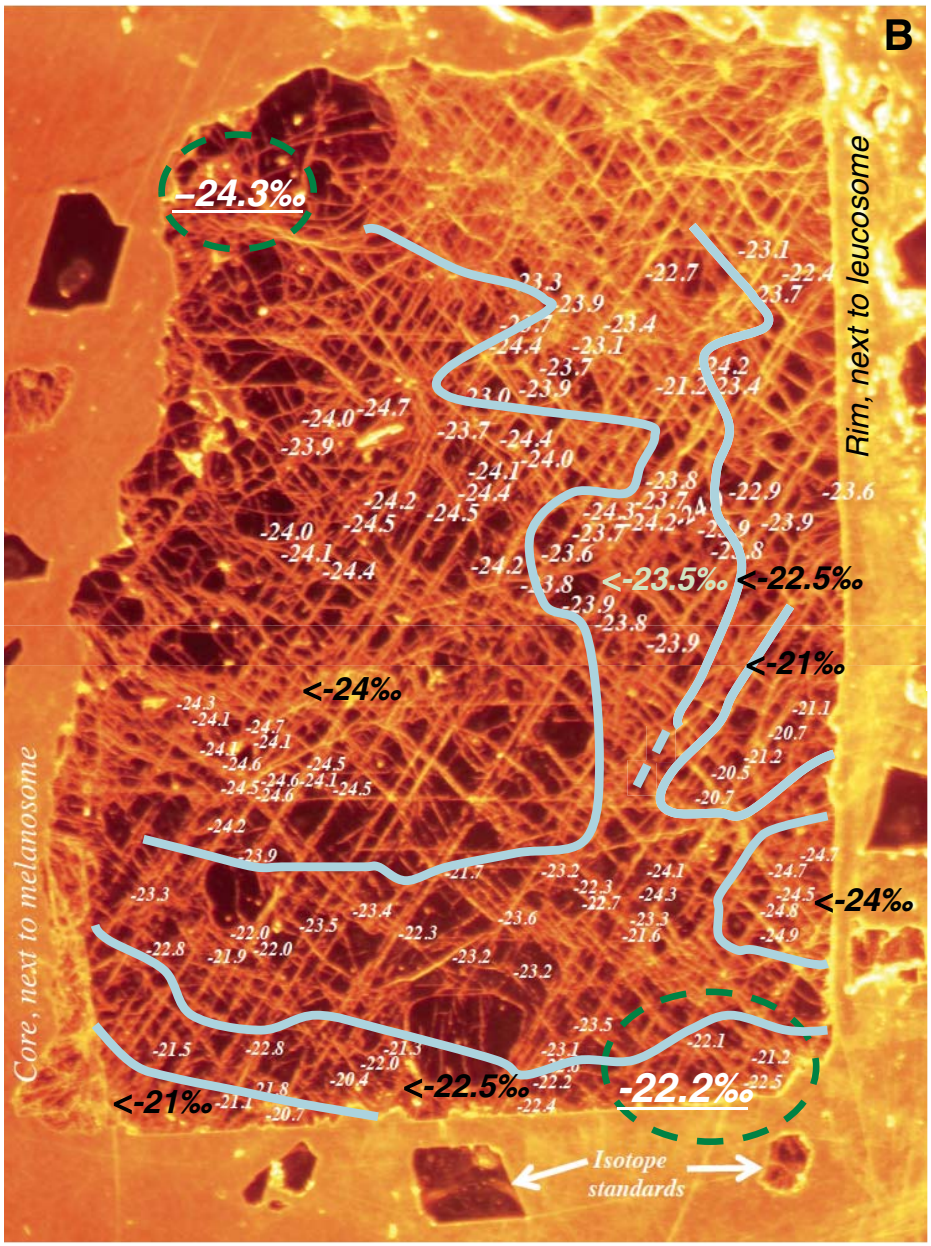

Figure 4. Ion microprobe investigation across a large corundum crystal (#K1-5) in sample K1 of Khitostrov with analyzed labeled crystal clusters 1 and 4 (Bindeman et al., 2010). (A) Original crystal showing corundum growth on the boundary of melanosome and leucosome (plagioclase dominated); (B) oxygen isotope distribution measured by ion microprobe. Notice the overall zoning pattern from ultralow-$\delta^{18}O$ core (<–24‰) attached to melanosome, ranging to higher $\delta^{18}O$ rims with –21 to –22‰ attached to plagioclase-dominated leucosome. This general trend is confirmed by two laser fluorination analyses (underlined numbers, shown by dashed circles). The crystal is 1 cm × 2 cm and has inclusions of other minerals as identified by the electron microprobe: garnet, rutile, ilmenite, zircon, and biotite. Cleavage cracks are filled with AlOOH compound with higher $\delta^{18}O$ values of >–8‰, likely derived from very late stage retrogressive hydration of the corundum crystal.

Geosphere, published online on 21 February 2014 as doi:10.1130/GES00952.1

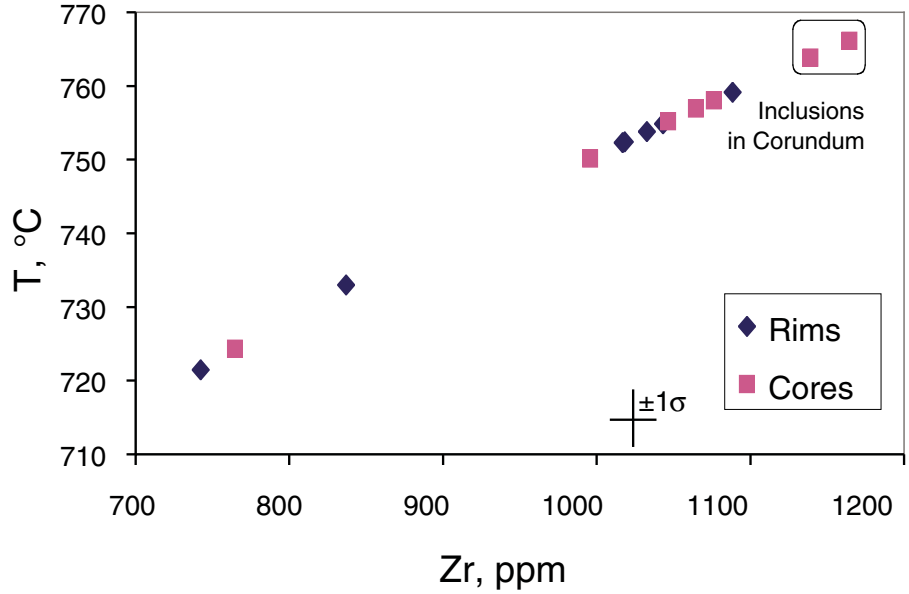

Figure 5. Zirconium in rutile thermometry (Ferry and Watson, 2007) of sample K1 (Fig. 4) based on inductively coupled plasma–mass spectrometry concentration measurements of rutile inclusions in corundum, and in the groundmass (cores and rims). Lower concentrations are interpreted to indicate retrogressive diffusive Zr loss (e.g., Blackburn et al., 2012), but inclusions reflect peak metamorphic conditions, consistent with upper amphibolitic metamorphic grade.

near-solidus hydrous melting process can generate a wide range of plagioclasite and quartz-muscovite plagioclasite compositions. These are evident in crosscutting, late-stage metasomatic overprinting of preexisting lithologies and are higher in $\delta^{18}O$ than the rocks they cut through (see Fig. 3; Serebryakov, 2004; Bindeman and Serebryakov, 2011). The increase in $\delta^{18}O$ is then simply explained by involving normal $\delta^{18}O$ fluids drawn into the zones of partial melting from outside the low-$\delta^{18}O$ zones during metamorphism. This water-rich partial melt (rather than a water-dominated fluid) is also capable of concentrating REE-bearing phosphates (monazite and xenotime), which impregnate zircon rims (see below) and whole-rock assemblages with high light rare-earth element (LREE) concentrations (see below; also Terekhov, 2007).

Triple Oxygen Isotope Analysis of Ultradepleted-$\delta^{18}O$ Rocks

The Belomorian Belt comprises rocks with the largest known terrestrial range in $\delta^{18}O$ values. These rocks range from +9 to 10‰ in the starting Chupa gneiss to –27.3‰ in corundum-bearing rocks from Khitostrov, for which the Chupa gneiss was the protolith. The triple oxygen isotope analysis was conducted to check for the mass independent, photolytic, or extraterrestrial origin of the ultralow-$\delta^{18}O$ rocks (e.g., oxygen having meteoritic or cometary origin with excesses or depletions in ^{17}O; Boss, 2011). We have determined $\delta^{17}O = {}^{17}O/{}^{16}O - 0.5X \times {}^{18}O/{}^{16}O$ at a precision on X <0.01–0.02‰ (Fig. 6 and Table A3 in the Supplemental File [see footnote 2]), and observe strict adherence to the terrestrial mass-dependent fractionation line (Fig. 5) precluding the possibility of extraterrestrial origins. Furthermore, the triple oxygen analysis is helpful to precisely determine the nature of the mass-dependent process that caused ^{18}O depletion and large-scale isotopic fractionation, because equilibrium or kinetic fractionation will result in different slopes (e.g., Clayton and Mayeda, 2009). The samples selected for $\delta^{17}O$ analyses strictly adhere to the *equilibrium* mass-fractionation line with a slope of 0.527, in agreement with earlier work regarding hydrothermal alteration elsewhere (e.g., Young et al., 2002). Evidence of equilibrium and solid-state processes has recently been precisely determined by laser fluorination and shows ^{17}O-^{18}O slopes in a narrow 0.526 to 0.528 range (Rumble et al., 2007; Spicuzza et al., 2007). Kinetic isotope fractionations involving gas have shallow slopes of ~0.516 (Young et al., 2002) or less (~0.503; Clayton and Mayeda, 2009). Thus, the 0.527 slope that we determined for extremely diverse Karelian rocks further suggests that the extreme hydrothermal process with significant mass dissolution and loss that was responsible for formation of these rocks is characterized by equilibrium mass-dependent oxygen fractionation.

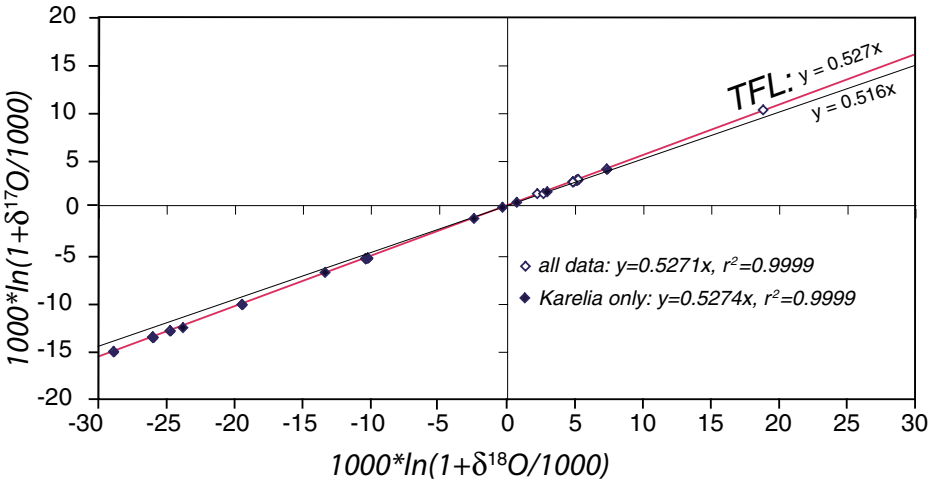

Figure 6. Triple oxygen isotope analysis of garnets in rocks from Khitostrov (filled symbols, mostly from a single outcrop), which displays a 37‰ range in $\delta^{18}O$ values, analyzed together with garnet standards and +18‰ Oregon sandstone (open symbols), with total $\delta^{18}O$ range of 48‰. Notice that triple oxygen defines a slope of 0.527, in strict adherence to the terrestrial-lunar fractionation line (Rumble et al., 2007; Spicuzza et al., 2007). Kinetic fractionation line with a slope 0.516 is shown for comparison. The coordinates of plotting are adapted from Miller (2002) and are meant to linearize the nonlinear delta scale. TFL—Terrestrial fractionation line.

$\delta^{18}O$ in Other Ultrahigh-Pressure Terrains

The Karelian amphibolite-grade metamorphic rocks host the world's lowest-$\delta^{18}O$ signature, but there are other low-$\delta^{18}O$ localities in metamorphic terrains, including the diamond-bearing ultrahigh-pressure (UHP) rocks from Dabie-Shan Sulu (Rumble and Yui, 1998; Zheng et al., 2004; Fu et al., 2012) and Kokchetav (Kazakhstan, Masago et al., 2003). In order to explore more deeply this counterintuitive connection between isotopic depletion and UHP metamorphism, to identify causes and effects, and to test whether ultrahigh-pressure rocks are generally associated with anomalously low-$\delta^{18}O$ values, we analyzed $\delta^{18}O$ in minerals within diamond- and coesite-bearing samples from nine other localities (Table 2). The $\delta^{18}O$ values for UHP rock range between ~5‰ (Alpe Arami, Alps) and +12.5‰ (Sederonero, Greece), characteristic for hydrothermally unaltered igneous and metasedimentary sources. We thus propose that association of low-$\delta^{18}O$ values with UHP metamorphism is purely coincidental. Presumably, these low-$\delta^{18}O$ anomalies were discovered fortuitously because of studying UHP minerals (Dabie Shan or Kokchetav) or nearly gem-quality ruby corundum (Karelia). This survey also suggests that the ultralow-$\delta^{18}O$ values in metamorphic and other inconspicuous rocks may be much more abundant than previously thought.

Zircon Age-$\delta^{18}O$ Relationships for Individual Localities

The descriptions below are from localities shown in Figures 1 and 2, with data presented in Table A1 in the Supplemental File (see footnote 2) and in Figures 7–11.

Khitostrov

We extracted zircons from corundum-bearing rocks from inside the Chupa gneiss (samples K5 and X424 in Bindeman et al., 2010 and Bindeman and Serebryakov, 2011, respectively). Backscatter electron and CL imaging reveals rounded igneous and metamorphic detrital cores sometimes overgrown by thin (<20 µm) metamorphic rims, similar to what was observed in another sample from these rocks previously imaged and dated by Serebryakov et al. (2007). New high-spatial resolution analyses of additional spots on cores and rims of zircons confirm previously published trends in $\delta^{18}O$ versus age (Fig. 8). Specifically, our combined data set shows that (1) zircon cores are exclusively older than 2.55 Ga and are normal $\delta^{18}O$ (~5.3–7‰; typical for metapelitic crustal rocks, e.g., Lackey et al., 2008) with the exception of one 2.72‰ grain; (2) cores are likely detrital because of their abraded shape and range of ages; (3) a minor population of zircon cores is oscillatory-zoned with ages of ca. 2.7–2.9 Ga mantled by uniformly gray CL ca. 2.6 Ga domains; both are normal in $\delta^{18}O$ (crystal KV10_1,2, Fig. 7); (4) low-$\delta^{18}O$ zircon rims are of Svecofennian metamorphic age (ca. 1.85 Ga) with $\delta^{18}O$ ranging from –27.3‰ to values identical with normal $\delta^{18}O$ cores; (5) most Khitostrov zircons (1.8 Ga rims and 2.6 Ga internal zones) have Th/U ratios <0.1 indicative of metamorphic growth (Hoskin and Schaltegger, 2003; Rubatto et al., 2009), with the exception of the ca. 2.7–2.9 Ga oscillatory-zoned zircon cores (Fig. 8B). Mostly low Th/U zircon crystals from corundum-bearing paragneiss contrast with higher Th/U zircon from neighboring mafic intrusions. These yield mostly ca. 1.85 Ga Svecofennian metamorphic ages (Table 1). We attribute the strong variability of U, Th, and REE in metamorphic zircon crystals to co-crystallization of coeval monazite (1.87 Ga; Bindeman et al., 2010) competing with zircon for Th and light REE (see further discussion below).

Varatskoye

Zircons in Varatskoye (Tables 1 and 2 and Fig. 9) were extracted from corundum-bearing rocks surrounded by Chupa paragneiss and from amphibolites that represent a metamorphosed ca. 2.4 Ga mafic intrusion. Our amphibolite sample is compositionally similar to a low-grade metamorphic mafic intrusion at 2 km distance from the Varatskoye location, which yielded U-Pb zircon ages of 2.40 Ga (Bibikova et al., 2004). Large zircons in Varatskoye rocks permitted co-registered U-Pb age and $\delta^{18}O$ analysis of clearly separated core and rim domains. Zircons in corundum-bearing rocks with gneiss as protolith display straightforward relationships between $\delta^{18}O$ and age: cores are exclusively 2.8–2.55 Ga with $\delta^{18}O$ = 5–7‰, and rim ages are 1.9–1.8 Ga with $\delta^{18}O$ = –19‰. The youngest cores interpreted to be metamorphic are ca. 2.55 Ga, and, similar to Khitostrov, are characterized by dark, featureless CL (Fig. 7). Zircons in the Varatskoye amphibolites were exclusively of Svecofennian age and display subtle rimward increases in $\delta^{18}O$ (Figs. 9B and 9C). Within the age range between 1.89 and 1.85 Ga, we observe a nearly linear increase in $\delta^{18}O$ of ~1–1.5‰. This temporal variation is too large to be caused by increasing zircon–whole-rock fractionation ($1000\ln\alpha^{18}O$(zircon-WR) during retrograde metamorphism and instead reflects a subtle increase in $\delta^{18}O$ for

TABLE 2. OXYGEN ISOTOPE ANALYSIS (THIS WORK) OF ULTRAHIGH-PRESSURE CRUSTAL ROCKS WITH DIAMONDS AND COESITES

Sample	Mineral	Locality of sample collection	Rock type	$\delta^{18}O$ (‰)	Pressure (P) (GPa)-temperature (T) (°C) conditions
6-AA-96	Garnet	Alpe Arami, Italy (Dobrzhinetskaya et al., 1996)	Garnet peridotite	5.39	P >10–12
7-AA96-1	Garnet	Alpe Arami, Italy (Dobrzhinetskaya et al., 2002)	Kyanite eclogite	3.93	P = ~7, T = 1100
ED05	Garnet	Erzgebirge, Germany (Dobrzhinetskaya et al., 2006)	Garnet-quartz-biotite gneiss with diamonds	10.58	P >7, T = 1200
20/1-93	Garnet	Fiortoft, Norway (Dobrzhinetskaya et al., 1995)	Garnet-biotite-kyanite gneiss with diamonds	12.18	P >4, T = 900
20-1/93	Garnet	Fiortoft, Norway (Dobrzhinetskaya et al., 1995)	Same with lenses of eclogite	7.29	P >4, T = 800
MP-1	Quartz	Kimi complex, Rhodope, Greece (Perraki et al., 2006)*	Garnet-biotite-gneiss with diamonds	11.32	P >4, T = 700†
126	Quartz	Sideronero complex, Rhodope, Greece§ (Schmidt et al., 2010)	Garnet-biotite-gneiss with diamonds	13.41	P >4, T = 700
K-210	Zircon	Kokchetav Massif, Kazakhstan (Dobrzhinetskaya et al., 2003)	Garnet-biotite-gneiss with diamonds	6.54	P >6–9, T = 980–1200
MakBal	Garnet	Makbal, Tajikistan# (Tagiri et al., 2010)	Garnet-eclogite with coesite	6.87	P = 2–3, T = 800

*Sample courtesy of M. Perraki.
†Mposkos and Kostopoulos (2001).
§Sample courtesy of T. Nagel and N. Frotzheim (Schmidt et al., 2010).
#Sample courtesy of A. Bakirov.

Geosphere, published online on 21 February 2014 as doi:10.1130/GES00952.1

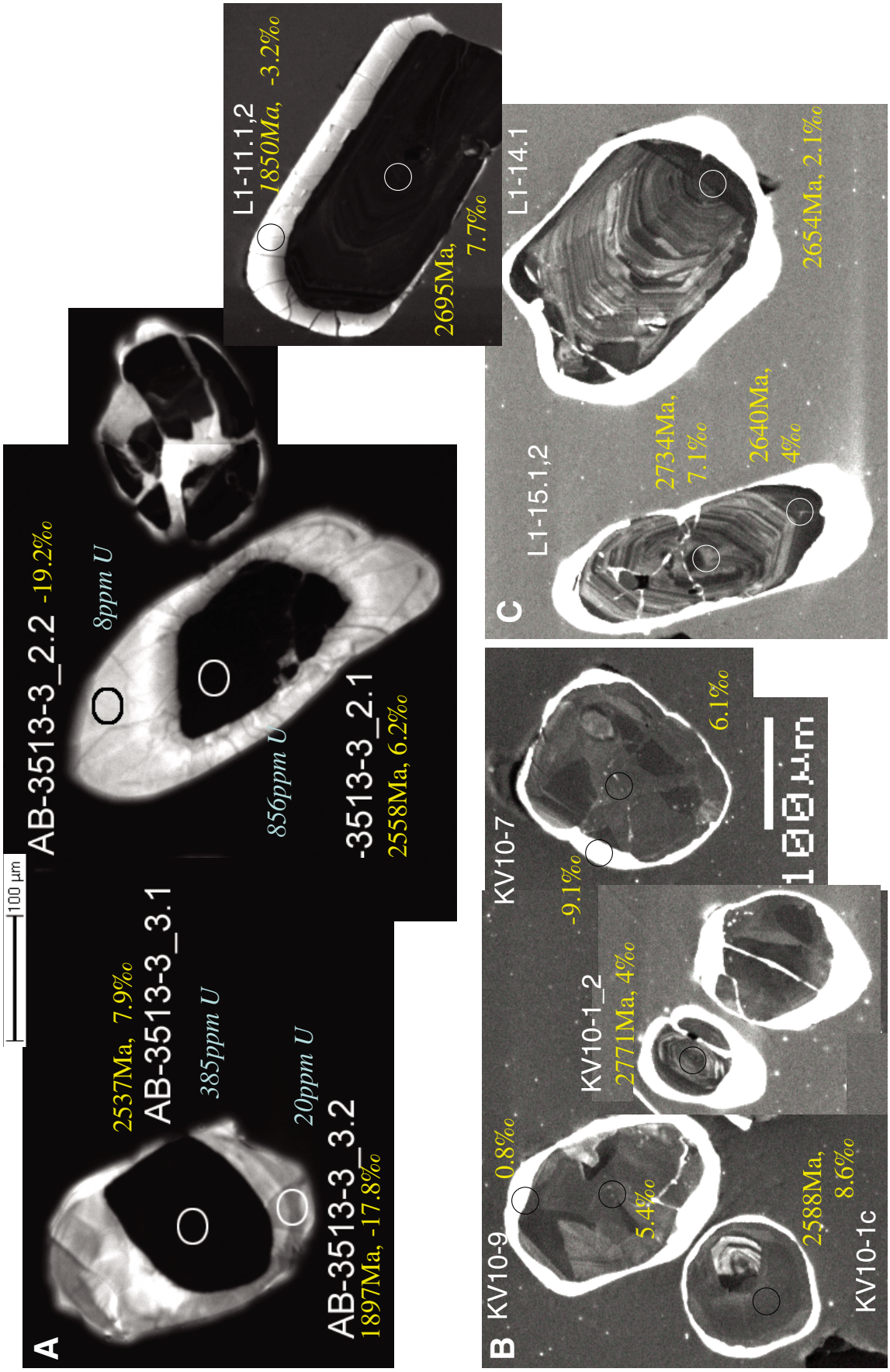

Figure 7 (*Continued on following page*). **Cathodoluminescence (CL) images of selected zircons from several samples showing core–metamorphic rim relationships and ion microprobe analyses spots for U-Pb age, oxygen isotopes, and trace elements relative to the internal zoning. See Table 1 for analyses and Figures 8–11 for plots. Panels a–e are for zircons in gneiss; panels f and g are for zircons in gabbro; B51 series is from high-Mg Varatskoye gabbro; panel f shows zircons in Khitostrov high-Fe gabbro with dark cores; panel h shows a generalized zircon zoning pattern in gneiss and gabbro and the most common zoning and age types. The youngest 2.55–2.6 Ga cores with dark CL crystallized as metamorphic (low Th/U) and are commonly rounded.**

Geosphere, published online on 21 February 2014 as doi:10.1130/GES00952.1

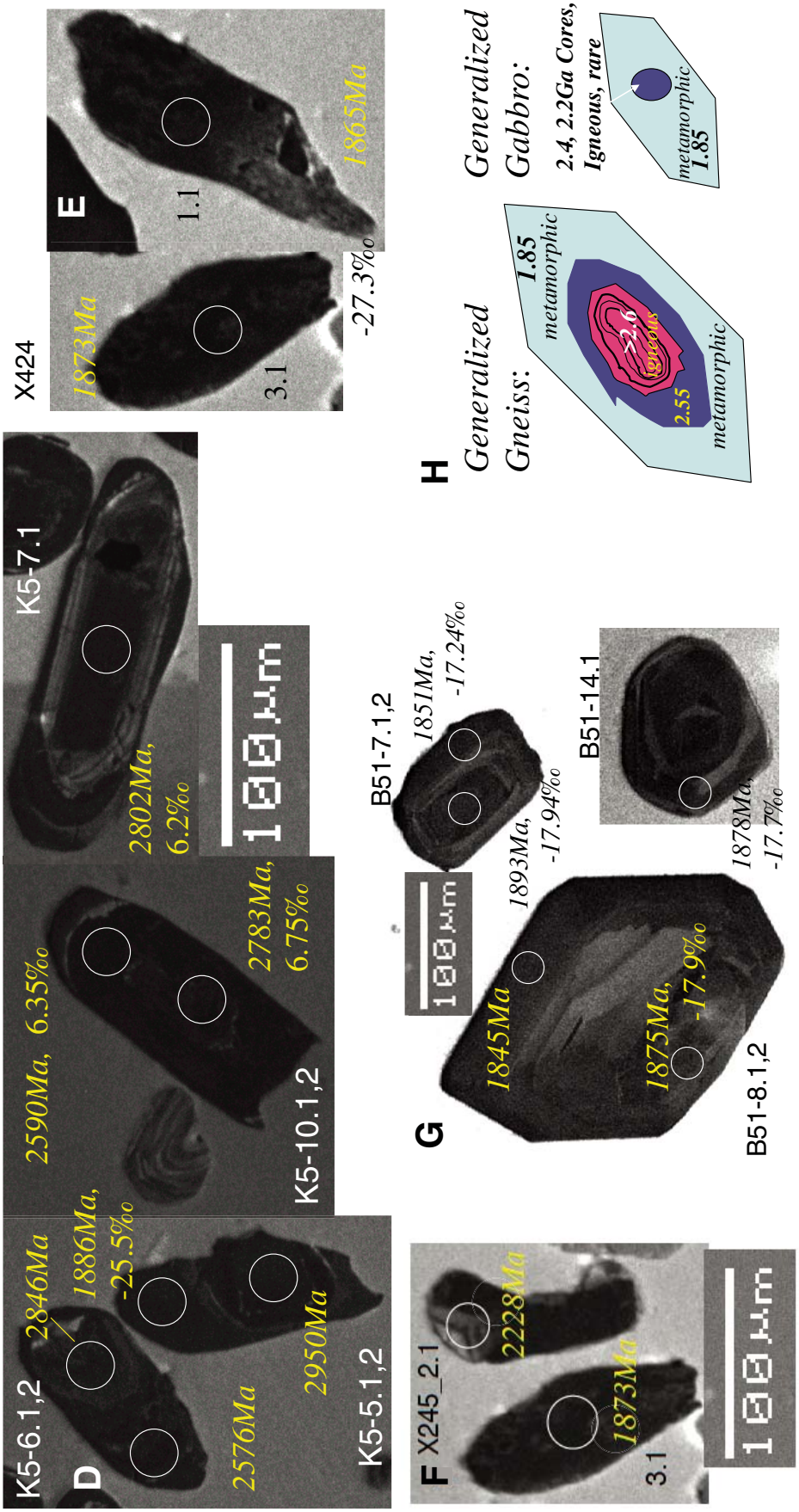

Figure 7 (*Continued*).

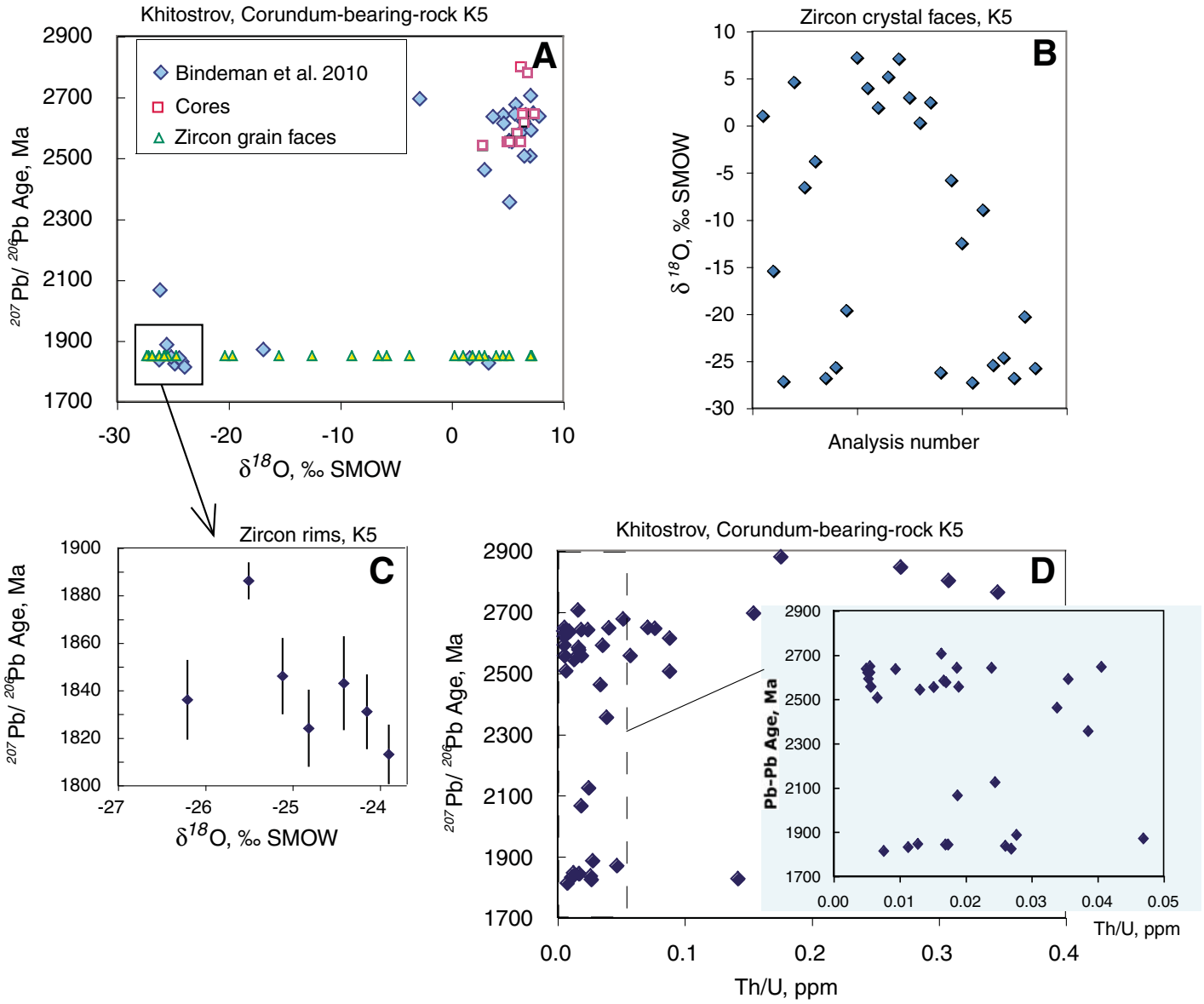

Figure 8. Zircons from sample K5 of the Khitostrov locality: ion microprobe–derived oxygen isotope values plotted versus ages measured on overlapping spots in individual zircons (see Fig. 7 for examples of cathodoluminescence [CL] images). (A) New analyses of zircon cores reveal uniformly normal-$\delta^{18}O$ zircons with a youngest age of 2.55 Ga, a few intermediate in age, and $\delta^{18}O$ values analyses from Bindeman et al. (2010) represent core/rim overlap. (B) $\delta^{18}O$ analyses of unpolished (and undated) zircon faces (outermost 1 µm); same data are plotted in (A) as triangles at a single metamorphic age of 1850 Ma. The $\delta^{18}O$ values range from expected –26 to –27‰ rim values to normal-$\delta^{18}O$, typical core values indicating lack of a rim. Intermediate in $\delta^{18}O$ values indicate rim/core overlap during zircon face penetration by an ion beam. (C) Detail of $\delta^{18}O$ rim versus age demonstrates subtle increase in $\delta^{18}O$ of dated polished rims versus age. (D) Th/U values of dated spots indicating exceedingly low (metamorphic) Th/U ratios characterize 1.85 Ga rims and many ca. 2.6 Ga cores; inset shows the detail of Th/U <0.05.

the metamorphic or intergranular fluids (e.g., Lackey et al., 2008; Peck et al., 2010; D'Errico et al., 2012). Unlike predominantly high-U concentrations and low-Th/U ratios at Khitostrov, at Varatskoye, U concentrations are mostly low (several to tens of ppm, resulting in comparatively large errors in the U-Pb ages), whereas Th/U ratios are highly variable.

Height 128 and Lyagkomina

Zircons in these two localities were extracted from corundum-bearing paragneiss samples. Height 128 zircons have dark CL, rounded cores with some oscillatory zoning and uniformly bright-CL rims that yielded 1.85 Ga ages (Figs. 7 and 10). The thickness of these Svecofennian rims varies from grain to grain, and they are extremely U and Th poor (<10 ppm) causing comparatively large U-Pb age uncertainties (Table 1). There are also few distinct intermediate zircon domains with dark CL and low Th/U that are metamorphic with 2.59–2.6 Ga ages. Zircon rims with dark CL and low Th/U have $\delta^{18}O$ = –9‰ (Figs. 7 and 10), in equilibrium with garnet and other minerals of the

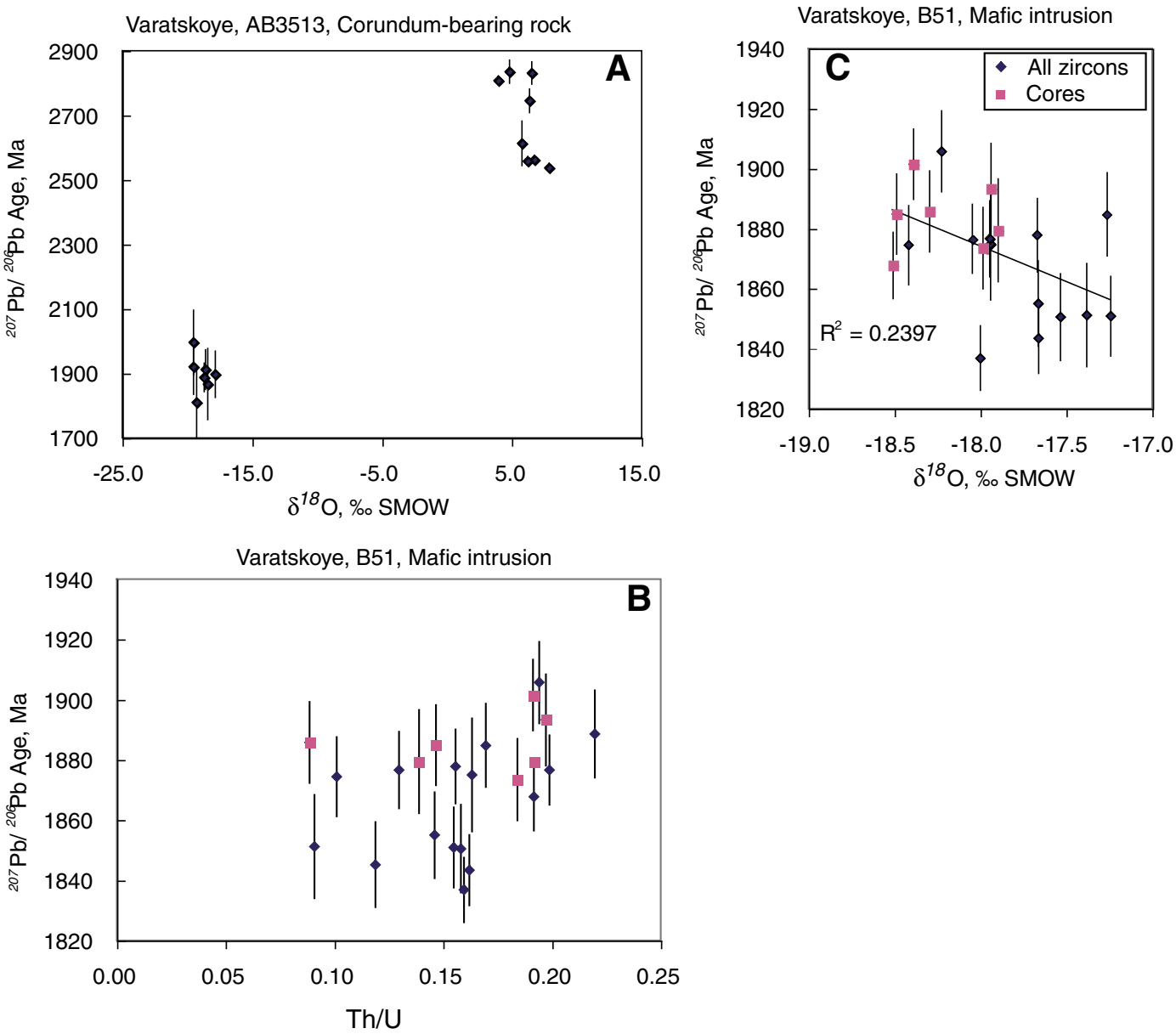

Figure 9. Zircons from the Varatskoye locality (see Fig. 7 examples of cathodoluminescence images). (A) Corundum-bearing rock AB3513 (former metapelite) showing inherited normal-δ^{18}O zircon cores and low-δ^{18}O 1.85 Ga zircon rim. The rims have very low U concentration (1–5 ppm, Table 1), resulting in large errors in age. (B) Th/U values of dated spots indicating low (metamorphic) Th/U ratios in both cores and rims of sample B51. (C) δ^{18}O analyses on dated spots zircons in amphibolite-grade ca. 2.45 Ga high-Mg mafic intrusion (sample B51), which shows non-preservation of 2.45 Ga zircon cores and overall increase in δ^{18}O in zircon rims with decreasing age.

host rock. Lyagkomina (sample L-1) zircons have oscillatory-zoned igneous cores with 2.7–2.75 Ga ages and δ^{18}O = 6.5–7.7‰ (n = 22) and the δ^{18}O at the rims of –4‰, also in equilibrium with the host assemblage. The Th/U ratios of interiors are typical for igneous crystallization, whereas rims are bright in CL and are low in Th/U and δ^{18}O values. In contrast to Height 128, crystal domains of 2.55–2.65 Ga age are absent. Intermediate age and δ^{18}O values (Fig. 9) are the result of beam overlap onto core and rim domains (marked C/R in Table 1), and are thus not considered further.

Mafic Intrusions

Two main types of mafic intrusions regionally occur in Fennoscandia (Figs. 1 and 2, and Fig. A2 in the Supplemental File [see footnote 2]) and are abundantly represented in the area: high-Mg gabbros (druzites) attributed to the 2.4–2.5 Ga global rifting episode (Amelin et al., 1995; Puchtel et al., 1997; Sharkov et al., 1997; Stepanova and Stepanov, 2010) and less abundant, high-Fe tholeiitic dikes tentatively dated at 2.1 Ga (Stepanov, 1981; Stepanova et al., 2003). The respective ages of 2.4–2.5 Ga and 2.1 Ga are thus typically assigned in the field on the basis of high-Mg and high-Fe composition. In the Belomorian Belt, both intrusion types are variably overprinted by 1.85 Ga Svecofennian metamorphism, and localities with extreme ^{18}O depletions also have intense chemical modification trends of desilication and aluminum

Geosphere, published online on 21 February 2014 as doi:10.1130/GES00952.1

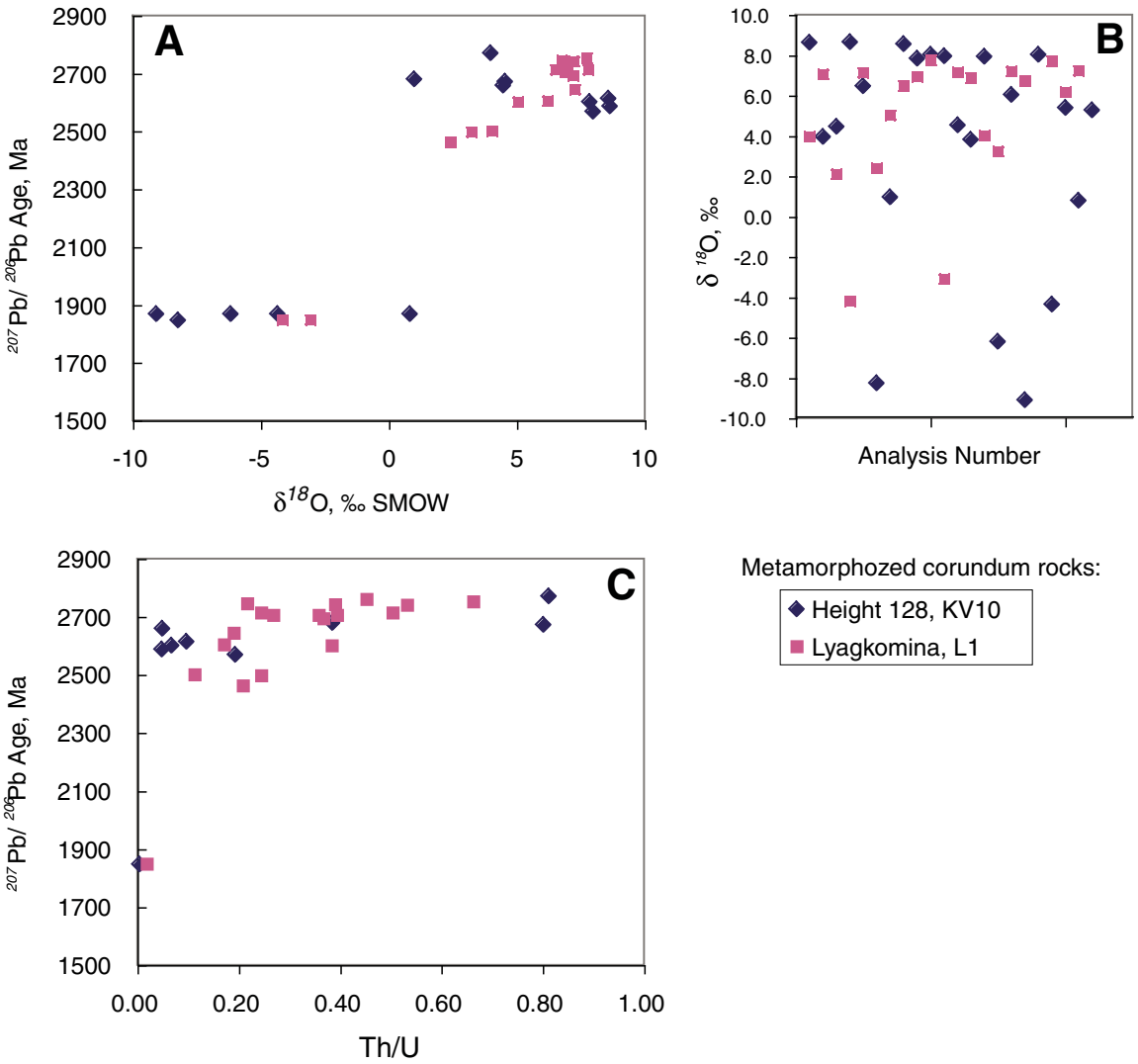

Figure 10. Zircons from Height 128 (sample KV10) and Lyagkomina (sample L1) localities (see Table 1 for analyses and Fig. 7 for selected cathodoluminescence images). (A) Corundum-bearing rocks (former metapelites) showing inherited normal-δ^{18}O zircon cores and low-δ^{18}O 1.85 Ga zircon rims. (B) δ^{18}O analyses of undated zircons showing expected ranges in both localities. (C) Th/U values of dated spots indicating low (metamorphic) Th/U ratios of 1.85 and ca. 2.6 Ga zircons.

enrichment. However, the composition-age designation, although more difficult to see, is still recognizable (e.g., sample X451, Table 1; Kulezhma KY21, Fig. 11). Both types of high-Mg and high-Fe intrusives sometimes occur in close proximity in the studied localities (e.g., at Kulezhma and Khitostrov).

In an attempt to determine the U-Pb age of mafic intrusions that host, or are in close proximity to, low-δ^{18}O localities, we extracted zircons from hand samples collected near the center of these bodies (Fig. 11) where normal, mantle-like δ^{18}O values for all major minerals prevail. The majority of zircon interior ages from Dyadina Gora, Khitostrov, and Varatskoye (Figs. 9 and 11) yielded 1.85 Ga Svecofennian ages with the exception of a single concordant zircon interior from Dyadina Gora, which returned a 2.39 ± 0.022 Ga (2σ) ^{207}Pb/^{206}Pb age. The least metamorphically modified high-Mg intrusive body at the Keret' River has been dated at 2.40 Ga in close proximity to the Varatskoye locality (Bibikova et al., 2004). A single slightly discordant zircon age from inside of high-Fe intrusion at Khitostrov gave a ^{207}Pb/^{206}Pb age of 2.228 ± 0.014 (2σ) Ga (sample X245, Fig. 10). Unfortunately, most zircons from this sample and all zircons extracted from high-Fe amphibolite (sample X451, Table 1) in close proximity to the contact with lowest-δ^{18}O corundum-bearing rocks yielded ca. 1.85 Ga Svecofennian ages indicative of overprinting and metamorphic zircon recrystallization. Zircon interiors in a high-Fe intrusion at Kulezhma were better preserved and yielded ^{207}Pb/^{206}Pb zircon core ages ranging between 2.15 and 2.04 Ga with highly variable Th/U ratios, and minor 1.85 Ga zircons, which suggest that some of these zircon ages represent metamorphic recrystallization. However, a recent compilation of intrusion ages determined by various zircon dating methods (mostly by ion microprobe) suggests that high-Fe dikes could also be older than 2.1 Ga (see Hanski and Melezhik, 2013, figs. 3.8 and 3.9 and references therein). Our single-zircon core age for

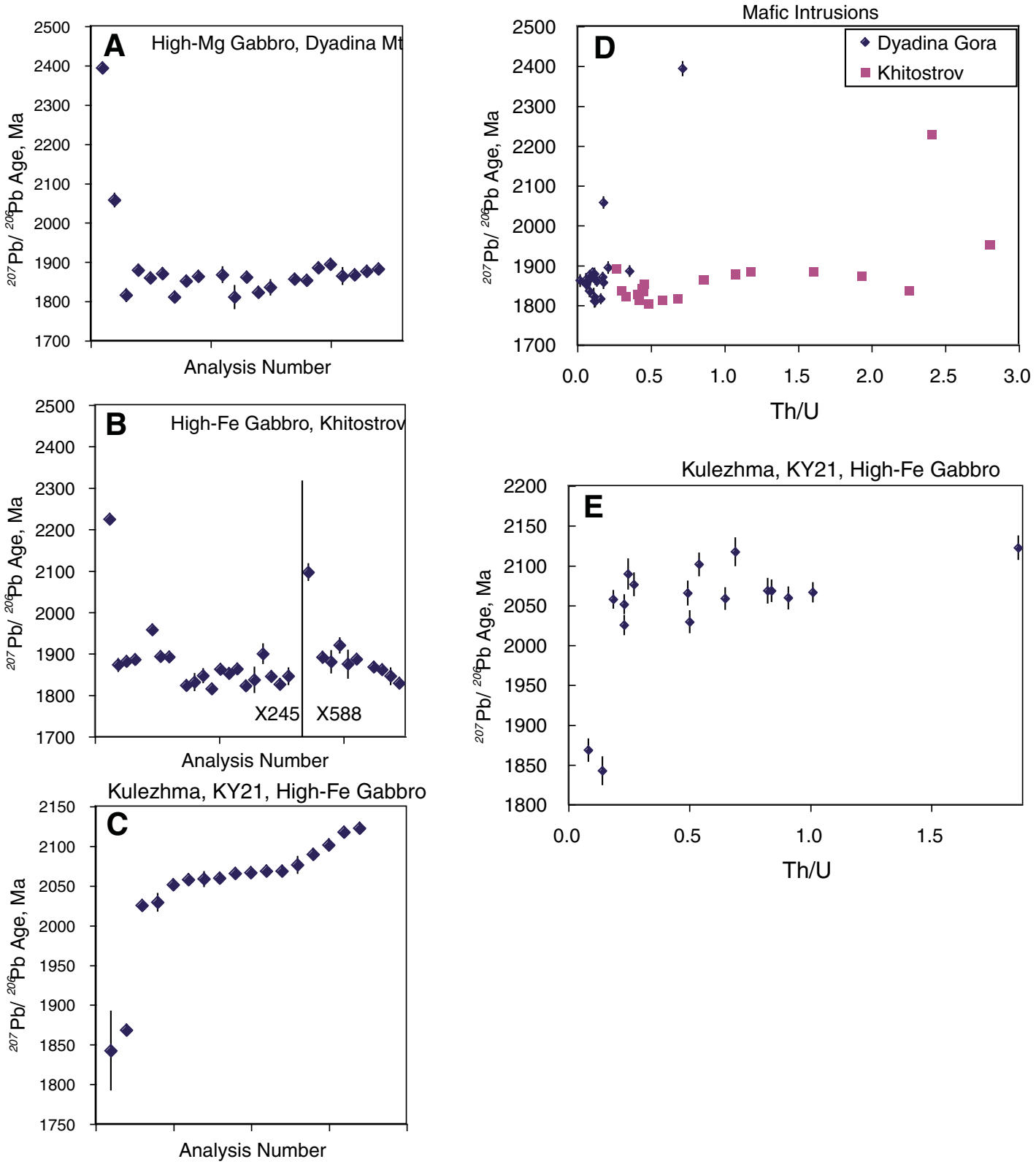

Figure 11. Zircons from mafic intrusions. Age versus analysis number (A–C) and Th/U ratios (D–E) of zircons in metamorphosed 2.45 Ga and 2.1–2.3 Ga mafic intrusions from three localities demonstrating that the majority of zircons in 2.45 Ga intrusions are of metamorphic 1.85 Ga age and only selected cores preserve older ages, likely because these intrusions originally contained few or no zircons. The 2.1 Ga intrusion at Kulezhma preserves older cores and metamorphic rims. See Table 1 for analyses.

Geosphere, published online on 21 February 2014 as doi:10.1130/GES00952.1

Khitostrov at 2.23 Ga could potentially also be a minimum age (Fig. 11B).

High-Spatial Resolution Core-Rim $\delta^{18}O$ Relationships in Zircons

The drastic isotopic gradients between normal $\delta^{18}O$ (detrital) zircon cores and ultralow-$\delta^{18}O$ rims in nearly all gneiss samples (Fig. 7) detected by conventional spot analyses are limited in spatial resolution to the lateral beam dimensions used (~25 µm). To constrain the spatial scale over which the $\delta^{18}O$ transition occurs, and to assess if this correlates with the sharp (<1 µm) CL contrast between cores and rims, we performed a high-spatial resolution isotope profiling using a ~0.5 µm diameter Ga^+ primary ion beam (Fig. 12). A zircon crystal from Varatskoye corundum-bearing rocks was selected because it had one of the thickest rims detected by CL imaging (Fig. 12). Over the length of the profile (~25 µm), the entire ~23‰ shift in $\delta^{18}O$ values occurs over a 5–6 µm interval. The shape of the $\delta^{18}O$ data array is symmetric, resembling a "Fickian" diffusion profile that is centered at the dark-light CL boundary between core and rim.

Rare-Earth Element Analyses of Zircons

Zircon rare-earth element (REE) abundances were determined synchronously with U-Pb ages for a subset of zircons (Fig. 13). In contrast to "normal" magmatic or metamorphic zircon REE patterns that are characteristically depleted in LREE, enriched in high HREE, and commonly have pronounced positive Ce and negative Eu anomalies (e.g., Rubatto and Hermann, 2007), many zircons from the low-$\delta^{18}O$ gneisses show a relative overabundance of LREEs and medium rare-earth elements (MREEs) (Fig. 13), sometimes with a positive Eu anomaly and a lack of a Ce anomaly (e.g., samples K5, KV10, and L1). Light rare-earth element–enriched zircons were also recently reported by Krylov et al. (2012) for Khitostrov locality using different instrumentation. Zircons from gabbros (samples X245 and DG150) also display concave-up REE patterns. To our knowledge, these are the most anomalous distributions observed for zircons anywhere in the world, even exceeding similar trends in detrital Hadean zircons from Western Australia (Cavosie et al., 2006). The rare exceptions to this anomalous behavior are zircons in sample B51 and several zircon cores (e.g., in sample K5; Table 1), which match the zircon-typical REE patterns (Hoskin and Schaltegger, 2003). Excess LREEs in zircon were interpreted to indicate "hydrothermal" or "hydrothermal-pegmatitic" origins (Hoskin and Schaltegger, 2003) because such compositions deviate from magmatic zircon-silicate melt partitioning (e.g., Rubatto and Hermann, 2007; Reid et al., 2011). Pettke et al. (2005), however, observed similar abundances of LREE in magmatic and hydrothermal zircons but found that hydrothermal zircons are characterized by strongly negative Eu anomalies, a feature entirely absent in zircons studied here. Co-crystallization of zircon with garnet cannot explain the observed relationships because garnet depletes the HREE.

At face value, chondrite-normalized LREE abundances of 10–500 suggest a "super"-pegmatitic parental solution or melt containing weight percent REE abundances. We consider such an interpretation improbable because: (1) no such melt has been described in nature and is uncharacteristic at 600–720 °C (e.g., Hermann et al., 2013), and (2) the anomalous distribution of LREE and MREE characterizes not only synmetamorphic zircon rims of Svecofennian 1.85 Ga age but also variably affects 2.9–2.5 Ga detrital zircon cores (see an example of diversity in REE profiles in sample K5).

The best explanation of this unusual phenomenon is the presence of an LREE- and MREE-enriched phase such as monazite ($CePO_4$) or xenotime (YPO_4), which contains 500,000 ppm of LREE and Y, and thus even tiny amounts can contaminate the zircon analysis. Monazite is present in analyzed rocks, and it has been dated specifically in sample K5 to yield Svecofennian 1.89 Ga age (Bindeman et al., 2010). We examined zircon crystals and analysis craters using electron beam imaging (secondary electrons [SE] and backscatter electrons [BSE]) to test whether the unusually large LREE enrichments are due to monazite or xenotime inclusions in zircon, but we found no recognizable monazite. If such inclusions existed, they would be smaller than detectable by SE or BSE imaging (<100 nm). To further test the hypothesis that accumulation of nanoinclusions occurred inside metamict, radioactively damaged zones, we analyzed selected spots in sample K5 using a CAMECA SX100 electron probe with wavelength dispersive spectrometers (calibrated relative to synthetic zircons, Fig. 13C; see Fig. A5 in the Supplemental File [see footnote 2]), exciting X-rays with high beam current (300 nA) and voltage (30 kV) to achieve high precision for trace elements (calculated detection limits are: P = 20 ppm, Ce = 90 ppm, and Y = 130 ppm). Because monazite and xenotime are both phosphate minerals, we concentrated on detecting

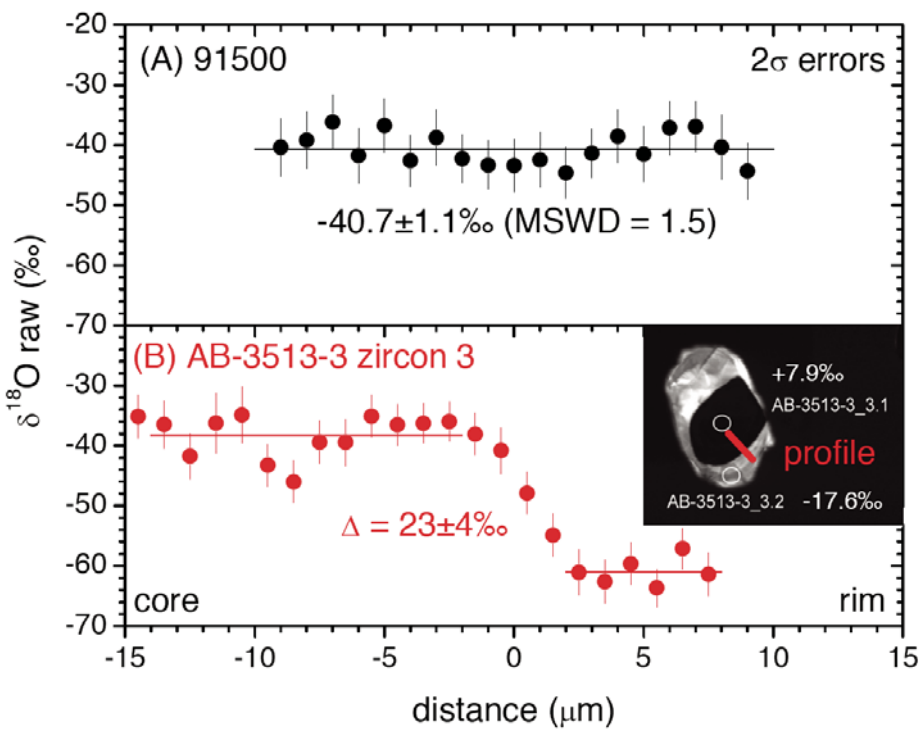

Figure 12. Small beam (<1 µm) ion microprobe profile across zircon core/rim boundary (sample AB3513, zircon 3 from Varatskoye). Note the rather abrupt (less than 6 µm) zoning, which suggests rapid dissolution and reprecipitation of zircon core, followed by overgrowth and limited subsequent oxygen diffusion. Raw $\delta^{18}O$ data are plotted, but the relative core-rim offset of 23 ± 4‰ is identical to regular spot analyses in this sample (Fig. 9A). MSWD—mean square of weighted deviates.

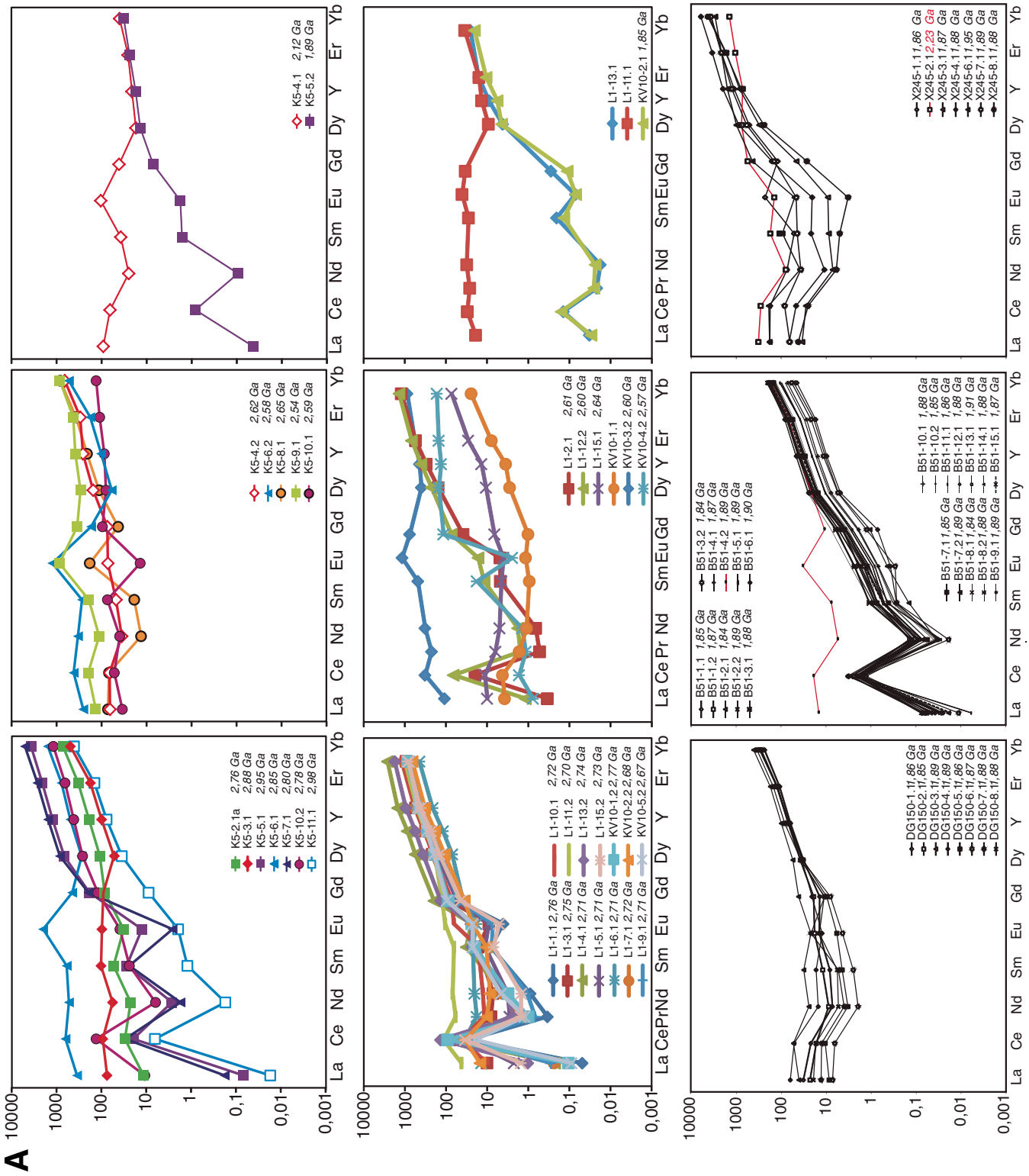

Figure 13 (*Continued on following 2 pages*).

Figure 13 (*Continued on following page*). Ion microprobe–determined concentrations of rare-earth elements (REE) in dated zircons from six samples. See the Supplemental File 2 (see footnote 2) for analyses. (A) REE as a function of sample identity and age. Notice very high and irregular concentration of REE in most samples, as compared to normal and expected REE distribution (e.g., K5-11.1 on first panel); overabundance of light and middle REE is pervasive in both cores and rims.

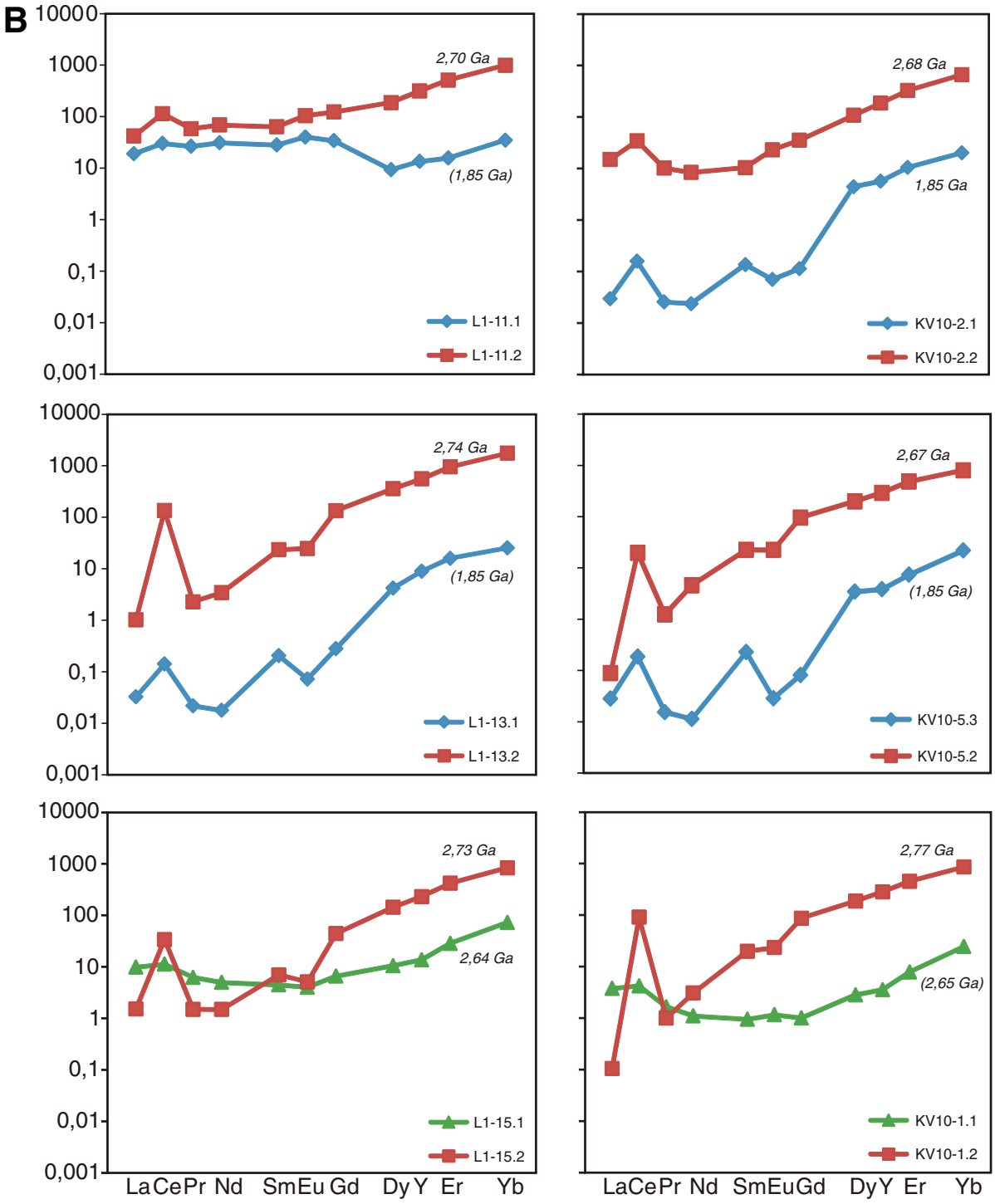

Figure 13 (*Continued*). (B) Analyses of core and the rim in the same crystal. Notice predominantly lower concentration of all REEs in metamorphic rims of studied samples.

Geosphere, published online on 21 February 2014 as doi:10.1130/GES00952.1

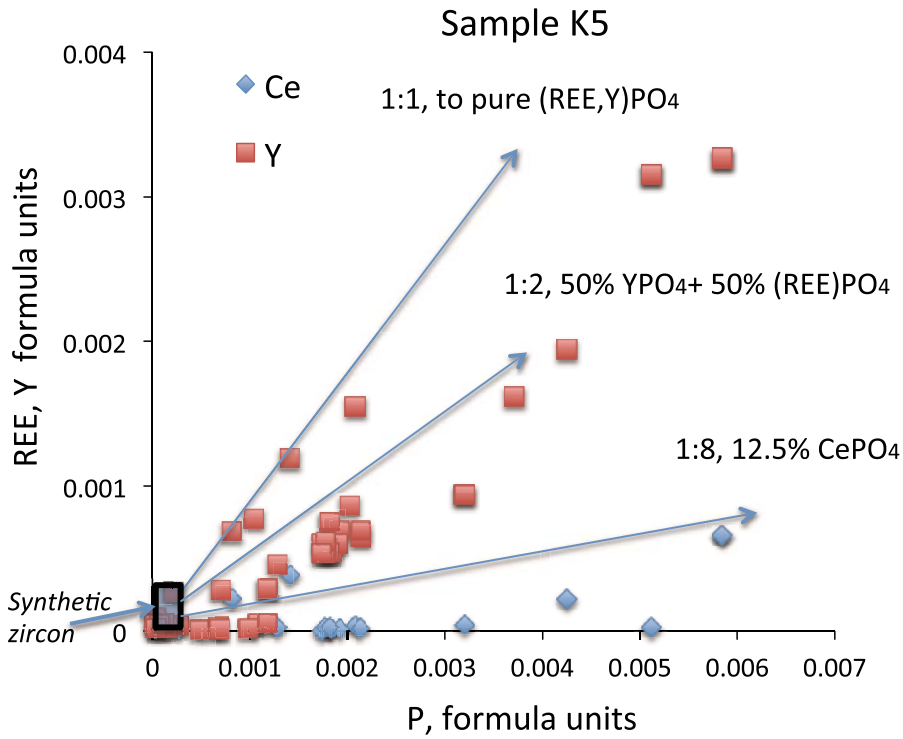

Figure 13 (*Continued*). (C) Electron microprobe analysis of ion microprobe pits and other areas in sample K5 demonstrating high concentration of P and correlation of P with Y and thus likely other REE (not measured); see the Supplemental File (see footnote 2) for analyses and images. We interpret elevated REE and their positive correlation with P as a feature caused by the presence of nano-sized Y and REE-phosphate in metamict zones of zircons (affecting U-richer and older cores more than the rims), below the spatial resolution of scanning electron micron imaging; see text for discussion.

phosphorous and correlations between REE and P. Analyzed zircons had up to 900 ppm P, and a positive correlation between Y and P exists. However, correlations between P and especially Ce are subtle. Although the amount of P in K5 zircons is abnormally high compared to common zircon (e.g., Hoskin and Schaltegger, 2003), it is still too low to account for the total abundance of REE (Fig. 13). This requires non-phosphate REE-rich phases in these zircons.

These measurements support our inference that zircons are "infected" by nanometer-scale inclusions, at least some of which would be monazite or xenotime like. Monazite recrystallizes and is dissolved in fluids at lower temperatures than zircons during regional metamorphism (Rubatto et al., 2001). The hydrous silicate melts that form plagioclasites, the leucosome in studied localities, serve as an appropriate transport media for these REE-rich phases. Our interpretations are in line with those of Cavosie et al. (2004, 2006), who attributed more modest LREE enrichment in >3.9 Ga Hadean detrital zircons to microinclusions formed at very low water/rock ratio inside of metamict zircon zones. These authors also found positive albeit scattered correlations between P and REE abundances.

High LREE abundances in zircons correspond to elevated and highly fractionated LREEs/heavy rare-earth elements (HREE) in corundum-bearing rocks across Karelia, which were reported by Terekhov (2007). Presence of just 0.01 wt% monazite (as detected in these rocks) is capable of explaining the elevated LREE budget.

The $\delta^{18}O$ Analyses of Nonmetamorphic Protoliths

In a reconnaissance study of coeval synrift sedimentary and igneous rocks that may preserve direct evidence for interaction with ultra-depleted glacial melt waters, we have sampled low-grade metamorphic rocks to the southeast (Vetreny Belt) and southwest (north of Petrozavodsk) of the Belomorian Belt (Fig. 1). We analyzed materials that reasonably could have interacted with low-$\delta^{18}O$ glacial meltwaters: glacial tillite, secondary minerals (amygdaloids and quartz vugs) inside basaltic lavas intercalated with glacial deposits, alteration minerals formed between margins of basaltic pillows, and quenched pillow basalt rinds (Table 3 and Fig. 14). For comparative purposes, we have also analyzed secondary quartz from Antarctica's Minna Bluff area, which represents subglacial and proximal alteration at 12–9 Ma (Antibus et al., 2012). Alteration history and isotope thermometry of these rocks have been studied in detail and confirm a 10–100 °C temperature window for deposition of quartz (Antibus, 2012), which constrains quartz-water isotope fractionation.

If alteration and secondary products in Karelian rocks were formed at low-temperatures (50° ± 30 °C) as suggested by comparison with Minna Bluff Antarctic quartz data, then the altering waters must have been ultra-low-$\delta^{18}O$, comparable to Antarctic ice. The Karelian quartz has $\delta^{18}O$ values that are 10–15‰ lower than subaerial Oligocene quartz vugs in Oregon, formed in temperate near-coastal conditions (Fig. 14).

DISCUSSION

Summary of Zircon Age-$\delta^{18}O$ Relationships

There are clear spatial and temporal patterns for $\delta^{18}O$ in zircon from corundum-bearing rocks in the Chupa gneiss that are consistent for all sampled localities: normal $\delta^{18}O$ cores with ages ranging from >2.9 to 2.55 Ga and ultralow-$\delta^{18}O$ rims with younger ca. 1.85 Ga Svecofennian ages. Zircon-rim $\delta^{18}O$ values are in isotopic equilibrium with the host-rock mineral assemblage, ranging from $\delta^{18}O$ = –4.1‰ in Lyagkomina to –27.3‰ in Khitostrov, which to our knowledge is the lowest value ever reported (samples X424 and X425). Rims also have universally low Th/U ratios characteristic for metamorphic zircon, whereas cores have variable but generally higher "igneous" Th/U. Some zircon cores have an internal mantle with dark CL and low Th/U values that date to a ca. 2.6 Ga metamorphic event previously reported for the Belomorian Belt (Bibikova et al., 1994, 2001, 2004). Importantly, these ca. 2.55–2.6 Ga internal mantle domains are normal in $\delta^{18}O$, and no unambiguously igneous zircon of this age is present in our data. The morphology of 2.6–2.55 Ga zircon cores is rounded and non-euhedral (Fig. 7) and represents metamorphic recrystallization of older cores. The sharp termination of 2.55–2.6 Ga metamorphic zircon growth zones suggests cooling potentially due to uplift and unroofing of the Chupa gneiss. The amount of denudation after 2.55 Ga but before regional rifting at 2.4 Ga remains

TABLE 3. OXYGEN-ISOTOPE ANALYSES OF SYNGLACIAL 2.4–2.5 GA MATERIALS FROM KARELIAN SARIOLIAN AND SUMIAN SEQUENCES AND THEIR COMPARISON WITH EQUIVALENT ANTARCTIC AND OREGON MATERIALS AND ESTIMATED OXYGEN-ISOTOPE VALUES OF WATERS ASSUMING FULL EXCHANGE AND QUOTED TEMPERATURES

Sample	Material	$\delta^{18}O$ (‰) SMOW	Latitude	Longitude	Locality, description	Water calculated§ (°C)			
						10	50	100	300
Onega Basin and Segozero Belts									
PZ-3	Quartz, vug-1	9.95	62°38'52.4"	33°41'30.3"	Girvas, Sariolian basalt interlayers with diamictites	–28.6	**–19.0**	–11.1	2.60
PZ-3	Basalt	4.55			Same				
PZ-4	Quartz, vug-1	5.06	62°25'50.9"	33°42'16.7"	Krasnaya Rechka, Sariolian basalt interlayers with diamictites	–33.4	**–23.9**	–15.9	–2.29
PZ-4	Basalt	4.8			Same				
PZ-5	Quartz, vug-1	11.4	62°25'50.4"	33°42'10.5"	50 m away, another flow	–27.1	**–17.5**	–9.6	4.09
PZ-6	Quartz, vug-1	11.7	62°25'49.9"	33°42'04.3"	50 m away, another flow	–26.9	**–17.3**	–9.4	4.30
PZ-7	Quartz cement	4.92	62°25'49.9"	33°42'04.3"	Fine conglomerate matrix (rock flower)	–33.6	**–24.0**	–16.1	–2.43
					Fresh surface or recently detached block	–38.5	**–29.0**	–21.0	–7.35
PZ-8	Basalt	5.2	62°43'58.11"	33°37'12.8"	Elmus Lake, pillow lavas, quartz fill between pillows				
PZ-8	Qz-1 vug	9.85	62°43'58.11"	33°37'12.8"	Same	–28.7	**–19.1**	–11.2	2.50
PZ-9	Hyaloclastite	4.91	62°43'58.11"	33°37'12.8"	Same, pillow rim material	–33.6	**–24.0**	–16.1	–2.44
PZ-10	Basalt	7.62	62°54'20.1"	34°22'04.9"	Road cut Petrozavodsk-Murmansk highway, Sariolian basalt				
PZ-10b	Quartz vug	9.68	62°54'20.1"	34°22'04.9"	Same	–28.8	**–19.3**	–11.3	2.33
PZ10b	Basalt	6.32	62°54'20.1"	34°22'04.9"	Same				
PZ-10c	Quartz vug	9.88	62°54'20.1"	34°22'04.9"	Road cut Petrozavodsk-Murmansk highway, Sariolian basalt	–28.6	**–19.1**	–11.1	2.53
PZ-11	Quartz, vug	11.8	63°11'04.3"	33°25'48.8"	Segezha Lake, Jatulian basalt	–26.7	**–17.1**	–9.2	4.49
PZ-13	Varves	11.9	63°12'02.2"	33°13'41.0"	Varves in the glacial lake, 2.4 Ga, between basalts	–26.6	**–17.1**	–9.1	4.52
PZ-25	Basalt	8.07					**–20.9**	–12.9	0.72
Vetreny Belt, 2.4 Ga (see Fig. 1A), subaqueous volcanics, sedimentary materials, and alteration products*									
230	Schist	0.69			Argillitic schist, Vilenchskaya Svita, Golets Mountain				
4115	Pillow rinds	3.60			area between pillows				
Makarukha	Quartz	6.05			Quartz vugs in Myandukha Mountain, fragments of komatiitic basalts		–22.9	–1.3	–1.3
Makarukha	Basalt	3.04			Host basalt in Myandukha Mountain, fragments of komatiitic basalts				
0230-K	Quartz	4.50			Quartz, breccia of volcanites, quartz-epidote aggregate, Golets Mountain		**–24.5**	–2.9	**–2.9**
KYL 02307	Epidote	–0.41			Epidote, volcanic breccia, quartz-epidote aggregate, Golets Mountain				
Minna Bluff, 12–9 Ma Antarctic basalt with quartz-calcite–filled vugs†									
Vug 1	Quartz core	7.42				–31.1	**–21.5**	–13.6	0.07
Vug 2	Quartz core	7.21				–31.3	**–21.7**	–13.8	–0.14
Vug 3	Quartz rim	6.38				–32.1	**–22.6**	–14.6	–0.97
Vug 4	Quartz core	4.50				–34.0	**–24.5**	–16.5	–2.85
Vug 5	Quartz rim	5.43				–33.1	**–23.5**	–15.6	–1.92
MP-07	Whole-rock basalt next to 5	3.5							
Vug 6	Quartz vein	1.65				–36.9	**–27.3**	–19.4	–5.70
MP-07	Whole-rock basalt next to 6	3.04							
Vug 7	Quartz rim	10.37				–28.1	**–18.6**	–10.6	3.02
Vug 8	Rim	6.15				–32.4	**–22.8**	–14.9	–1.21
Vug 9	Quartz rim	7.57				–30.9	**–21.4**	–13.4	0.22
Vug 10	Quartz core	5.47				–33.0	**–23.5**	–15.5	–1.88
Vug 11	Quartz core	0.68				–37.8	**–28.3**	–20.3	–6.67
Vug 11	Quartz core	1.23				–37.3	**–27.7**	–19.8	–6.12
Oregon's 55 Ma subaerial basalts with quartz-filled vugs									
Yachats	Quartz vug	24.40				–14.1	**–4.5**	**3.4**	17.05
Bobs Creek	Quartz vug	18.66				–19.8	**–10.3**	**–2.3**	11.31
Ilwaco, Washington	Quartz vug	21.05				–17.5	**–7.9**	**0.1**	13.70

*Samples kindly provided by V.S. Kulikov (Karelian Institute of Geology, Petrozavodsk).
†Samples of J. Antibus and K. Panter (Antibus et al., 2012).
§Assuming equilibrium at quoted temperatures (Clayton et al.,1972; Kawabe,1978).
SMOW—standard mean ocean water.

Geosphere, published online on 21 February 2014 as doi:10.1130/GES00952.1

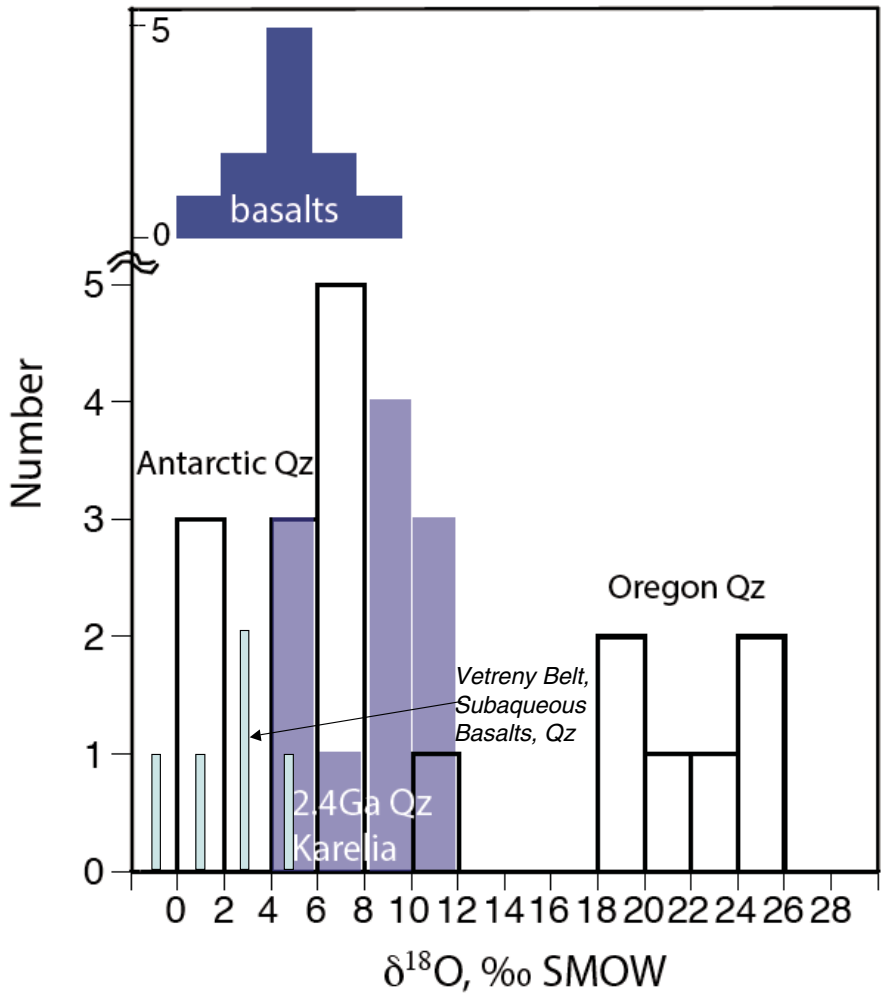

Figure 14. Oxygen isotope analysis of secondary quartz (Qz) vugs (amygdaloids) from 2.5 to 2.3 Ga Sariolian and Sumian basalts from Karelia (see Table 3 for analyses); these are compared to the quartz vugs in Antarctic and Oregon basalts. Quartz-basalt and quartz-epidote isotope fractionations in Vetreny Belt samples suggest temperature of formation for quartz amygdaloids in basalts to be in a broad ~50 to 250 °C range, and likely involved isotopically shifted meteoric waters due to interaction with rocks. Low-$\delta^{18}O$ values of many quartz and basalts suggest that the interaction involved low-$\delta^{18}O$ water at elevated temperatures relative to surface conditions. Although the values in Karelian quartz are not particularly low, the close match of 2.4 Ga Karelian vugs with Antarctic vugs, and not Oregon vugs, suggests by *analogy* that the Karelian basalts could have been altered by low-$\delta^{18}O$ glacial meltwaters.

unknown, but rocks must have resided at this time at depths *shallow enough* to enable open fractures and attendant alteration by meteoric water at large water/rock ratios to imprint the observed ultralow-$\delta^{18}O$ glacial meltwater signature on them shortly thereafter.

The next episodes of zircon growth that reflect a regional geologic event are recorded exclusively in gabbroic intrusions but not in the gneisses they intrude. The zircon record of the high-Mg gabbros yields only a single magmatic core of 2.4 Ga (i.e., in DG150-11, Fig. 11), which is in agreement with similarly aged zircon crystals described for mafic intrusions at locations that are not surrounded by low-$\delta^{18}O$ depletions (Puchtel et al., 1997; Bibikova et al., 2004). Rare zircons in high-Fe intrusions (e.g., 2.23Ga in Khitostrov) characterize less abundant high-Fe magmatism with nominal 2.1Ga age but may be locally older (ca 2.2–2.3 Ga, Hanski and Melezhik, 2013). Pervasive 1.85 Ga Svecofennian metamorphism appears to have obliterated much of the pre–1.85 Ga zircon record in the mafic intrusives immediately adjacent to the low-$\delta^{18}O$ localities. This is not surprising because the odds for survival and detection of any older igneous or metamorphic zircons in such mafic intrusions, if they were ever present, are low because of low Zr abundance and small grain sizes typical for such rocks. It should be mentioned, however, that the cores are better preserved (and dated) in the least metamorphosed mafic intrusions 1–2 km away from localities of interest (2.4 Ga at Varatskoye; Bibikova et al., 1994, 2004).

The last episode of zircon growth is during the 1.85 Ga Svecofennian metamorphism, affecting zircons in both gneisses and mafic intrusions. This stage is represented by zircon overgrowths on existing cores and crystallization of new zircons (Fig. 7).

Zircon geochronology reveals a rather short (~50–100 m.y.) time gap between the 2.55 Ga youngest metamorphic crystallization of zircons in the gneiss and their inferred shallow hydrothermal alteration by glacial meltwaters near the surface by 2.45–2.4 Ga in the vicinity of superplume-related (Evans and Pisarevsky, 2008), high-Mg gabbroic intrusions. Two scenarios are possible. (1) Cessation of zircon growth after 2.55 Ga but before 2.45 Ga can be reasonably achieved at comparatively slow metamorphic unroofing (and cooling) rates of ~1 mm/yr: uplift from amphibolite-grade depths (15–18 km) to the near surface would take ~15–36 m.y. Unroofing in response to postcollisional erosion-driven isostatic uplift (removal of the mountain top overburden) or by lateral gravitational flow of the thickened crust, as is observed in the Alps (Ruppel et al., 1988; Champagnac et al., 2009), is conceivable. At such rates, uplift and cooling (Fig. 14) will be completed ~50 m.y. before the superplume event and the inferred initiation of rifting at 2.5 to 2.45 Ga. (2) Uplift caused by extension during the 2.5–2.4 Ga rifting episode, a known regional (Rybakov et al., 2000) and global event. In this scenario, rifting resulted in rapid exhumation from mid-crustal depths. For this tectonically driven uplift history, exhumation would have been completed in less than 10 m.y.

The Khitostrov locality may require hydrothermal alteration to take place at 2.23 Ga, coincident with high-Fe gabbro intrusions.

Origin of Sharp Isotope Boundaries inside Zircon

Karelian zircons show sharp isotopic shifts across the core-rim boundaries, with the rims being in isotopic equilibrium with the host assemblage (Fig. 12). For a ~3 μm

half-thickness of the $\delta^{18}O$ diffusion profile in the Varatskoye zircon, and assuming that the zircons spent *at least* 10 m.y. at high peak metamorphic conditions of ~700 °C indicated by the metamorphic paragenesis and Zr-in-rutile geothermometry (Fig. 5), the estimated oxygen-diffusion coefficients are ~10^{-23} to 10^{-24} m^2/s, in agreement with Watson and Cherniak's (1997) "dry" diffusion coefficients for zircon. For "wet" diffusion coefficients, complete annealing of the zircon crystals would occur over the same timescale, even at a lower metamorphic temperature of ~600 °C, which is contrary to our observations. "Wet" diffusion would produce the observed diffusion profile in ~0.1 m.y., a duration that is too brief to be reconciled with reasonable cooling rates for regional retrograde metamorphism. There are several considerations here for explaining the comparatively sharp $\delta^{18}O$ diffusion profile we have observed: (1) experimental uncertainties in wet versus dry diffusion coefficients, in particular the "wet" diffusion coefficients of Watson and Cherniak (1997) being too large (e.g., Page et al., 2007; Bowman et al., 2011); (2) the metamorphism occurred under drier conditions than usually assumed for such rocks (Kohn, 1999); (3) metamorphic rims crystallized at much lower "metasomatic" temperatures (<500 °C), where diffusion was vanishingly small[3]; and/or (4) the metamorphic event was unusually short. Under these conditions, zircon-rim crystallization should have occurred at a maximum temperature 510–485 °C for only a few million years. However, such low temperatures contradict metamorphic grade, Zr-in-rutile temperatures (Fig. 5), and Ti in zircon temperatures recently reported by Krylov et al. (2012) for the Khitostrov locality, all suggesting 650–770 °C for zircon-rim crystallization. The age difference between amphibolitic zircon and monazite crystallization age of 1.89 Ga (Bindeman et al., 2010) and inferred ca. 1.75 Ga ages of exhumation of these rocks (Terekhov, 2007) suggests a normal duration of metamorphism and exhumation, lasting tens of millions of years. We thus prefer explanation (1) because it is in agreement with geological evidence (e.g., Page et al., 2007; Bowman et al., 2011).

[3]To quantify the maximum temperature at which the zircon rims could have crystallized without significantly reequilibrating with the zircon cores, we modeled metamorphic cooling using fast grain boundary diffusion model (Eiler et al., 1992; Peck et al., 2003) over reasonable metamorphic temperatures and cooling duration of 10 m.y. using "wet" diffusion coefficients (Watson and Cherniak, 1997); see figure A1 in Bindeman and Serebryakov (2011).

Search for a Nonmetamorphic Low-$\delta^{18}O$ Protolith

The Karelian ultralow-$\delta^{18}O$ anomaly is exclusively hosted by amphibolite-grade metamorphic rocks of the 1.85 Ga Belomorian Belt extending >450 km, but oxygen isotope depletion of the protolith is likely associated with a Paleoproterozoic "Slushball Earth" episode of subglacial alteration around rift-related mafic intrusions (Fig. 1). No ultralow-$\delta^{18}O$ rocks have yet been reported in coeval low-grade volcanic and sedimentary rocks (Table 3 and Fig. 14). Although ultralow-$\delta^{18}O$ supracrustal rocks would be the ultimate proof for extremely ^{18}O-depleted glacial waters (which, if present at low latitudes would indicate a "Slushball Earth" condition; Hoffman, 2009; Bindeman et al., 2010), we have reason to surmise that such evidence would be difficult to find, or be uncommon. First, this is because water-rock interaction is kinetically restricted in supracrustal rocks, and isotope fractionation factors are large at low temperatures, favoring higher-$\delta^{18}O$ solids. In contrast, isotopic exchange is rapid and extensive in hydrothermal systems, and $1000\ln\alpha_{rock\text{-}water}$ whole-rock–water fractionation is close to 0‰, thus more reliably recording water $\delta^{18}O$ values at large water/rock ratios. Second, there are uncertainties regarding the geological position of sediments and lavas as representing subglacial or lacustrine environments (low-$\delta^{18}O$ water), or marine environments (~0‰ $\delta^{18}O$ SMOW seawater values). Nonetheless, despite the unknown temperature of formation, the $\delta^{18}O$ values in supracrustal samples from Karelia (Fig. 14) are at the lower end of geologically more recent analogues, overlapping with the Antarctic quartz data.

Protolithic versus Synmetamorphic Low-$\delta^{18}O$ Signatures

Our isotope mapping for the Khitostrov zone of ultralow-$\delta^{18}O$ rocks shows concentric zonation in the proximity of elongated mafic intrusion, sheared during 1.85 Ga Svecofennian metamorphism (Fig. 2). *If* the elongated concentric isotopic pattern were to be explained by infiltration of ultralow-$\delta^{18}O$ synmetamorphic fluids at 1.85 Ga (as suggested by Terekhov, 2007; Ustinov et al., 2008), the following very specific conditions must be met.

(1) In the absence of any recognized reservoirs of mantle- or crustal-derived, low-$\delta^{18}O$ and low-δD, high-temperature fluids, the only conceivable source of such ultralow-$\delta^{18}O$ fluids is devolatilization of (previously surface-exposed) buried metamorphic rocks.

(2) Because typical gneisses and amphibolites contain only 1–2 wt% H_2O (Fig. 15A) and because at amphibolite-grade temperatures of 600–700 °C, $1000\ln\alpha_{water\text{-}rock}$ water–whole-rock fractionation is close to zero (Fig. 15B), the devolatilizing protolith would have to be: (a) essentially the same ultralow-$\delta^{18}O$ composition to yield ultralow-$\delta^{18}O$ fluids that are inferred for Karelia; and (b) it would take 50–100 times (Fig. 15D) the mass of the devolatilizing ultralow-$\delta^{18}O$ rock to produce cubic kilometers of –10 to –27‰ rocks documented in outcrops (Fig. 2).

(3) Isotopic effects are maximized only if fluids were escaping through the same metamorphic shear zone, thus integrating fluid/rock ratios (Figs. 14C and 14D). On an equimolar-oxygen basis, *and* assuming that fluids are following the same path with 100% exchange efficiency, it will take equal amounts of fluids to rocks to bring $\delta^{18}O$ value of rocks closer to that of the fluid, again requiring 100 times the volume of the known low-$\delta^{18}O$ exposures (6 × 2 km, Fig. 2C). If the isotope exchange reaction is only 50% efficient, and/or if increments of fluids are following different (non-integrating) paths, the total isotopic effects are significantly reduced, and thus the required amount of devolatilizing rocks at depth is significantly increased.

(4) The flushing fluids will induce progressively lower (but still significant) isotopic effects on rocks down the path of exchange (up the fault). Thus the exposed –27‰ rocks would require an even lower $\delta^{18}O$ devolatilizing source (Fig. 15C).

(5) If metamorphic fluids were CO_2 rich (e.g., Valley, 1986; Lackey and Valley, 2004), they should have been derived from decarbonation of ultralow-$\delta^{18}O$ carbonate, unknown in the area or worldwide. While mass balance would require less rock on an equimolar-oxygen basis (~10–20 times the amount of decarbonating marble versus 50–100 times the amount of dehydrating amphibole-bearing rock), the fractionation factors required are still problematic: $\delta^{18}O$ of CO_2 is heavier than coexisting calcite by 3.3‰ (900 °C) to 6‰ (700 °C; Zheng, 1993; Rosenbaum, 1994), thus diminishing the overall fluxing effect of CO_2 and requiring an even lighter devolatilizing carbonate source of –30 to –35‰ $\delta^{18}O$ SMOW.

In summary, a synmetamorphic fluid-fluxing hypothesis would require >100 times ^{18}O-depleted rocks underneath the Khitostrov and other Karelian localities, making an even stronger case for widespread pre–1.85 Ga surface altered rocks. Additionally, investigated eclogites of the Belomorian Belt (Fig. 1A and Table A1 in the Supplemental File [see footnote 2]), devolatilized equivalents of studied rocks, are structurally below the examined localities, but these eclogites lack low-$\delta^{18}O$ minerals.

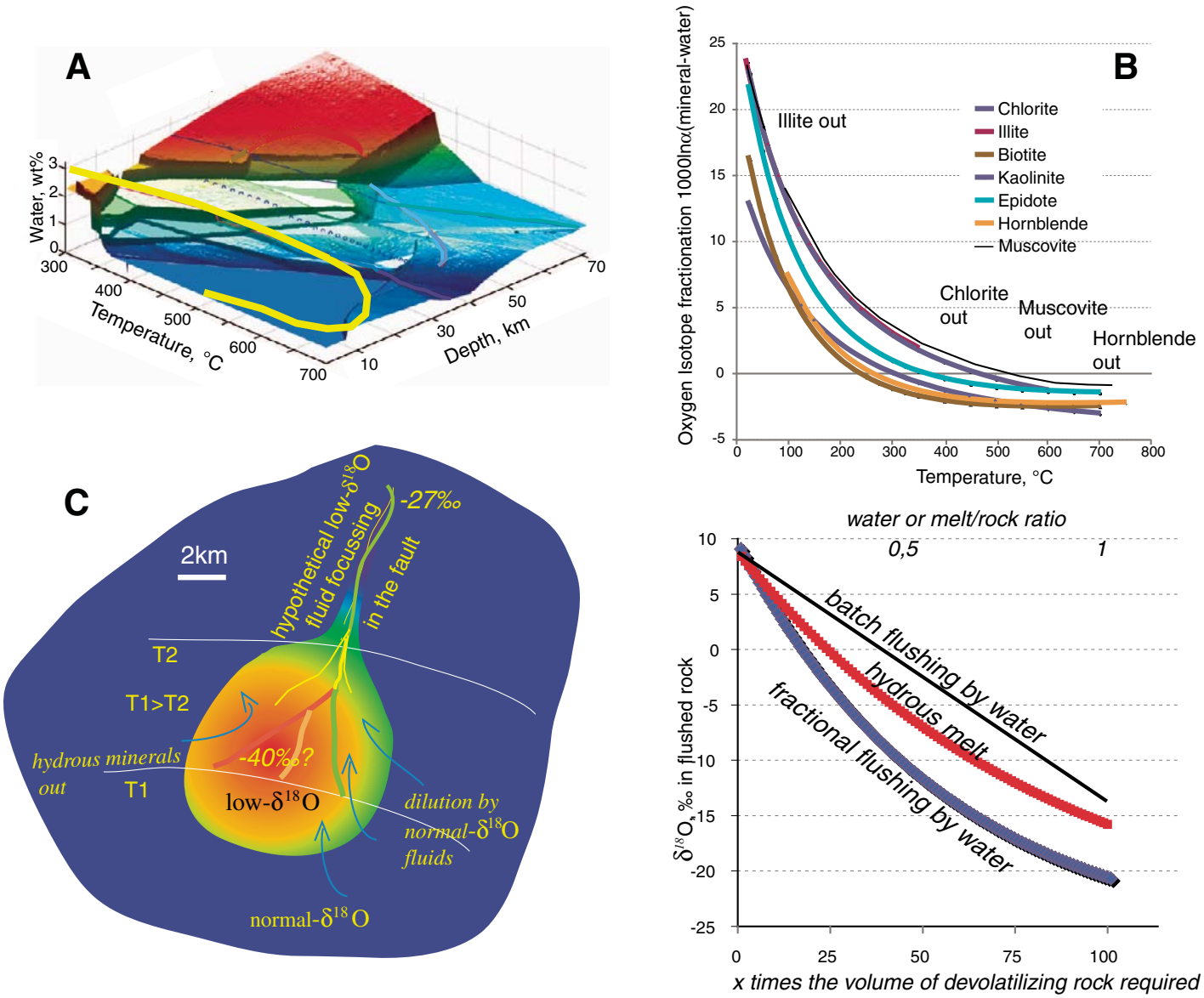

Figure 15. Isotope effects during metamorphic dehydration and metamorphic fluid flow, demonstrating that the Karelian depletions were unlikely to have formed by this process. (A) A generic metapelite P-T-X_{H2O} diagram (adopted from Connolly, 2010) with a superimposed reaction path for studied localities of the Belomorian Belt. Note the stepwise dehydration pattern showing hydrous mineral breakdown at specific temperatures. (B) A diagram showing compiled oxygen isotope fractionation factors (see the Supplemental File [see footnote 2]) and approximate temperature ranges of hydrous mineral stability; their dehydration at T > 200–400 °C results in small 0 ± 2‰ water-rock oxygen isotope fractionations. (C) A cartoon explaining the focusing of fluid-flow paths along the fault zone. The mass of devolatilizing low-δ18O rocks at depth should greatly exceed the mass of altered rocks proximal to the fault. (D) Oxygen isotope depletion effects in response to putative incremental percolation of low-δ18O hydrous fluid (89% oxygen) or hydrous plagioclasite melt (59% oxygen) through the fault zone. Shown are the water-rock ratios and the large amounts of devolatilizing protolith required.

We consider shallow heated glacial meltwater interaction with rocks as the most parsimonious explanation. This would result in a circular symmetric depletion pattern formed around mafic intrusions prior to 1.85 Ga metamorphism, which, in turn, deformed these depletion zones into elongated and thus likely fault-controlled, ultralow-$\delta^{18}O$ localities. Later local devolatilization of the low-$\delta^{18}O$ protolith during metamorphism generated zones of equally low-$\delta^{18}O$ synmetamorphic fluids, plagioclasite leucosomes (Fig. 3), which caused localized formation of zoned metamorphic minerals, zircon rims, smoothed and/or obscured preexisting $\delta^{18}O$ zonation in outcrops, enriching metamict zones in zircons, and whole rocks with LREEs.

Alternative Isotopic Ways to Produce Ultralow-$\delta^{18}O$ Fluids?

Are there other conceivable processes that can produce the isotopic ranges observed? We are aware of only three processes other than hydrothermal alteration that are capable of producing large (>20‰) depletion of $\delta^{18}O$: (1) kinetic isotope fractionation, e.g., during devolatilization or evaporation with significant mass loss (Clayton and Mayeda, 2009; Mendybayev et al., 2010); (2) thermal diffusion in water-bearing rocks (Bindeman et al., 2013); and (3) extreme Rayleigh distillation.

Rapid thermal decomposition of hydrous phases (e.g., brucite and serpentine; Clayton and Mayeda, 2009) at low pressure or vacuum involves kinetic removal of increments of low-$\delta^{18}O$ water. The process can be viewed as isotope disproportionation into high-$\delta^{18}O$ residue and low-$\delta^{18}O$ fluid. However, contrary to the Karelian data, such a process generates shallow "kinetic" slopes of $\delta^{17}O$ versus $\delta^{18}O$ fractionation of 0.503–0.516, which are different from the equilibrium mass-dependent slopes that we measured (0.527, Fig. 6). The kinetic devolatilization process is also unlikely to explain the genesis of the Karelia rocks because high-$\delta^{18}O$ anhydrous residues are absent. Moreover, evidence is lacking that high-pressure metamorphic devolatilization would be kinetically equivalent to low-pressure devolatilization.

For thermal isotope redistribution (or "thermal migration"; e.g., Lundstrom, 2009), the sense of O- and H-isotope redistribution in a temperature gradient is low $\delta^{18}O$ at a hotter end and high $\delta^{18}O$ at the colder end, in spatial agreement to the observed contact relationships between gabbro and gneiss. Covariant mass-dependent fractionations as much as 28‰ for $\delta^{18}O$ and 144‰ for δD are possible in a ~500 °C temperature gradient (Bindeman et al., 2013) using natural, normal-$\delta^{18}O$ rocks with 2–4 wt% H_2O. As is the case with kinetic devolatilization above, both low- and high-$\delta^{18}O$ values are generated in the process, while Karelia rocks universally show a decreasing trend from normal-$\delta^{18}O$ gneiss or gabbro to ultralow-$\delta^{18}O$ values in corundum-bearing rocks. However, further tests can be applied to explore both of these possibilities: oxygen and hydrogen isotopes should be covariant with other isotopic species (e.g., Si, Mg, and Fe) in a predictable mass-dependent way (Mendybayev et al., 2010; Bindeman et al., 2013).

Finally, an extreme Rayleigh fractionation process of incremental fluid removal, which we can call the "underground distillery model," can accentuate isotopic differences. However, at high temperatures, isotope fractionation factors are small (Fig. 15B), the amount of ultra-distilled fluid is measured at a few percent of the original, and thus the possibility of any significant "underground distillation" is also unlikely. We suggest that interaction between normal $\delta^{18}O$ rocks and ultralow-$\delta^{18}O$ glacial meltwater presents the simplest and most realistic explanation to the observed results.

Insights into Duration of Paleoproterozoic Slushball Earth Glaciations

The Paleoproterozoic glaciation on different continents is inferred to have lasted from ca. 2.45 Ga to as late as 2.26 Ga based on existing and newly appearing geochronologic data on diamictites worldwide (see Hoffman, 2013, for review). Three to four individual glacial episodes, each of unknown but likely global or near-global extent, characterized the Earth during this time interval, each lasting multiple millions of years. Coeval to glaciation was the appearance of oxygen in the Earth's atmosphere and disappearance of the mass-independent sulfur photolysis reactions between 2.4 and 2.26 Ga (Bekker et al., 2004). When exactly the Great Oxidation Event (GOE) occurred remains a matter of debate.

Our work contributes to this discussion because ultralow-$\delta^{18}O$ values in Karelian rocks provide direct evidence for low-$\delta^{18}O$ glacial meltwaters and thus terrestrial glaciation at low latitudes. The majority of Karelia localities record a 2.4 Ga episode, during coeval rifting and high-Mg plume magmatism (Fig. 16; also Bindeman and Serebryakov, 2011). The new evidence from the most depleted locality at Khitostrov is adjacent to high-Fe gabbro that yielded a single-zircon core of 2.23 Ga, suggesting that hydrothermal alteration could have been caused by the youngest glaciation dated at 2.26 Ga by Rasmussen et al. (2013) in South Africa and Canada. Thus there is a need to date post–2.4 Ga high-Fe intrusions in the Belomorian Belt and their unmetamorphosed variety in Karelia to confirm the age designation. If this evidence is confirmed, then the Karelian low-$\delta^{18}O$ rocks record the oldest and the youngest of glaciations during the Paleoproterozoic, so that every shallow intrusion likely underwent subglacial or near-glacial meteoric-hydrothermal alteration.

CONCLUSIONS

(1) Eleven newly discovered low- and ultralow-$\delta^{18}O$ Paleoproterozoic Karelian localities extend the previously known geographical range of such rocks in the Belomorian Belt to 450 km.

(2) At the Khitostrov locality, which hosts the world's lowest $\delta^{18}O$ rocks (–27.3‰), the mapped zone of depletion is now extended to ~6 × 2 km, tracing the high-Fe gabbro body in an exposed regional fault.

(3) Isotopic mass balance supports the idea of near-surface alteration by glacial meltwaters at large water-rock ratio as the most likely mechanistic interpretation of the observed depletion patterns, prior to metamorphism.

(4) Zircon crystals in corundum-bearing rocks associated with the Chupa paragneiss display systematic zoning patterns with normal-$\delta^{18}O$, 2.9–2.7 Ga igneous cores that are commonly mantled by normal-$\delta^{18}O$ 2.55–2.6 Ga metamorphic domains and ultralow-$\delta^{18}O$ Svecofennian 1.85 Ga metamorphic rims. Zircons in metamorphosed mafic intrusions are predominantly of the younger metamorphic Svecofennian age.

(5) Zircon ages of gabbroic intrusions in most low-$\delta^{18}O$ localities indicate intrusive ages coincident with 2.45 Ga rifting and the oldest Paleoproterozoic glaciation. Hydrothermal alteration in the rift zones involved heated glacial meltwaters at large water-rock ratios, implying shallow residence of the studied localities at that time.

(6) Whether the depletion at Khitostrov is younger than 2.4 Ga, and is associated with ca. 2.23 Ga high-Fe intrusions, needs to be further tested. If proven, Khitostrov will document a hydrothermal alteration event during the youngest of Paleoproterozoic glaciations.

(7) Svecofennian 1.85 Ga burial and metamorphism have resulted in very limited devolatilization of low-$\delta^{18}O$ rocks diluted by the fluids from ambient normal-$\delta^{18}O$ rocks, leading to increasing $\delta^{18}O$ in metamorphic minerals and zircon rims. This small fluid-rock ratio or hydrous low-degree melting may explain unusually enriched REE and P concentrations in zircons. We invoke dispersed LREE-rich nanometer-sized REE-phosphate inclusions in metamict zones within these zircons.

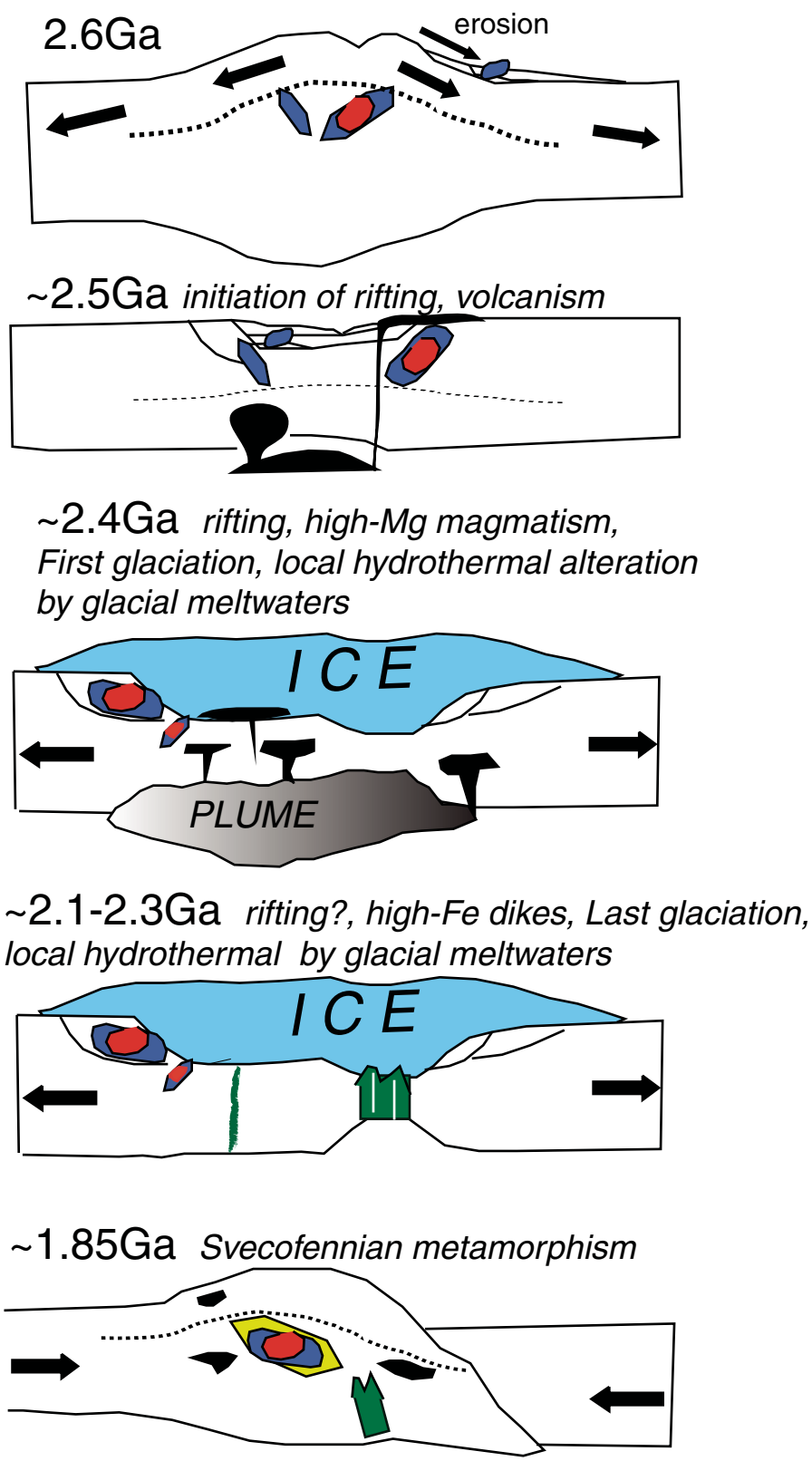

Figure 16. Interpreted sequence of tectonic events as recorded by zircons and rocks. Zircons crystallize and/or recrystallize below the dashed line of inferred isotherm (defining closure temperature in P-T-X_{H_2O} space). See text for detail.

(8) Geochronologic and geologic evidence indicates depletion in $\delta^{18}O$ happened between 2.55 and 1.85 Ga, which is broadly coincidental with glacial deposits of the Sariolian and Sumian age of Karelia. These coeval volcanic and sedimentary rocks and their alteration products have $\delta^{18}O$ values broadly comparable to those in modern Antarctica but lack ultralow-$\delta^{18}O$ values due to lower (and uncertain) temperatures of alteration as compared to high-temperature hydrothermal alteration around magmatic intrusions.

(9) The redefined range of $\delta^{18}O$ in Karelian rocks (from +10 to −27.3‰) allows a more precise determination of exponents of the $\delta^{17}O$ versus $\delta^{18}O$ fractionation exponent, as 0.527, in strict adherence to the equilibrium distribution of isotopes in the process, suggesting that intense hydrothermal alteration obeys equilibrium mass dependency.

ACKNOWLEDGMENTS

We thank the National Science Foundation for funding of grants EAR-1049351 and EAR-CAREER 0805972; IF-EAR funding of the CAMECA 1270 ion microprobe facility; the University of California, Los Angeles; and the Russian Foundation for Basic Research for grant 12-05-00706a. We also thank Pavel Medvedev, Sergei Svetov, and Denis Korpechkov for help during fieldwork of 2011 and 2012, and Markus Walle for help with LA-ICP MS. V. Kulikov kindly supplied samples from Vetreny Belt, and Kurt Panter is thanked for collaboration on Antarctic secondary quartz. J. Eiler and Caltech Ion microprobe facility are thanked for hosting I. Bindeman during sabbatical, and Cliff Dax is thanked for electronics support. Associate Editor Aaron Cavosie and two anonymous reviewers are thanked for their careful reviews.

REFERENCES CITED

Amelin, Y.V., Heaman, L.M., and Semenov, V.S., 1995, U-Pb geochronology of layered mafic intrusions in the eastern Baltic Shield—Implications for the timing and duration of Paleoproterozoic continental rifting: Precambrian Research, v. 75, p. 31–46, doi:10.1016/0301-9268(95)00015-W.

Antibus, J.V., 2012, A petrographic, geochemical, and isotopic (Sr, O, H, and C) investigation of alteration minerals in volcaniclastic rocks at Minna Bluff, Antarctica: Petrogenesis and implications for paleoenvironmental conditions [M.S. thesis]: Bowling Green, Kentucky, Bowling Green State University, 272 p.

Antibus, J.V., Panter, K.S., Wilch, T., Dunbar, N., McIntosh, W., Blusztajn, J., Traipati, A., and Bindeman, I., 2012, A petrographic, geochemical, and isotopic (O, H, C, and Sr) investigation of secondary minerals in volcaniclastic rocks at Minna Bluff, Antarctica: Petrogenesis of alteration and implications for paleoenvironmental conditions: San Francisco, California, American Geophysical Union, Abstract V21A-2758, 2012 Fall Meeting.

Balagansky, V.V., Bogdanova, M.N., and Kozlova, N.E., 1986, Evolution of Northwest Belomorian Belt: USSR Academy of Sciences, Kola Filial, Apatity, 100 p. [in Russian].

Barth, A.P., and Wooden, J.L., 2010, Coupled elemental and isotopic analyses of polygenetic zircons from granitic rocks by ion microprobe, with implications for melt evolution and the sources of granitic magamas: Chemical Geology, v. 227, p. 149–159.

Bekker, A., 2011, Huronian glaciation, *in* Encyclopedia of Astrobiology: Springer-Verlag, p. 768–772.

Bekker, A., Holland, H.D., Wang, P.-L., Rumble, D., III, Stein, H.J., Hannah, J.L., Coetzee, L.L., and Beukes, N.J., 2004, Dating the rise of atmospheric oxygen: Nature, v. 427, p. 117–120, doi:10.1038/nature02260.

Bibikova, E.V., Skiold, T., Bogdanova, S.V., Drugova, G.M., and Lobach-Zhuchenko, S.B., 1994, Belomoride Geochronology: Interpretation of multi-stage history: Geokhimia, v. 10, p. 1393–1411.

Bibikova, E.V., Claesson, S., Glebovitsky, V.A., Sedova, I.S., and Ruchev, A.M., 2001, Isotope dating of the Svecofennian metamorphism of the Belomorian Belt, Baltic Shield: Geokhimia, v. 10, p. 1116–1119.

Bibikova, E.V., Bogdanova, S.V., Glebovitsky, V.A., Claesson, S., and Skiold, T., 2004, Evolution of the Belomorian Belt: NORDSIM U-Pb zircon dating of the Chupa paragneisses, magmatism, and metamorphic stages: Petrology, v. 12, p. 195–210.

Bindeman, I., 2011, When do we need pan-global freeze to explain ^{18}O-depleted zircons and rocks?: Geology, v. 39, p. 799–800, doi:10.1130/focus082011.1.

Bindeman, I.N., 2008, Oxygen isotopes in mantle and crustal magmas as revealed by single crystal analysis: Reviews in Mineralogy and Geochemistry, v. 69, p. 445–478, doi:10.2138/rmg.2008.69.12.

Bindeman, I.N., and Serebryakov, N.S., 2011, Geology, Petrology and O and H isotope geochemistry of remarkably ^{18}O-depleted Paleoproterozoic rocks of the Belomorian Belt, Karelia, Russia, attributed to global glaciation 2.4 Ga: Earth and Planetary Science Letters, v. 306, p. 163–174, doi:10.1016/j.epsl.2011.03.031.

Bindeman, I.N., Schmitt, A.K., and Evans, D.A.D., 2010, Origin of the lowest-known δ^{18}O silicate rock on Earth in Paleoproterozoic Karelian rift: Geology, v. 38, p. 631–634, doi:10.1130/G30968.1.

Bindeman, I.N., Lundstrom, C., Bopp, C., and Huang, F., 2013, Stable isotope (O, H, Li) fractionation by thermal diffusion through partially molten wet and dry silicate rocks: The unrealized behavior of dissolved H_2O in a temperature gradient: Earth and Planetary Science Letters, v. 365, p. 51–62, doi:10.1016/j.epsl.2012.12.037.

Black, L.P., Kamo, S.L., Allen, C.M., Davis, D.W., Aleinikoff, J.N., Valley, J.W., Mundil, R., Campbell, I.H., Korsch, R.J., Williams, I.S., and Foudoulis, C., 2004, Improved ^{206}Pb/^{238}U microprobe geochronology by the monitoring of a trace-element-related matrix effect; SHRIMP, ID–TIMS, ELA–ICP–MS and oxygen isotope documentation for a series of zircon standards: Chemical Geology, v. 205, p. 115–140, doi:10.1016/j.chemgeo.2004.01.003.

Blackburn, T., Shimizu, N., Bowring, S.A., Schoene, B., and Mahan, K.H., 2012, Zirconium in rutile speedometry: New constraints on lower crustal cooling rates and residence temperatures: Earth and Planetary Science Letters, v. 317–318, p. 231–240, doi:10.1016/j.epsl.2011.11.012.

Boss, A.P., 2011, Evolution of the solar nebula. XI. Gradients in the spatial heterogeneity of the short-lived radioisotopes ^{60}Fe and ^{26}Al and the stable oxygen isotopes: The Astrophysical Journal, v. 739, doi:10.1088/0004-637X/739/2/61.

Bowman, J.R., Moser, D.E., Valley, J.W., Wooden, J.L., Kita, N.T., and Mazdab, F.K., 2011, Zircon U-Pb isotope, δ^{18}O and trace element response to 80 My of high temperature metamorphism in the lower crust: Sluggish diffusion and new records of Archean craton formation: American Journal of Science, v. 311, p. 719–772, doi:10.2475/09.2011.01.

Cavosie, A.J., Liu, D., Wilde, S.A., Weiblen, P.W., and Valley, J.W., 2004, Internal structure and U-Th-Pb chemistry of Jack Hills detrital zircons: A mineral record of Early Archean to Mesoproterozoic (4348–1576 Ma) magmatism: Precambrian Research, v. 135, p. 251–279, doi:10.1016/j.precamres.2004.09.001.

Cavosie, A.J., Valley, J.W., and Wilde, S.A., 2006, Correlated microanalysis of zircon: Trace element, δ^{18}O, and U-Th-Pb isotopic constraints on the igneous origin of complex >3900 Ma detrital grains: Geochimica et Cosmochimica Acta, v. 70, p. 5601–5616, doi:10.1016/j.gca.2006.08.011.

Champagnac, J.-D., Schunegger, F., Norton, K., von Blanckenburg, F., Abbühl, L.M., and Schwab, M., 2009, Erosion-driven uplift of the modern Central Alps: Tectonophysics, v. 474, p. 236–249, doi:10.1016/j.tecto.2009.02.024.

Claiborne, L.L., Miller, C.F., Walker, B.A., Wooden, J.L., Mazdab, F.K., and Bea, F., 2006, Tracking magmatic processes through Zr/Hf ratios in rocks and Hf and Ti zoning in zircons: An example from the Spirit Mountain batholith, Nevada: Mineralogical Magazine, v. 70, no. 5, p. 517–543.

Clayton, R.N., and Mayeda, T.K., 2009, Kinetic isotope effects in oxygen in the laboratory dehydration of magnesian minerals: The Journal of Physical Chemistry A, v. 113, p. 2212–2217, doi:10.1021/jp808621n.

Clayton, R.N., O'Neil, J.R., and Mayeda, T.K., 1972, Oxygen isotope exchange between quartz and water: Journal of Geophysical Research, v. 77, p. 3057–3067.

Connolly, J.A.D., 2010, The mechanics of metamorphic fluid expulsion: Elements, v. 6, p. 165–172, doi:10.2113/gselements.6.3.165.

D'Errico, M.E., Lackey, J.S., Surpless, B.E., Loewy, S.L., Wooden, J.L., Barnes, J.D., Strickland, A., and Valley, J.W., 2012, A detailed record of shallow hydrothermal fluid flow in the Sierra Nevada magmatic arc from low-δ^{18}O skarn garnets: Geology, v. 40, p. 763–766, doi:10.1130/G33008.1.

Dobrzhinetskaya, L.F., Eide, E.A., Larsen, R.B., Sturt, B.A., Tronnes, R.G., Smith, D.C., Taylor, W.R., and Posukhova, T.V., 1995, Microdiamond in high-grade metamorphic rocks of the Western Gneiss Region, Norway: Geology, v. 23, p. 597–600, doi:10.1130/0091-7613(1995)023<0597:MIHGMR>2.3.CO;2.

Dobrzhinetskaya, L.F., Green, H.W., II, and Wang, S., 1996, Alpe-Arami: A peridotite massif from depth of more than 300 kilometers: Science, v. 271, p. 1841–1845, doi:10.1126/science.271.5257.1841.

Dobrzhinetskaya, L.F., Schwienehage, R., Massonne, H.-J., and Green, H.W., II, 2002, Silica precipitates in omphacite from eclogite at Alpe Arami, Switzerland: Evidence of deep subduction: Journal of Metamorphic Geology, v. 20, p. 481–492, doi:10.1046/j.1525-1314.2002.00383.x.

Dobrzhinetskaya, L.F., Green, H.W., Bozhilov, K.N., Mitchell, T.E., and Dickerson, R.M., 2003, Crystallization environment of Kazakhstan microdiamonds: Evidence from their nanometric inclusions and mineral associations: Journal of Metamorphic Geology, v. 21, p. 425–437, doi:10.1046/j.1525-1314.2003.00452.x.

Dobrzhinetskaya, L.F., Liu, Z., Cartigny, P., Zhang, J., Tchkhetia, N.N., Green, H.W., II, and Hemley, R.J., 2006, Synchrotron infrared and Raman spectroscopy of microdiamonds from Erzgebirge, Germany: Earth and Planetary Science Letters, v. 248, p. 340–349, doi:10.1016/j.epsl.2006.05.037.

Eiler, J.M., Baumgartner, L., and Valley, J.W., 1992, Intercrystalline stable isotope diffusion: A fast grain boundary model: Contributions to Mineralogy and Petrology, v. 112, p. 543–557, doi:10.1007/BF00310783.

Evans, D.A.D., and Pisarevsky, S.A., 2008, Plate tectonics on the early Earth?: Weighing the paleomagnetic evidence, *in* Condie, K., and Pease, V., eds., When Did Plate Tectonics Begin on Planet Earth?: Geological Society of America Special Paper 440, p. 249–263.

Ferry, J., and Watson, E., 2007, New thermodynamic models and revised calibrations for the Ti-in-zircon and Zr-in-rutile thermometers: Contributions to Mineralogy and Petrology, v. 154, p. 429–437, doi:10.1007/s00410-007-0201-0.

Fu, B., Kita, N.T., Wilde, S.A., Liu, X., Cliff, J., and Greig, A., 2012, Origin of the Tongbai-Dabie-Sulu Neoproterozoic low-δ^{18}O igneous province, east-central China: Contributions to Mineralogy and Petrology, v. 165, p. 641–662, doi:10.1007/s00410-012-0828-3.

Ghiorso, M.S., and Sack, R.O., 1995, Chemical mass transfer in magmatic processes. IV. A revised and internally consistent thermodynamic model for the interpolation and extrapolation of liquid-solid equilibria in magmatic systems at elevated temperatures and pressures: Contributions to Mineralogy and Petrology, v. 119, p. 197–212, doi:10.1007/BF00307281.

Glebovitsky, V.A., and Bushmin, S.A., 1983, Aftermigmatitic metasomatism: Leningrad, Nauka Publisher, 216 p. [in Russian].

Hanski, E.J., and Melezhik, V.A., 2013, Litho and chronostratigraphy of Paleoproterozoic Karelian formations. Chapter 3.2, *in* Melezhik, V.A., et al., eds., Reading the Archive of Earth's Oxygenation: Volume 3: Global Events and the Fennoscandian Arctic Russia—Drilling Earth Project: Springer, 1552 p.

Hermann, J., Zheng, Y.F., and Rubatto, D., 2013, Deep fluids in subducted continental crust: Elements, v. 9, p. 281–287, doi:10.2113/gselements.9.4.281.

Hoffman, P.F., 2009, Pan-glacial—A third state in the climate system: Geology Today, v. 25, p. 100–107, doi:10.1111/j.1365-2451.2009.00716.x.

Hoffman, P.F., 2013, The Great Oxidation and a Siderian snowball Earth: MIF-S based correlation of Paleoproterozoic glacial epochs: Chemical Geology, v. 362, p. 143–156, doi:10.1016/j.chemgeo.2013.04.018.

Hoskin, P.W., and Schaltegger, U., 2003, The composition of zircon and igneous and metamorphic petrogenesis: Reviews in Mineralogy and Geochemistry, v. 53, no. 1, p. 27–62, doi:10.2113/0530027.

Kawabe, I., 1978, Calculation of oxygen isotope fractionation in quartz-water system with special reference to the low temperature fractionation: Geochimica et Cosmochimica Acta, v. 42, p. 613–621, doi:10.1016/0016-7037(78)90006-6.

Kohn, M.J., 1999, Why most "dry" rocks should cool "wet": The American Mineralogist, v. 84, p. 570–580.

Kohn, M.J., and Valley, J.W., 1998, Effect of cation substitutions in garnet and pyroxene on equilibrium oxygen isotope fractionations: Journal of Metamorphic Geology, v. 16, p. 625–639, doi:10.1111/j.1525-1314.1998.00162.x.

Krylov, D.P., Glebovitsky, V.A., Skublov, S.G., and Tolmacheva, E.V., 2012, Rare-earth elements in zircons of diverse age from corundum-bearing rocks of Khitostrov (Northern Karelia): Doklady Akademii Nauk, v. 443, p. 352–357.

Lackey, J.S., and Valley, J.W., 2004, Complex patterns of fluid flow during wollastonite formation in calcareous sandstones at Laurel Mountain, Mt. Morrison Pendant, California: Geological Society of America Bulletin, v. 116, p. 76–93, doi:10.1130/B25239.1.

Lackey, J.S., Valley, J.W., Chen, J.H., and Stockli, D.F., 2008, Dynamic magma systems, crustal recycling, and alteration in the central Sierra Nevada batholith: The oxygen isotope record: Journal of Petrology, v. 49, p. 1397–1426, doi:10.1093/petrology/egn030.

Lundstrom, C.C., 2009, Hypothesis for origin of convergent margin granitoids and Earth's continental crust by thermal migration zone refining: Geochimica et Cosmochimica Acta, v. 73, p. 5709–5729, doi:10.1016/j.gca.2009.06.020.

Masago, H., Rumble, D., Ernst, W.G., Parkinson, C.D., and Maruyama, S., 2003, Low δ^{18}O eclogites from the Kokchetav massif, northern Kazakhstan: Journal of Metamorphic Geology, v. 21, p. 579–587, doi:10.1046/j.1525-1314.2003.00465.x.

Mattinson, C.G., Wooden, J.L., Liou, J.G., Bird, D.K., and Wu, C.L., 2006, Age and duration of eclogite-facies metamorphism, North Qaidam HP/UHP terrane, Western China: American Journal of Science, v. 306, no. 9, p. 683–711, doi:10.2475/09.2006.01.

Melezhik, V.A., Prave, A.R., Hanski, E.J., Fallick, A.E., Lepland, A., Kump, L.R., and Strauss, H., 2013, Reading the archive of Earth oxygenation. Volume 1, Paleoproterozoic of Fennoscandia as context for Fennoscandian Arctic Russia—Drilling Early Earth Project: Springer, 490 p.

Mendybayev, R.A., Richter, F.M., Spicuzza, M.J., and Davis, A.M., 2010, Oxygen isotope fractionation during evaporation of Mg- and Si- rich CMAS-liquid in vacuum: Lunar and Planetary Institute Science Conference Abstracts, v. 41, p. 2725.

Miller, M.F., 2002, Isotopic fractionation and the quantification of ^{17}O anomalies in the oxygen three-isotope system: An appraisal and geochemical significance: Geochimica et Cosmochimica Acta, v. 66, p. 1881–1889, doi:10.1016/S0016-7037(02)00832-3.

Miller, Yu.V., and Milkevich, R.I., 1995, Tectonic cover-folded structure of the Belomorian Belt and its relations with the Karelian granite-greenschist region: Geotectonics, v. 6, p. 80–92.

Mposkos, E.D., and Kostopoulos, D.K., 2001, Diamond, former coesite and supersilicic garnet in metasedimentary rocks from the Greek Rhodope: A new ultrahigh-

pressure metamorphic province established: Earth and Planetary Science Letters, v. 192, p. 497–506, doi:10.1016/S0012-821X(01)00478-2.

Myskova, T.A., Mil'kevich, R.I., L'vov, A.B., and Miller, 2000, Origin of the Belomorian Chupa Gneiss in the light of new lithogeochemical data: Lithology and Mineral Resources, v. 35, p. 583–593, doi:10.1023/A:1026653600124.

Myskova, T.A., Glebovitskii, V.A., and Miller, Y.V., 2003, Supracrustal sequences of the Belomorian mobile belt: Protoliths, age, and origin: Stratigraphy and Geological Correlation, v. 11, p. 535–549.

Page, F.Z., Ushikubo, T., Kita, N.T., Riciputi, L.R., and Valley, J.W., 2007, High-precision oxygen isotope analysis of picogram samples reveals 2 um gradients and slow diffusion in zircon: The American Mineralogist, v. 92, p. 1772–1775, doi:10.2138/am.2007.2697.

Peck, W.H., Valley, J.W., and Graham, C.M., 2003, Slow oxygen diffusion rates in igneous zircons from metamorphic rocks: The American Mineralogist, v. 88, p. 1003–1014.

Peck, W.H., Bickford, M.E., McLelland, J.M., Nagle, A.N., and Swarr, G.J., 2010, Mechanism of metamorphic zircon growth in a granulite-facies quartzite, Adirondack Highlands, Grenville Province, New York: The American Mineralogist, v. 95, p. 1796–1806, doi:10.2138/am.2010.3547.

Perraki, M., Proyer, A., Mposkos, E., Kaindl, R., and Hoinkes, G., 2006, Raman micro-spectroscopy on diamond, graphite and other carbon polymorphs from the ultrahigh-pressure metamorphic Kimi Complex of the Rhodope Metamorphic Province, NE Greece: Earth and Planetary Science Letters, v. 241, p. 672–685, doi:10.1016/j.epsl.2005.11.014.

Pettke, T.A., Audetat, A., Schaltegger, U., and Heirich, C.A., 2005, Magmatic-to-hydrothermal crystallization in the W-Sn mineralized Mole Granite (NSW, Australia): Chemical Geology, v. 220, p. 191–213, doi:10.1016/j.chemgeo.2005.02.017.

Puchtel, I.S., Haase, K.M., Hofmann, A.W., Chauvel, C., Kulikov, V.S., Garbe-Schonberg, C.-D., and Nemchin, A.A., 1997, Petrology and geochemistry of crustally contaminated komatiitic basalts from Vetrenny Belt, SW Baltic Shield: Evidence for an early Proterozoic mantle plume beneath rifted Archean continental lithosphere: Geochimica et Cosmochimica Acta, v. 61, p. 1205–1222, doi:10.1016/S0016-7037(96)00410-3.

Rasmussen, B., Bekker, A., and Fletcher, I.A., 2013, Correlation of Paleoproterozoic glaciations based on U-Pb zircon ages for tuff beds in the Transvaal and Huronian Supergroups: Earth and Planetary Science Letters, v. 382, p. 173–180, doi.org/10.1016/j.epsl.2013.08.037.

Reid, M.R., Vazquez, J.A., and Schmitt, A.K., 2011, Zircon-scale insights into the history of a Supervolcano, Bishop Tuff, Long Valley, California, with implications for the Ti-in-zircon geothermometer: Contributions to Mineralogy and Petrology, v. 161, p. 293–311, doi:10.1007/s00410-010-0532-0.

Rosenbaum, J.M., 1994, Stable isotope fractionation between carbon dioxide and calcite at 900 °C: Geochimica et Cosmochimica Acta, v. 58, p. 3747–3753, doi:10.1016/0016-7037(94)90164-3.

Rubatto, D., and Hermann, J., 2007, Experimental zircon/melt and zircon/garnet trace element partitioning and implications for the geochronology of crustal rocks: Chemical Geology, v. 241, p. 38–61, doi:10.1016/j.chemgeo.2007.01.027.

Rubatto, D., Williams, I.S., and Buick, I.S., 2001, Zircon and monazite response to prograde metamorphism in the Reynolds Range, central Australia: Contributions to Mineralogy and Petrology, v. 140, p. 458–468, doi:10.1007/PL00007673.

Rubatto, D., Hermann, J., Berger, A., and Engi, M., 2009, Protracted fluid-induced melting during Barrovian metamorphism in the Central Alps: Contributions to Mineralogy and Petrology, v. 158, p. 703–722, doi:10.1007/s00410-009-0406-5.

Rumble, D., and Yui, T.F., 1998, The Qinglongshan oxygen and hydrogen isotope anomaly near Donghai in Jiangsu Province, China: Geochimica et Cosmochimica Acta, v. 62, p. 3307–3321, doi:10.1016/S0016-7037(98)00239-7.

Rumble, D., Miller, M.F., Franchi, I.A., and Greenwood, R.C., 2007, Oxygen three-isotope fractionation lines in terrestrial silicate minerals: An inter-laboratory comparison of hydrothermal quartz and eclogitic garnet: Geochimica et Cosmochimica Acta, v. 71, p. 3592–3600, doi:10.1016/j.gca.2007.05.011.

Ruppel, C., Royden, L., and Hodges, K.V., 1988, Thermal modeling of extensional tectonics: Application to pressure-temperature-time histories of metamorphic rocks: Tectonics, v. 7, p. 947–957, doi:10.1029/TC007i005p00947.

Rybakov, S.I., Golubev, A.I., Slusarev, V.D., Stepanov, V.S., Lavrov, M.M., and Trofimov, N.N., 2000, Proterozoic rifts and their role in forming Belomorian Mobile Belt, *in* Geology and Ore Deposits in Karelia: Petrozavodsk, no. 2, p. 4–11 (in Russian).

Schmitt, A.K., Grove, M., Harrison, T.M., Lovera, O., Hulen, J.B., and Walters, M., 2003, The Geysers–Cobb Mountain magma system California (Part 1): U-Pb zircon ages of volcanic rocks conditions of zircon crystallization and magma residence times: Geochimica et Cosmochimica Acta, v. 67, p. 3423–3442, doi:10.1016/S0016-7037(03)00140-6.

Schmidt, S., Nagel, T.J., and Froitzheim, N., 2010, A new occurrence of microdiamond-bearing metamorphic rocks, SW Rhodopes, Greece: European Journal of Mineralogy, v. 22, no. 2, p. 189–198, doi:10.1127/0935-1221/2010/0022-1999.

Serebryakov, N.S., 2004, Petrology of corundum-bearing rocks of the Chupa sequence of Belomorian Mobile Belt [Ph.D. thesis]: Russian State Library, 208 p. [in Russian].

Serebryakov, N.S., and Aristov V.V., 2004, Conditions of localization of gem-quality corundum in rocks of Chupa sequence of the Belomorian complex of Northern Karelia: Izvestiia Visshikh Uchebnikh Zavedenii, Geologia I Razvedka 4, p. 36–42 [in Russian].

Serebryakov, N.S., and Rusinov, V.L., 2004, High-T high-pressure Ca, Na metasomatism and formation of corundum in the Precambrian Belomorian mobile belt: Doklady, Earth Science Sections, v. 395, p. 549–553.

Serebryakov, N.S., Astafiev, B.Y., Voinova, O.A., and Presnyakov, S.L., 2007, First single zircon dating of metasomatites from the Belomorian Belt: Doklady, Earth Science Sections, v. 413, p. 388–392, doi:10.1134/S1028334X07030154.

Sharkov, E.V., Smolkin, V.F., and Krassivskaya, I.S., 1997, Early Proterozoic igneous province of siliceous high-Mg boninite-like rocks in the eastern Baltic Shield: Petrology, v. 5, p. 448–465.

Shipansky, A.A., Khodorevskaya, L.I., Konolov, A.N., and Slabunov, A.I., 2012, Eclogites of the Belomorian Belt, geology and petrology: Russian Geology and Geophysics, v. 53, p. 3–29.

Slabunov, A.I., Lobach-Zhuchenko, S.B., and Bibikova, E.V., 2006, The Archean of the Baltic Shield: Geology, geochronology, and geodynamic settings: Geotectonics, v. 40, p. 409–433, doi:10.1134/S001685210606001X.

Spicuzza, M.J., Day, J.M.D., Taylor, L.A., and Valley, J.W., 2007, Oxygen isotope constraints on the origin and differentiation of the Moon: Earth and Planetary Science Letters, v. 253, p. 254–265, doi:10.1016/j.epsl.2006.10.030.

Stepanov, V.S., 1981, Precambrian Basic magmatism of the western Belomorian Belt: Leningrad, Nedra Press, 216 p. (monograph in Russian).

Stepanova, A., and Stepanov, V., 2010, Paleoproterozoic mafic dyke swarms of the Belomorian Province, eastern Fennoscandian Shield: Precambrian Research, v. 183, p. 602–616, doi:10.1016/j.precamres.2010.08.016.

Stepanova, A.I., Larionov, A.N., Bibikova, E.V., Stepanov, V.S., and Slabunov, A.I., 2003, Early Proterozoic (2.1 Ga) Fe-tholeiitic magmatism of the Belomorian Province, Baltic Shield: Geochemistry and Geochronology: Doklady, Earth Science Sections, v. 390, p. 607–610.

Tagiri, M., Takiguchi, S., Ishida, C., Noguchi, T., Kimura, M., Bakirov, A., Sakiev, K., Takahashi, M., Takasu, A., Bakirov, A., Togonbaeva, A., and Suzuki, A., 2010, Intrusion of UHP metamorphic rocks into the upper crust of Kyrgyzian Tien-Shan: *P-T* path and metamorphic age of the Makbal Complex: Journal of Mineralogical and Petrological Sciences, v. 105, p. 233–250, doi:10.2465/jmps.071025.

Taylor, H.P., 1974, The applications of oxygen and hydrogen isotope studies to problems of hydrothermal alteration and ore deposition: Economic Geology and the Bulletin of the Society of Economic Geologists, v. 69, p. 843–883, doi:10.2113/gsecongeo.69.6.843.

Terekhov, E.N., 2007, REE distribution in corundum-bearing and other metasomatic rocks during the exhumation of metamorphic rocks of the Belomorian Belt of the Baltic Shield: Geochemistry International, v. 45, p. 364–380, doi:10.1134/S0016702907040040.

Trail, D., Mojzsis, S.J., Harrison, T.M., Schmitt, A.K., Watson, E.B., and Young, E.D., 2007, Constraints on Hadean zircon protoliths from oxygen isotopes, Ti thermometry, and rare earth elements: Geochemistry Geophysics Geosystems, v. 8, no. 6, doi:10.1029/2006GC001449.

Ustinov, V.I., Baksheev, I.A., and Serebryakov, N.S., 2008, Oxygen isotopic composition of the mineral forming fluids of corundum-bearing metasomatic rocks at the Khitoostrov and Varaka mineral occurrences, N. Karelia: Geokhimia, v. 46, p. 1174–1177.

Valley, J.W., 1986, Stable isotope geochemistry of metamorphic rocks: Reviews in Mineralogy, v. 16, p. 445–489.

Valley, J.W., 2003, Oxygen isotopes in zircon: Reviews in Mineralogy and Geochemistry, v. 53, no. 1, p. 343–385, doi:10.2113/0530343.

Valley, J.W., and O'Neil, J., 1984, Fluid heterogeneity during granulite facies metamorphism in the Adirondacks: Stable isotope evidence: Contributions to Mineralogy and Petrology, v. 85, p. 158–173, doi:10.1007/BF00371706.

Watson, E.B., and Cherniak, D.J., 1997, Oxygen diffusion in zircon: Earth and Planetary Science Letters, v. 148, p. 527–544, doi:10.1016/S0012-821X(97)00057-5.

Young, E.D., Galy, A., and Nagahara, H., 2002, Kinetic and equilibrium mass-dependent fractionation laws in nature and their geochemical and cosmochemical significance: Geochimica et Cosmochimica Acta, v. 66, p. 1095–1104, doi:10.1016/S0016-7037(01)00832-8.

Young, G.M., 2004, Earth's earliest glaciations: Tectonic setting and stratigraphic context of Paleoproterozoic glaciogenic deposits, *in* Jenkins, G.S., McMenamin, M.A.S., McKay, C.P., and Sohl, L., eds., The Extreme Proterozoic: Geology, Geochemistry, and Climate: American Geophysical Union Monograph Series 146, 161–181.

Zheng, Y.F., 1993, Calculation of oxygen isotope fractionation in hydroxyl-bearing silicates: Earth and Planetary Science Letters, v. 120, p. 247–263, doi:10.1016/0012-821X(93)90243-3.

Zheng, Y.-F., Wu, Y.-B., Chen, F.K., Gong, B., Li, L., and Zhao, Z.-F., 2004, Zircon U-Pb and oxygen isotope evidence for a large-scale ^{18}O depletion event in igneous rocks during the Neoproterozoic: Geochimica et Cosmochimica Acta, v. 68, p. 4145–4165, doi:10.1016/j.gca.2004.01.007.